

**Aspects of lithium-ion micro-batteries with
a novel silicon anode:**

**Investigation of the impact of electrolyte additives on the electrochemical
performance and of the adhesive bond of possible enclosure materials**

Masterarbeit

zur Erlangung des akademischen Grades
Diplomingenieur (Dipl.-Ing.)

an der Fakultät für Technische Chemie,
Verfahrenstechnik und Biotechnologie
der Technischen Universität Graz (TU Graz)

vorgelegt von

Gabriel SCHROTTER

Institut für Chemische Technologie von Materialien

Betreuer: Univ.-Prof. Dr.rer.nat. Martin Wilkening

Graz, 2013/14

Abstract

The aim of this thesis was to investigate the effects of selected electrolyte additives (vinylene carbonate, vinylethylene carbonate, 4-fluorophenyl isocyanate and 2,3,4-trifluorophenyl isocyanate) on the electrochemical performance of a novel silicon electrode for lithium-ion batteries. With the help of two different test setups (pouch cells for long term cycling, Swagelok cells for short term cycling) and a SEM analysis of the electrodes, it could be determined that the additives were able to effectively decrease the irreversible capacity loss during SEI formation and increase the morphological stability of the microstructure.

Another aspect investigated was the quality and strength of an adhesive bond between different modified silicon surfaces and a possible enclosure material (aluminium laminated film, pouch foil) for a micro battery. For this purpose, a peel test was carried out and analyzed and it could be shown that the bond between modified surfaces and pouch foil showed superior characteristics compared to unmodified silicon.

Acknowledgments

My deepest gratitude goes to my supervisor and professor, **Univ.-Prof. Dr.rer.nat. Martin Wilkening**, for the possibility of doing this thesis, as well as for his patience and helpfulness.

I would also like to thank Univ.-Prof. Dipl.-Ing. Dr.techn. Franz Stelzer and all other members of the Institute for Chemistry and Technology of Materials for the good collaboration.

I would like to express my gratitude to the team I was part of, the “AG Wilkening”, especially to Dipl.-Ing. Dr.techn Michael Sternad, for his ideas and input and to Georg Hirtler and Veronika Pregartner for their assistance.

I would also like to thank Sanja Simic, from the Institute of Electron Microscopy and Nanoanalysis, for doing the SEM images.

I would like to thank Infineon Technologies Austria AG for their support and their supply of materials and samples.

Special thanks go to my parents for their generous support and patience during my studies, my friends for always distracting me and my girlfriend for being there whenever I needed someone.

This thesis was made possible by the financial support of the Austrian Federal Ministry of Economy, Family and Youth, and the Austrian National Foundation for Research, Technology and Development as part of the Christian Doppler Laboratory for Lithium-ion Batteries, Graz University of Technology, Institute for Chemistry and Technology of Materials, Stremayrgasse 9, 8010 Graz, Austria.



Table of Contents

| | |
|---|-----------|
| 1. Introduction | 1 |
| 1.1. Target and hypothesis | 1 |
| 1.1.1. Impact of electrolyte additives on the electrochemical performance | 1 |
| 1.1.2. Adhesive bond of possible enclosure materials | 2 |
| 1.2. Fundamentals of batteries | 3 |
| 1.2.1. Basic aspects of batteries | 4 |
| 1.2.2. Battery characteristics | 6 |
| 1.2.2.1. Theoretical and terminal voltage | 6 |
| 1.2.2.2. Theoretical capacity and specific energy | 7 |
| 1.2.2.3. Coulometric efficiency and cycle life | 8 |
| 1.3. Practical battery systems | 8 |
| 1.3.1. Battery systems with aqueous electrolyte | 9 |
| 1.3.1.1. Alkaline-manganese battery | 9 |
| 1.3.1.2. Lead-acid battery | 10 |
| 1.3.1.3. Nickel-Cadmium and Nickel-MH batteries | 11 |
| 1.3.2. Battery systems with nonaqueous electrolyte | 12 |
| 1.3.2.1. Primary lithium batteries | 12 |
| 1.3.2.1.1. Lithium-manganese dioxide batteries | 14 |
| 1.3.2.1.2. Lithium-thionyl chloride batteries | 14 |
| 1.3.2.2. Lithium-ion batteries | 15 |
| 1.3.2.2.1. Electrode materials for Li-ion batteries | 15 |
| 1.3.2.2.2. Lithium-ion battery schemata | 17 |
| 1.3.2.2.3. Electrolyte and SEI | 18 |
| 1.3.2.2.4. Practical usage and outlook | 19 |
| 2. Experimental | 20 |
| 2.1. Long term cycling experiments in pouch cells | 20 |
| 2.1.1. Cathode preparation for pouch cells | 20 |

| | | |
|-----------|---|-----------|
| 2.1.2. | Anode preparation for pouch cells | 20 |
| 2.1.3. | Electrolyte preparation | 22 |
| 2.1.4. | Assembling of the pouch cells | 23 |
| 2.1.5. | Long term electrochemical testing | 24 |
| 2.1.6. | Post mortem investigation of pouch cells | 25 |
| 2.2. | Short term cycling experiments in Swagelok cells | 25 |
| 2.2.1. | Cathode preparation for Swagelok cells | 25 |
| 2.2.2. | Anode preparation for Swagelok cells | 26 |
| 2.2.3. | Electrolyte preparation | 26 |
| 2.2.4. | Assembling the Swagelok cells | 27 |
| 2.2.5. | Short term electrochemical testing | 27 |
| 2.2.6. | Post mortem investigation of Swagelok cells | 28 |
| 2.3. | SEM investigations | 29 |
| 2.4. | Peel test of pouch foil sealing tape welded on different surfaces | 29 |
| 2.4.1. | Sample preparation | 29 |
| 2.4.2. | Peel test | 30 |
| 2.4.3. | Analysis of the peel test | 31 |
| 3. | Results and discussion | 32 |
| 3.1. | Impact of electrolyte additives: Long term cycling experiments | 32 |
| 3.1.1. | Cycling behavior | 32 |
| 3.1.2. | Cumulative irreversible capacity | 37 |
| 3.1.3. | Post mortem images | 38 |
| 3.1.3.1. | Standard electrolyte (EC:EMC 3:7 w/w, 1 M LiPF ₆) | 38 |
| 3.1.3.2. | Standard electrolyte + 0.5 % VC | 39 |
| 3.1.3.3. | Standard electrolyte + 1.0 % VC | 39 |
| 3.1.3.4. | Standard electrolyte + 2.0 % VC | 40 |
| 3.1.3.5. | Standard electrolyte + 0.5 % VEC | 40 |
| 3.1.3.6. | Standard electrolyte + 1.0 % VEC | 41 |
| 3.1.3.7. | Standard electrolyte + 2.0 % VEC | 41 |
| 3.1.3.8. | Standard electrolyte + 0.5 % 4-FP | 42 |

| | | |
|-----------|---|----|
| 3.1.3.9. | Standard electrolyte + 1.0 % 4-FP | 42 |
| 3.1.3.10. | Standard electrolyte + 2.0 % 4-FP | 43 |
| 3.1.3.11. | Standard electrolyte + 0.5 Tri-FP | 43 |
| 3.1.3.12. | Standard electrolyte + 1.0 Tri-FP | 44 |
| 3.1.3.13. | Standard electrolyte + 2.0 % Tri-FP | 44 |
| 3.1.3.14. | Observations | 45 |
| 3.1.4. | SEM images | 45 |
| 3.1.4.1. | Not cycled LIBC 13 and LIBC 23 anodes | 46 |
| 3.1.4.2. | Standard electrolyte (EC:EMC 3:7 w/w, 1 M LiPF ₆) | 47 |
| 3.1.4.3. | Standard electrolyte + 0.5 % VC | 48 |
| 3.1.4.4. | Standard electrolyte + 1.0 % VC | 49 |
| 3.1.4.5. | Standard electrolyte + 2.0 % VC | 49 |
| 3.1.4.6. | Standard electrolyte + 0.5 % VEC | 51 |
| 3.1.4.7. | Standard electrolyte + 1.0 % VEC | 51 |
| 3.1.4.8. | Standard electrolyte + 2.0 % VEC | 52 |
| 3.1.4.9. | Standard electrolyte + 0.5 % 4-FP | 52 |
| 3.1.4.10. | Standard electrolyte + 1.0 % 4-FP | 53 |
| 3.1.4.11. | Standard electrolyte + 2.0 % 4-FP | 54 |
| 3.1.4.12. | Standard electrolyte + 0.5 % Tri-FP | 54 |
| 3.1.4.13. | Standard electrolyte + 1.0 % Tri-FP | 55 |
| 3.1.4.14. | Standard electrolyte + 2.0 Tri-FP | 56 |
| 3.1.5. | Analysis and comparison of the results | 56 |
| 3.1.5.1. | Standard electrolyte and VC | 59 |
| 3.1.5.2. | Standard electrolyte and VEC | 60 |
| 3.1.5.3. | Standard electrolyte and 4-FP | 61 |
| 3.1.5.4. | Standard electrolyte and Tri-FP | 63 |
| 3.1.6. | Conclusion | 64 |
| 3.2. | Impact of electrolyte additives: Short term cycling experiments | 66 |
| 3.2.1. | Target and hypothesis | 66 |
| 3.2.2. | Cumulative irreversible capacity | 66 |
| 3.2.3. | SEM images | 67 |
| 3.2.3.1. | Standard electrolyte (EC:EMC 3:7 w/w, 1 M LiPF ₆) | 67 |
| 3.2.3.2. | Standard electrolyte + 0.5 % VC | 68 |

| | | |
|-----------|--|-----------|
| 3.2.3.3. | Standard electrolyte + 1.0 % VC | 69 |
| 3.2.3.4. | Standard electrolyte + 2.0 % VC | 69 |
| 3.2.3.5. | Standard electrolyte + 0.5 % VEC | 70 |
| 3.2.3.6. | Standard electrolyte + 1.0 % VEC | 71 |
| 3.2.3.7. | Standard electrolyte + 2.0 % VEC | 71 |
| 3.2.3.8. | Standard electrolyte + 0.5 % 4-FP | 72 |
| 3.2.3.9. | Standard electrolyte + 1.0 % 4-FP | 72 |
| 3.2.3.10. | Standard electrolyte + 2.0 % 4-FP | 73 |
| 3.2.3.11. | Standard electrolyte + 0.5 % Tri-FP | 73 |
| 3.2.3.12. | Standard electrolyte + 1.0 % Tri-FP | 74 |
| 3.2.3.13. | Standard electrolyte + 2.0 % Tri-FP | 74 |
| 3.2.4. | Analysis | 75 |
| 3.2.4.1. | VC/VEC vs. 4-FP/Tri-FP | 76 |
| 3.2.5. | Conclusion | 78 |
| 3.3. | Adhesion of pouch foil sealing tape welded on different surfaces | 79 |
| 3.3.1. | Analysis | 79 |
| 3.3.1.1. | Reference (unmodified silicon wafer) | 79 |
| 3.3.1.2. | Mechanically thinned silicon on glass | 81 |
| 3.3.1.3. | Etched silicon on glass | 82 |
| 3.3.1.4. | ECD-Cu on silicon | 83 |
| 3.3.1.5. | RU302507V01 (5) | 84 |
| 3.3.1.6. | TiW/AlCu on silicon | 85 |
| 3.3.1.7. | 1300 nm TEOS on silicon | 86 |
| 3.3.2. | Conclusion | 87 |
| 4. | Summary | 89 |
| 5. | References | 91 |

1. Introduction

1.1. Target and hypothesis

1.1.1. Impact of electrolyte additives on the electrochemical performance

The ever growing demand for lithium-ion batteries with a higher specific energy and a higher energy density leads to the need for new electrode materials. A very promising candidate for a high capacity anode material is silicon (Si), which has a very high theoretical capacity of nearly 4200 mAh g^{-1} [1] and was already studied extensively to replace graphite [2, 3]. However, during lithiation, silicon suffers from a volume expansion of up to 300 % [4]. Therefore, various approaches for silicon electrodes were taken including the use of Si-composites [5], different Si particle sizes [6] and Si-thin films or amorphous Si [7, 8].

Another important factor for the performance of a silicon anode is the quality and durability of the SEI that is formed on its surface, as the SEI properties strongly influence the cycle life and the reversible capacity [9]. The addition of additives to the electrolyte is one of the most effective ways to influence the critical formation of the SEI and other important cell characteristics. A lot research on this topic was already carried out on graphite anodes [10], but with the increasing importance of silicon, studies on the influence of additives on silicon are increasing too.

This thesis investigates the effects of selected electrolyte additives on the electrochemical performance of a novel silicon electrode for a lithium-ion micro battery. These electrodes are prepared from a single crystal silicon wafer and they are micro-structured. The selected additives are used for their ability to influence SEI formation and thus should prolong cycle life of the Si-anode and reduce the irreversible capacity. For this purpose, vinylene carbonate (VC), vinylene carbonate (VEC), 4-fluorophenyl isocyanate (4-FP) and 2,3,4-trifluorophenyl isocyanate (Tri-FP) are used.

VC was already proposed early on [11] and is the most used additive. It was extensively studied in combination with a graphite anode [12] and is a good candidate for improving Si-electrodes as well [13]. VEC has not been used with silicon before, but has similar characteristics to VC [14]. Various aromatic isocyanates like 4-FP and Tri-FP are said to have similar SEI forming properties to VC or VEC too, although their reaction mechanisms are different and depend on the number and nature of the heteroatoms within the molecule [15, 16].

The investigation is carried out using a cycling experiment with capacity limitation. The influence of the additive on the cycle stability and irreversible capacity is measured and compared to results from cells without additive. Additionally, SEM images are made from the silicon anodes after the cycling experiments, to examine the morphological changes of the micro-structured surface and the possible influences of the additive.

1.1.2. Adhesive bond of possible enclosure materials

One possibility for the realization of a silicon micro-battery is to place the electrochemical active materials into a cavity on a silicon wafer. The silicon at the bottom of this cavity has the function of the negative active material, the cavity itself is filled with separator and electrolyte and then closed with some kind of lid on whose inside the positive active material is applied. For this lid, aluminium laminated film [17] can be used, which is also used as packaging material for lithium-ion battery pouches (therefore the name pouch foil). However, to achieve air and watertight sealing the pouch foil has to be welded onto the surface of the silicon wafer and this is only possible with the addition of a sealing tape between those layers. To further increase the adhesive bond between the wafer and the lid, the surface of the silicon substrate can be modified.

The target of this examination was to determine the quality and strength of the adhesive bond between the wafer and the lid and to find factors with which the different possible surface modifications can be compared to the unmodified silicon. Ultimately, the best suited modification shall be identified. For this reason, a simple 180 ° peel test was carried out and analyzed [18-20].

1.2. Fundamentals of batteries

When Alessandro Volta (1745-1827) invented the voltaic pile in 1800, inspired by Luigi Galvani's (1737-1798) discovery of a dissected frog leg twitching when touched with two different metals, he laid the foundation for a whole new field of discoveries for electrochemistry and electrical engineering. In fact, the voltaic pile (see Figure 1) was the first real battery, consisting of several identical galvanic cells made of zinc and copper discs separated by a layer of cloth or cardboard soaked with brine that were stacked on top of each other. This device provided enough voltage to deliver small electric shocks. Volta even experimented with different materials and found out that different metals caused electrical effects of varying intensity (with zinc and copper being the strongest) [21, 22]. Finally, this led to the understanding that the properties of batteries are strongly dependent on the used electrode materials and electrolytes.

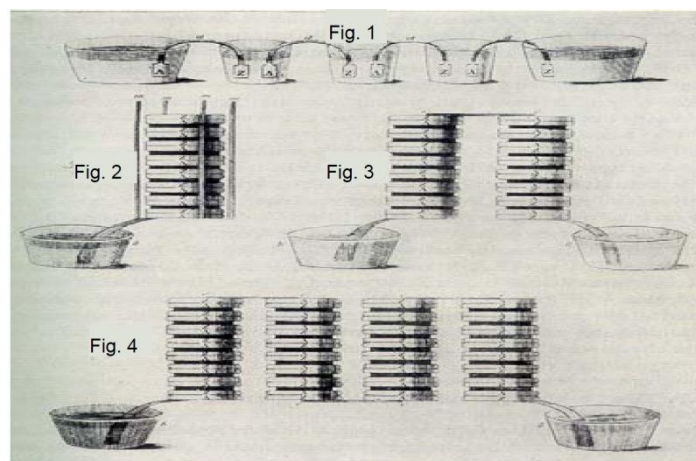


Figure 1: Voltaic pile of various proportions. Fig. 1: Galvanic element connected in series. Fig. 2 to Fig. 4: One, two and four voltaic piles connected in series [22].

Since then, batteries have become an important part of our everyday lives. Their scope of application is as broad and varied as are the possible combinations of usable materials and different battery geometries. This abundance of possibilities allows to create battery systems customized for particular fields of application. On the other hand, this means that not every system can be used for every purpose, even though the working fundamentals of all cell and battery systems are more or less the same.

1.2.1. Basic aspects of batteries

Batteries are electrochemical power sources. More specifically, a battery is a device that contains one or more electrochemical cells, mostly connected in series alongside some other components ensuring its safe and reliable use inside battery housing. Most of the time, however, the term “battery” directly refers to the electrochemical cell. These electrochemical cells are able to convert the chemical energy stored inside their active materials directly into electric energy through an electrochemical oxidation reduction reaction. This so called discharge reaction consists of two separated partial reactions that are connected to each other. First, the material with the lower redox potential, i.e. the anode or negative electrode, is oxidized generating electrons for the external circuit. The material with the higher redox potential, i.e. the cathode or positive electrode, accepts the same amount of electrons from the external circuit and is therefore reduced. To complete the circuit, an internal liquid or gel-like ionic conductor, i.e. the electrolyte, transfers electrons, in the form of ions, from the cathode to the anode. To prevent internal short circuits between the anode and the cathode, an additional separator mechanically separates the electrodes in practical cell designs [23, 24]. Figure 2 shows a schematic example of an electrochemical cell during discharge with all according reactions.

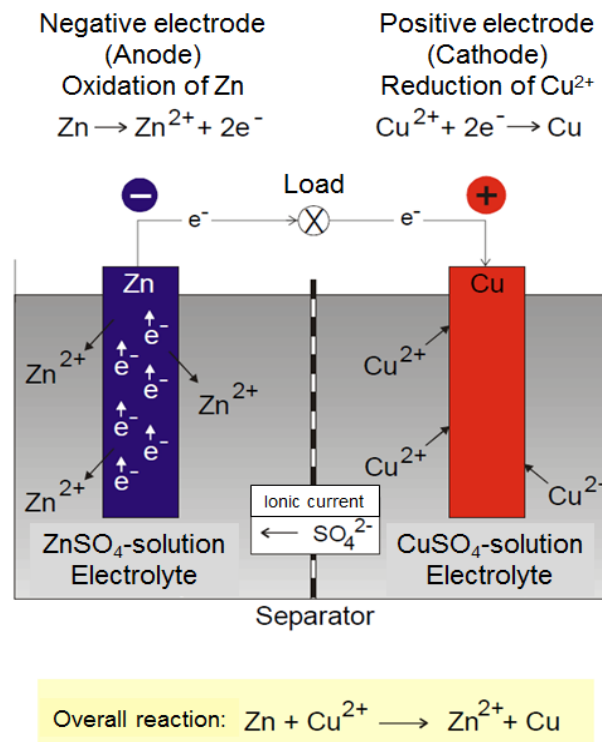


Figure 2: Schematic image of a Daniell cell (1836): Discharge reactions of an electrochemical cell with a zinc anode, a copper cathode and sulfuric acid as electrolyte [23].

If all those reactions inside the cell are reversible, it is possible to recharge the cell through the reversion of the external current flow. In this case, the negative electrode is reduced and the positive electrode is oxidized, which means, that if the anode is defined as the electrode at which oxidation occurs and the cathode as the one where reduction takes place, the negative electrode is now the cathode and the positive one the anode [24]. Therefore it is difficult to explicitly define anode and cathode in a rechargeable cell, as the charge and discharge cycle is repeated many times. To prevent confusion, the terms negative electrode and positive electrode, should be used as the potential of the negative or positive electrode will always be more negative or positive as that of the other electrode. Alternatively, by convention, the electrodes can be named after their function during discharge [23].

These concepts led to a classification of practical batteries according their ability to be recharged.

1. Primary cells or batteries are non-rechargeable, which means that the electrochemical reactions inside them are irreversible. They can only be discharged once, contain a fixed amount of active materials, which are consumed during use, and the cells are discarded afterwards. Advantages of primary batteries are their convenient and easy use, good shelf life and low to moderate discharge rates [24, 25].
2. Secondary cells or batteries are rechargeable, which means that the electrochemical reactions inside them are highly reversible. After the battery is discharged, an external current flow forces the electrochemical process to be reversed and the cell's active materials are restored to their former state. This means that after charging, the cell can be discharged again. This cycle can be repeated hundreds or even thousands of times and thus prolongs the lifetime of the cell. This advantage over primary cells sets off their higher costs and lower charge retention [24, 25].

As noted before, batteries have numerous fields of application, but typically they are used for portable systems such as mobile phones, laptops, other cordless power tools, starter-light-ignition batteries for cars, electrically powered vehicles and a growing number of stationary energy storage devices.

All these different applications led to the development of all kinds of different battery systems, the preference for any particular system depending on the field of application. For example, for devices that are rarely used like household flashlights or for long term applications with low current consumption like watches or pacemakers, primary cells like zinc-carbon or alkaline-manganese are selected. For applications like laptops, mobile phones or starter batteries in cars, secondary battery systems like lithium-ion batteries or lead-acid batteries have far more advantages from an economical and ecological point of view.

With that in mind, it is obvious that nowadays there is no single battery system that can cover the great variety of demands and that the chosen battery system for a given application may often be a compromise. This means that to be able to evaluate different battery systems, their characteristics need to be compared [25].

1.2.2. Battery characteristics

1.2.2.1. Theoretical and terminal voltage

The theoretical voltage of an electrochemical cell can be calculated from the standard electrode potential E^0 of the active materials the electrodes of the cell are made of. These empirical values can be found in the electrochemical series of metals, a listing of standard electrode potentials, where the potentials are sorted relative to the normal hydrogen electrode (NHE), which was arbitrarily set to 0 V under standard conditions (25 °C temperature and 101.13 kPa pressure).

The standard potential of a cell is the difference between the electrode with the higher standard potential and that with the lower one. For example, the following theoretical potential can be calculated for the Daniell element in Figure 2:

| | |
|---------------------|-------------------|
| Cu/Cu ²⁺ | +0.34 V |
| Zn/Zn ²⁺ | <u>-(−0.76 V)</u> |
| Cell potential | +1.10 V |

The terminal cell voltage that can be measured between the poles of a battery will always differ slightly from the theoretical potential, as a result of other factors like inhibited equilibrium state or side reactions [25].

1.2.2.2. Theoretical capacity and specific energy

The capacity of a cell or battery is the total amount of electric charge, in the form of electrons or ions that can be generated or stored through the electrochemical reactions of the active materials and is generally expressed in ampere-hours (Ah). This value depends on the mass of the active materials of the cell and the number of electrons involved in the reactions. This means that for a given battery system, based only on active materials, the theoretical capacity, expressed in ampere-hours per kilogram (Ah/kg), can be calculated from the specific capacity (the amount of charge generated per kilogram reactant) of its electrode materials [23, 24].

The theoretical specific energy, in watt-hours per kilogram (Wh/kg), or energy density, in watt-hours per litre (Wh/l), is the amount of energy that can be harvested from an electrochemical cell of certain dimensions. It is the product of the cell voltage (V) and the theoretical capacity (Ah/kg) of a cell. This means that battery systems consisting of materials with high theoretical capacity and those that have electrochemical reactions with reduction potentials that are far apart (which leads to a high theoretical voltage) are most desirable. Table 1 compares a number of primary and secondary battery systems and it is apparent that the practical specific energies are much lower than the theoretical. The reason for this is that practical cells are not made out of active materials only, but always include a lot of other components that are inactive for electrochemical reasons like housing parts, separator or current collectors [23].

Table 1: Comparison of various battery systems in terms of their energy [25].

| System | Specific energy (theoretical) / Wh/kg | Specific energy (practical) / Wh/kg | Energy density (practical) / Wh/l |
|--------------------------------|--|--|--|
| Alkaline (zinc)-manganese cell | 336 | 50-80 | 120-150 |
| Zinc-carbon | 358 | 60-90 | 140-200 |
| Lead-acid | 170 | 35 | 90 |
| Nickel-cadmium | 209 | 50 | 90 |
| Nickel-metal hydride | 380 | 60 | 80 |
| Lithium-ion-metal oxide | 500-550 | 150 | 220 |

1.2.2.3. Coulometric efficiency and cycle life

These two properties apply only to secondary battery systems. The coulometric efficiency of a cell or battery is the ratio between the electric charge or energy released during discharge and the charge or energy needed to fully load the cell. As for all energy conversions, the amount used will always be higher than the amount gained in the process, meaning that this efficiency factor will always be lower than 1. In the case of batteries, this is due to the generation of heat through useless side reactions or the incomplete formation of useable reaction products. The coulometric efficiency of secondary battery systems is a very important factor in their performance and has to be as high as possible. For example the coulometric efficiency of a nickel-cadmium system is about 70-90 %, while that for a lithium-ion battery is nearly 100 %.

The cycle life of a secondary battery is the number of cycles it can achieve during its lifetime. It determines how often a secondary cell can be discharged and charged repeatedly until a defined, lower limit of capacity is reached (for example, until 80 % of the nominal capacity are reached). The cycle life is strongly influenced by the coulometric efficiency, as with each cycle the amount of capacity that is lost through side reactions sums up with each subsequent cycle, leading to shorter cycle lives, the lower the efficiency. Another factor that can influence the cycle life or lifetime of a battery is the unwanted self-discharge during storage, which is affected by cell design, temperature and electrochemical system [25].

1.3. Practical battery systems

As mentioned before, the ever growing demand and new possible applications for batteries led to the development of many different battery systems. Alongside the battery systems that were developed early on, such as the Leclanché cell, which was further developed into alkaline-manganese cells, the lead-acid cell and newer developments like the nickel-cadmium and nickel-metal hydride (MH) batteries, primary and secondary lithium batteries were commercialized two decades ago and most recently lithium-ion batteries were developed. What the first systems have in common is that their electrolyte solutions are based on water and thus have a bad cold temperature behavior ($< -40\text{ }^{\circ}\text{C}$) and a limitation of the terminal voltage for a single cell because of the relatively low electrochemical stability window of water (1.23 V vs. NHE). Lithium and lithium-ion batteries, on the other hand, can reach much higher terminal voltages, because of the

more active materials that are used, but this is only possible with the use of more stable nonaqueous electrolytes. Such electrolytes typically consist of a conducting salt dissolved in a liquid or polymeric organic solvent. The downside of the use of those electrolytes is that they have a lower conductivity and higher safety requirements than aqueous electrolytes [23, 26].

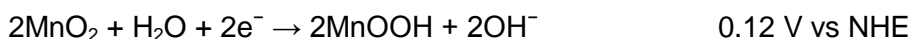
The first part of the following chapter will give an overview of common battery systems with electrolytes based on water, while the second part will deal with lithium and especially lithium-ion battery technology.

1.3.1. Battery systems with aqueous electrolyte

1.3.1.1. Alkaline-manganese battery

The alkaline-manganese dioxide battery is a primary system that has its name from the concentrated alkaline aqueous solution (generally 30-45 % potassium hydroxide) that is used as electrolyte for this cell. Due to the high conductivity of the electrolyte solution, they are considered high-power cells. During operation, the zinc anode is oxidized to form zinc oxide, while the manganese dioxide cathode is reduced to form MnOOH:

Cathode reaction:



Anode reaction:



Overall reaction:



The initial terminal voltage is about 1.5 V and alkaline-manganese dioxide batteries are mostly constructed in cylindrical shape as shown in Figure 3. They are still widely used and have a good shelf life [25].

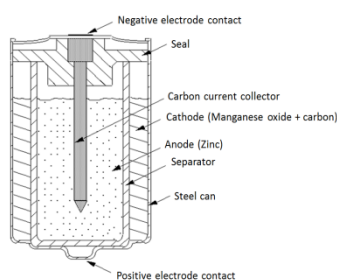


Figure 3: Cell construction of an alkaline-manganese dioxide battery. Inside a steel can serving as current collector the manganese dioxide cathode, a separator and zinc powder with the electrolyte solution is located [27].

1.3.1.2. Lead-acid battery

The lead-acid battery that was already invented 1859, was the first battery that could be recharged. It is still the most reliable and widely used battery for starter, light and ignition applications in vehicles and as reserve battery for emergencies. Lead-acid cells use an aqueous sulfuric acid solution as electrolyte, metallic lead as anode and lead oxide as cathode. During discharge, the anode is oxidized to form lead sulfate and the cathode is reduced to lead sulfate too. This is a unique characteristic, as in a fully discharged state both electrodes consist of the same material. Another uncommon trait is that the electrolyte, sulfuric acid, takes an active part in the electrochemical reactions and thus can be viewed as a type of active material too. The reason for this is that during discharge, sulfate ions are used up to form the solid lead sulfite on the electrodes and water. The mechanism of these reactions is not fully understood yet. Figure 4 shows discharge and charge reactions of the lead-acid battery as well as a simplified scheme. The initial voltage of a single lead-acid cell is about 2.0 V. At this value electrolysis of the electrolyte may occur, but is kinetically inhibited so that the very small amount of gases generated can be neglected. To reach higher values, which is important for most applications, those cells are often connected in series [23].

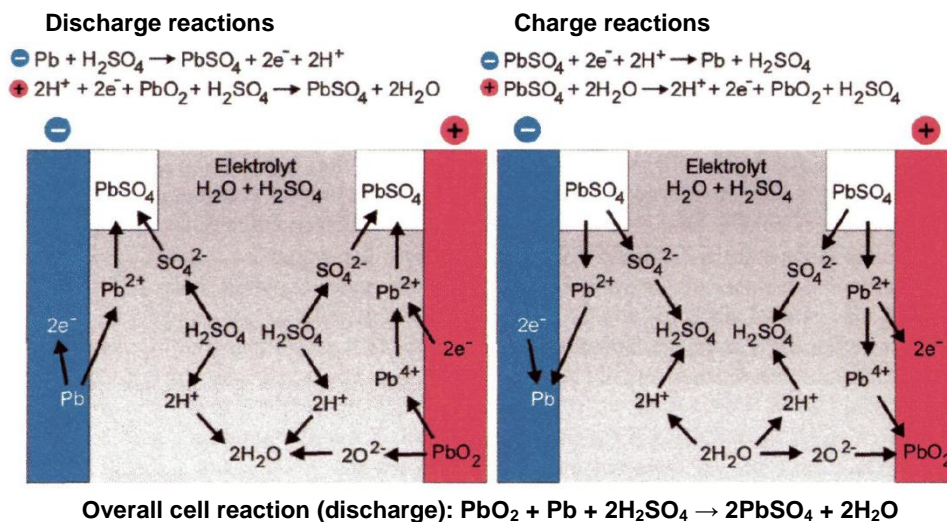
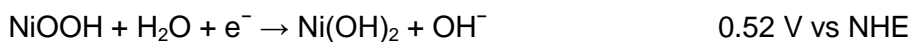


Figure 4: Simplified reactions and mechanisms of the lead-acid battery. Left: Discharge. Right: Charge [23].

1.3.1.3. Nickel-Cadmium and Nickel-MH batteries

In nickel-cadmium batteries, nickel hydroxide is used as positive electrode and a cadmium compound is used as negative electrode. A potassium hydroxide solution is used as electrolyte. During discharge, the following reactions take place, during charge they are reversed.

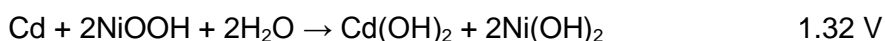
Cathode reaction:



Anode reaction:



Overall reaction:



Similar to the lead-acid cell, hydrogen and oxygen gases evolve from the electrolysis of water in the electrolyte and lead to self-discharge and safety problems because of pressure increases inside the cell. To prevent this from happening, the negative electrode is fitted with a discharge and charge reserve, which reduces hydrogen generation during overdischarge and overcharge. With this protection, it is possible to manufacture cells that have a completely sealed structure and thus are easy to use and maintenance free. Nickel-cadmium batteries have excellent characteristics, such as a long service life (exceeding 500 charge-discharge cycles), a high rate of discharge and constant discharge voltage, which makes them an excellent power source for any battery-powered device.

The nickel-MH battery, commercial available since the late 1980s, is very similar to the nickel-cadmium battery in cell design and structure. The negative electrode in the nickel-cadmium battery (the cadmium) is replaced with a hydrogen-absorbing alloy (M) that is able to form a metal hydride (MH), while all other cell compounds remain the same. This means that the second active species is actually hydrogen.

Cathode reaction:



Anode reaction:



Overall reaction:



This change leads to several advantages of nickel-MH over nickel-cadmium batteries. The capacity and energy density of the nickel-MH battery is about 1.5-1.8 times higher than that of the nickel-cadmium battery. It has an even longer service life (up to 1000 cycles and more) and does not use compounds that are critical for the environment like cadmium. Most nickel-MH batteries are available in cylindrical and prismatic form. They replace nickel-cadmium batteries in many of their applications like computers, mobile phones and other handheld devices, but can be used as power source for electric vehicles as well [23, 25].

1.3.2. Battery systems with nonaqueous electrolyte

1.3.2.1. Primary lithium batteries

In lithium batteries, metallic lithium is used as the negative active material. As listed in Table 2 and compared to the materials already mentioned, lithium has a very high specific capacity due to its very low electrochemical equivalent mass and the lowest electrode potential of all metals. Moreover, it has the lowest density of all solids. As a consequence of these physical properties, the use of lithium as negative electrode material in batteries with nonaqueous electrolyte leads to the possibility of manufacturing cells that have high voltage and high energy density [25].

Table 2: Comparison of various negative active materials in their charged state. $F = \text{Faraday constant} = 96485 \text{ As/mol}$. Electrode potential at equilibrium conditions against the NHE [23].

| Active material | Atomic mass / g/mol | Electro-chemical equivalent | Electrochemical equivalent mass / g/(mol F) | Specific capacity / Ah/kg | Electrode potential / V |
|---------------------------------------|---------------------|-----------------------------|---|---------------------------|-------------------------|
| Pb | 207.20 | 2 | 103.60 | 259 | -0.13 |
| Cd | 112.42 | 2 | 56.21 | 477 | -0.40 |
| LaNi ₅ H ₆ (MH) | 438.40 | 6 | 73.07 | 366.7 | ±0.00 |
| Zn | 65.38 | 2 | 32.69 | 820 | -0.76 |
| Li | 6.94 | 1 | 6.94 | 3862 | -3.05 |
| Na | 22.94 | 1 | 22.94 | 1168 | -2.71 |

To achieve this, an adequate stability of electrolyte and electrodes (lithium or other alkaline metals with low electrode potentials are highly reactive) is required. Therefore certain aprotic organic and inorganic solvents are used as electrolytes. Another important advantage of lithium is that it is kinetically stable in such electrolytes, although it is thermodynamically unstable. This is possible because of the formation of an electronically insulating interface layer that is formed at first contact between the metal and certain electrolytes. Because of its ability to still be permeable for small Li^+ -ions this film, called solid electrolyte interphase (SEI), is most important for the use of lithium as active material in batteries, as it prevents the electrode from further corrosion (see Figure 5) [26].

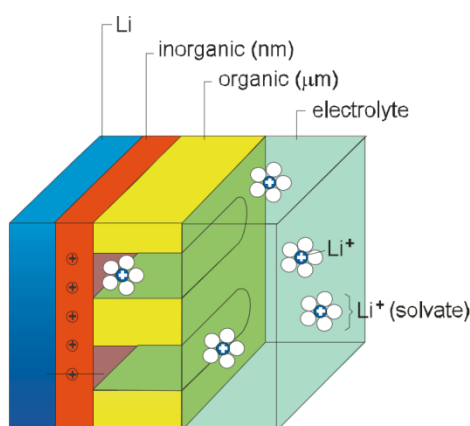


Figure 5: Schematic image of the SEI on a lithium electrode in an organic electrolyte. The exact compositions of the inorganic and organic portions depend on the used electrolyte. The model of viewing the film as a new phase that functions as a solid electrolyte for Li^+ -ions was proposed by Peled 1979 [28].

The good Li^+ -ion conductivity of the SEI allows for lithium to be precipitated from the electrolyte on the negative electrode and thus offers the possibility of lithium batteries to be recharged. However, because this reaction basically takes place in areas with a poorly formed SEI, specular, dendrite like lithium structures are formed. This lithium is only partially reusable during discharge as it is mechanically unstable and may simply break off of the main electrode or become isolated through new formed SEI layers. This means that efficiency drops to a maximum of 99 % and excess lithium, as well as excess electrolyte (both are irreversibly lost) have to be integrated in the cell to reach high cycle lives. The real problem, however, is a safety aspect. These lithium dendrites may grow so long that they get in contact with the positive electrode. If this happens, the cell is short-circuited and enough heat is generated to partially melt the lithium that is in contact with a flammable organic electrolyte and as a result thermal runaway may occur [26].

This means that although technically possible and attractive as a high energy secondary system, secondary lithium batteries are only used in limited applications

Primary lithium batteries on the other hand offer superior characteristics compared to common batteries with aqueous electrolytes. They have high voltage, a wide operable temperature range, high specific energy and energy density as well as low self-discharge rates that lead to storage stabilities of up to ten years. Because of the high reduction potential of lithium, many different materials can be considered as cathode material for those batteries and various types are available.

1.3.2.1.1. Lithium-manganese dioxide batteries

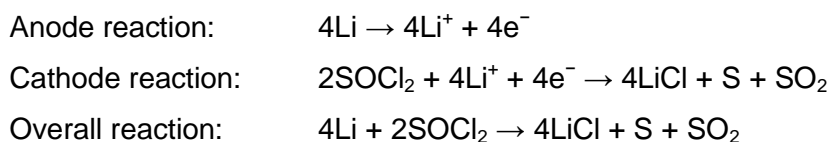
Lithium-manganese dioxide batteries are the cheapest and most common among lithium batteries. MnO_2 functions as positive active material, as it does in the already mentioned alkaline cells (see chapter 1.3.1.1.), but in a different manner. As electrolyte solution, a mixture of propylene carbonate (PC) and 1,2-dimethoxyethane (DME), as solvents, and lithium perchlorate (LiClO_4) or lithium trifluoromethanesulfonate (LiCF_3SO_3), as conducting salt, is used. The following reactions occur during operation and the end product $\text{MnO}_2^-(\text{Li}^+)$ refers to a lithium ion that is intercalated into the MnO_2 crystal lattice.



These batteries provide a stable voltage of 3 V and are available as coin cells or cylindrical cells with varying capacities depending on their size. One lithium-manganese dioxide battery can easily replace at least two regular alkaline-manganese batteries [25].

1.3.2.1.2. Lithium-thionyl chloride batteries

In the lithium-thionyl chloride battery, the cathode consists of a porous carbon current collector and a liquid thionyl chloride solution, in which a salt (lithium tetrachloroaluminium, LiAlCl_4), is dissolved. Thionyl chloride serves as electrolyte solution and positive active material as well. The discharge reaction takes place on the catalytic surface of the carbon, which serves as a depository for the insoluble products of the reaction, lithium chloride and sulfur.



These batteries have a very high operating voltage of 3.6 V, are capable of operation in a temperature range of between -55 to 85 °C and are available in cylindrical form of various dimensions and capacities [25].

1.3.2.2. Lithium-ion batteries

With the trend (since the 1980s) of portable electronic equipment to be designed ever smaller and lighter, the demand for rechargeable batteries that fit these parameters has increased dramatically too. With the introduction of primary batteries with metallic lithium as negative material, a system which was able to meet these requirements was available and much effort has been put into the development of secondary batteries that uses lithium as negative active material. However, for reasons already mentioned, practical problems (poor cycle performance and safety characteristics because of the formation of dendritic lithium during the charging process, see chapter 1.3.2.1.) with that battery system were encountered and the potential of rechargeable lithium metal batteries could not be exploited. To overcome those problems, lithium-storing materials have been studied and finally the metallic lithium anode was replaced with a carbonaceous material into which lithium ions could be inserted. This led to the first commercially available lithium-ion battery that was released in 1991 [29].

1.3.2.2.1. Electrode materials for Li-ion batteries

Various lithium insertion or intercalation materials are available for the use as electrodes in lithium ion batteries. Among the materials most suitable for the negative electrode are carbons and lithium-alloy forming metals (for example Al, Sb, Sn and Si [30]). Lithium-alloys offer a very high specific capacity that can be equivalent to or even surpass that of metallic lithium. The reason for this is that the very small lithium ions that are inserted into the metallic matrix can reach higher packing factors than in metallic lithium. The downside of this characteristic is that the lithium insertion leads to enormous structure and volume changes (up to 300 %). Thus, these highly preferable anode materials suffer from great mechanical stress, which results in a drastic decrease of cycling stability and life time of practical cells with such anodes. For this reason the next best suited materials (carbons, especially graphitic carbon) are used as anodes in commercial lithium-ion batteries. Here,

the lithium ions are inserted into specified gaps between the layers of carbon. Although they have a lower specific capacity than lithium-alloys (see Table 3), carbons suffer from almost no structure and volume changes during lithium insertion which results in a remarkable cycling stability (up to 1000 cycles) [26].

The most frequently used positive active materials for lithium-ion batteries are lithium containing transition-metal oxides. Among them, LiCoO_2 , LiNiO_2 and LiMn_2O_4 have gained the most commercial importance. The first two have a layered structure, comparable to graphite, while the third has a three dimensional spinel-type structure. Additionally, mixed layered oxides of the composition $\text{LiNi}_x\text{Co}_y\text{Mn}_z\text{O}_2$ or $\text{LiNi}_x\text{Co}_y\text{Al}_z\text{O}_2$ (“NCA”) were used for partly superior characteristics (for example higher specific capacity). These structures allow the reversible insertion and deinsertion of ions, but only to a certain degree (only half of the lithium ions per metal can be extracted unless the material suffers from irreversible structural damages). For this reason, the specific capacity of these materials is much lower compared to the anode materials (see Table 3). An advantage of these materials is that they are water and oxygen-proof and that no further lithium source has to be included during cell construction [26, 30].

Table 3 shows some values for specific capacities of electrode materials for lithium-ion batteries:

Table 3: Theoretical specific capacity of negative and positive electrode materials for lithium-ion batteries [30].

| Electrode material | Theoretical specific capacity / Ah/kg | Electrode |
|-------------------------------------|--|------------------|
| Li (primary) | 3862 | negative |
| LiC_6 (graphite) | 372 | negative |
| LiAl (alloy) | 993 | negative |
| $\text{Li}_{22}\text{Si}_5$ (alloy) | 4200 | negative |
| LiCoO_2 | 137 | positive |
| LiNiO_2 | 192 | positive |
| LiMn_2O_4 | 148 | positive |

Another aspect according to which electrode materials can be selected is their reduction potential. For a battery to have high voltage it is important that the potentials of the negative and positive electrode are as far apart as possible. Figure 6 shows the reduction potential of various electrode materials vs. Li/Li^+ . Negative active materials like LiAl or graphite have a very low potential while positive materials (LiCoO_2 , LiMn_2O_4) have a very high one. Combining one of these in a battery leads to a voltage of around 4 V in a lithium-ion battery.

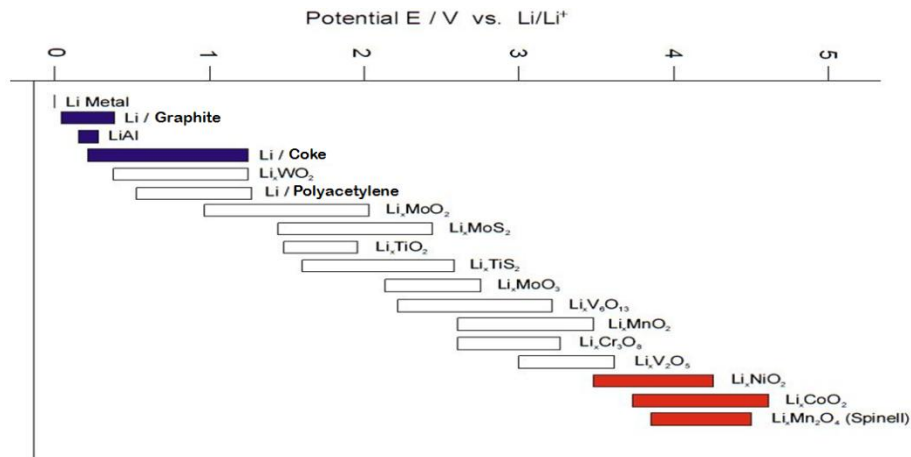


Figure 6: Reduction potential chart of electrode materials for lithium-ion batteries. The blue materials are negative electrode materials with very low potentials and the red ones are positive electrode materials with high potentials [26].

1.3.2.2.2. Lithium-ion battery schemata

In Figure 7 a schematic image of a commercial lithium-ion battery is shown. As cathode, a lithium containing transition-metal oxide is used and as anode a carbon material. The cell is constructed in the discharged state and when charged, lithium ions move from the positive electrode (cathode) through the electrolyte (a carbonate based organic liquid containing a lithium salt) to the negative electrode (anode) and the appropriate electrons move through the external circuit. During discharge, the lithium ions and electrons move into the opposite direction and energy can be obtained. This means that the electrode materials are the electrochemical active parts, not the lithium ions [25].

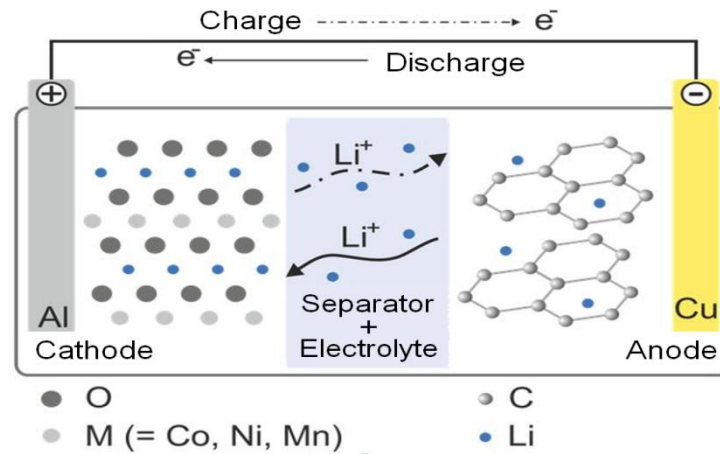
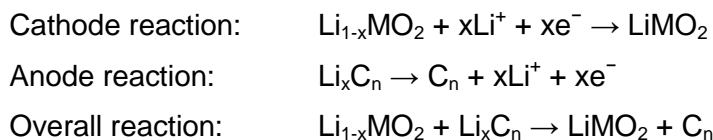


Figure 7: Schematic image of a lithium-ion battery with graphitic carbon as negative electrode and a lithium transition-metal oxide as positive electrode [31].

The cell reactions of the shown lithium-ion cell are as follows (the shown reactions occur during discharge, during charge they run in the opposite direction, M = Co, Ni, Mn):



1.3.2.2.3. Electrolyte and SEI

For commercial lithium-ion batteries, liquid electrolyte solutions based on aprotic organic solvents like propylene carbonate (PC) or ethylene carbonate (EC) are used. Those liquids have a high dielectric constant and thus favor the solubility of the lithium salt that is added for conductivity reasons. Because of the low viscosity at low temperatures of this solution, another solvent with low viscosity is added, generally dimethyl carbonate (DMC), ethylmethyl carbonate (EMC) or diethyl carbonate (DEC). This mixture takes no active part in the electrochemical reactions and can thus be applied in a very thin film or it can be immobilized inside a polymer matrix or as part of a gel [26].

The lithium salts that are used in the electrolyte solutions should have the following overall properties: good stability (chemically, electrochemically and thermally), good solubility in the used solvent, high conductivity of the solution, low molecular weight, cost and toxicity. For these reasons salts with large monovalent anions like LiClO_4 , LiPF_6 , LiAsF_6 , LiBF_4 or lithium bis(oxalate)borate are used. Neither of those salts meets all the requirements and among those mentioned above, lithium hexafluorophosphate (LiPF_6) is the one that is currently the most used because it moderately fulfills all required properties [32].

Another very important factor for lithium-ion batteries is the behavior of the interfaces between electrodes and electrolyte. As already mentioned in chapter 1.3.2.1, the solid electrolyte interphase (SEI) between electrolyte and lithium metal electrode plays a central role in the functionality of these systems. Due to the formation of the SEI out of degradation products of the electrolyte, the lithium salt and the electrode, electrolyte and anode are protected from further corrosion. The SEI is electronically non-conductive and only the small lithium-ions are able to permeate these layers.

When carbons or lithium-alloy materials are used for the anode as replacement for lithium metal, the SEI is formed not at first contact between anode and electrolyte but will be formed during the first charging of the cell. Nonetheless, the SEI is even more important for those rechargeable batteries as it has to be stable over many cycles of operation and it should only be permeable for lithium ions. On the other hand, SEI formation and similar irreversible reactions account for most of the capacity losses and self-discharge rates. This is why a lot of efforts have been made in the study of these phenomena [26].

1.3.2.2.4. Practical usage and outlook

Because of the possibility of assembling the actual electrochemical system out of the available parts (different anode and cathode materials, electrolytes and conducting salts) depending on the targeted application, lithium-ion batteries can be used for a great many applications. Lithium-ion batteries are the battery of choice for handheld electronics like mobile phones, mp3 players or camcorders to other portable devices like laptop computers, as a power source for electric vehicles and even for big stationary applications like energy storage for renewable resources,.

With the ever growing demand they are still getting cheaper and a lots of effort is made to increase the specific energy and overall performance through the introduction of new materials for almost every part of the battery. Especially lithium-alloy materials have been researched increasingly during the last few years, e.g. silicon for the use as negative electrode because of its unbeatable specific capacity

2. Experimental

2.1. Long term cycling experiments in pouch cells

2.1.1. Cathode preparation for pouch cells

A slurry of lithium cobalt nickel aluminium oxide (NCA) “dry-blend” (88 wt.% $\text{LiNi}_{0.85}\text{Co}_{0.10}\text{Al}_{0.05}\text{O}_2$ active material; 3 wt.% Kynar 2801 and 3 wt.% Kynar 761 binder; 3 wt.% carbon black and 3 wt.% KS6 graphite as conductive agents) and *N*-methyl-2-pyrrolidone (NMP, Sigma Aldrich, anhydrous 99.5 %) 7:3 (m/m) was prepared and stirred for 24 h. Aluminium foil (8 cm width, 20 μm thickness) was etched in KOH (60 °C, 35 wt.%) for 20 s, rinsed with distilled water, dried and used as substrate for the slurry in a blade coating process (550 μm thickness, Erichson COATMASTER 510). The cathode film was dried for 24 h at 60 °C and compressed with a calender (from 320-340 μm to 270-290 μm). 5 x 50 mm single electrode stripes with the NCA on the top 5 x 5 mm area were cut out and stored for further use (see Figure 8).

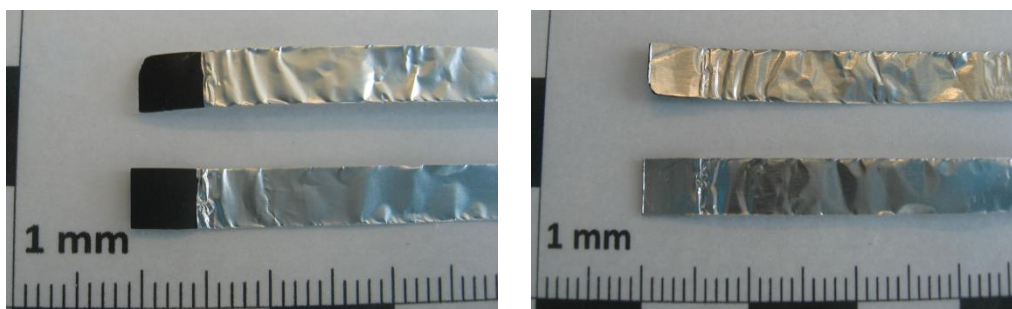


Figure 8: Images of the cathodes: Single Al stripes with the NCA active material on the top 5 x 5 mm area. Left: Front. Right: Back.

2.1.2. Anode preparation for pouch cells

Single crystal, micro-structured (50 x 50 x 50 μm cubic structure) silicon anodes (4 x 4 mm, 200 μm thick) with boron doping, TiW interlayer and copper backside, subsequently referred as LIBC 13, were obtained from Infineon Technologies Austria (IFX). A copper strip, acting as a current collector (1 x 50 mm, 60 μm thickness), was glued on the cleaned backside with conductive varnish (50 wt.% dendritic copper 3 μm particle size, 43 wt.% NMP, 7 wt.% PVdF binder) and left to dry for 24 h at 60 °C. To permanently connect the current collector and the electrode, the backside was copper-plated using an acidic copper sulfate bath (302 g/l $\text{CuSO}_4 \cdot 5 \text{H}_2\text{O}$, Sigma Aldrich, ~99 %;

0.025 g/l thiourea, Riedel-de Haën, puriss.; 30 g/l sulfuric acid, Roth, $\geq 95\%$ p.a.) as an electrolyte and a pure copper plate as an anode ($J = 0,1 \text{ mA/mm}^2$, $t = 30 \text{ min}$, resulting layer thickness 50-60 μm) while the front side was protected with Parafilm. The combined electrode/current collector was washed with warm water (60 °C), dried and stored. Figure 9 shows the electrodes before and after copper plating. Figure 10 shows the copper plating equipment.

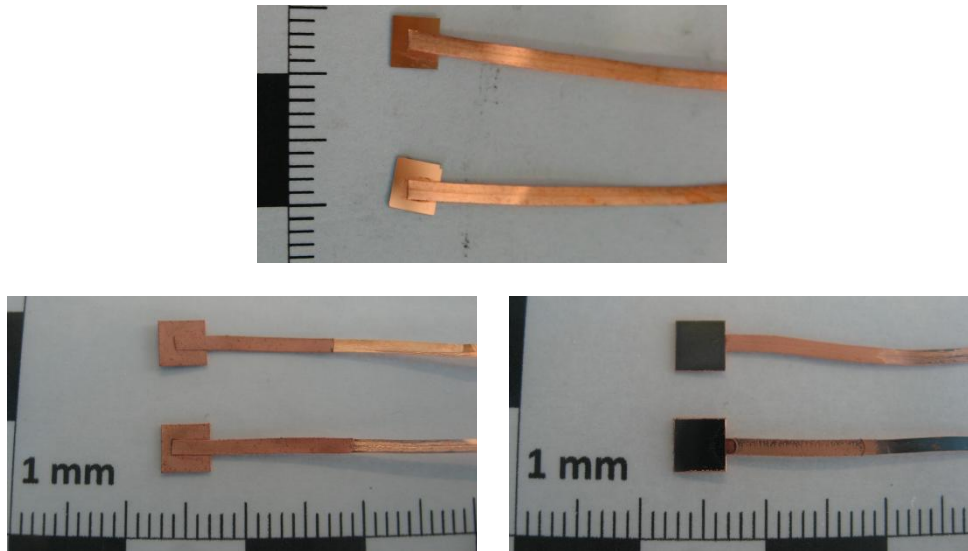


Figure 9: Images of the anodes: LIBC 13 active material first glued and then copper plated onto a Cu strip. Upper image: Back of the anodes after gluing. Lower left image: Back of the anode after copper plating. Lower right image: Front of the anode after copper plating.

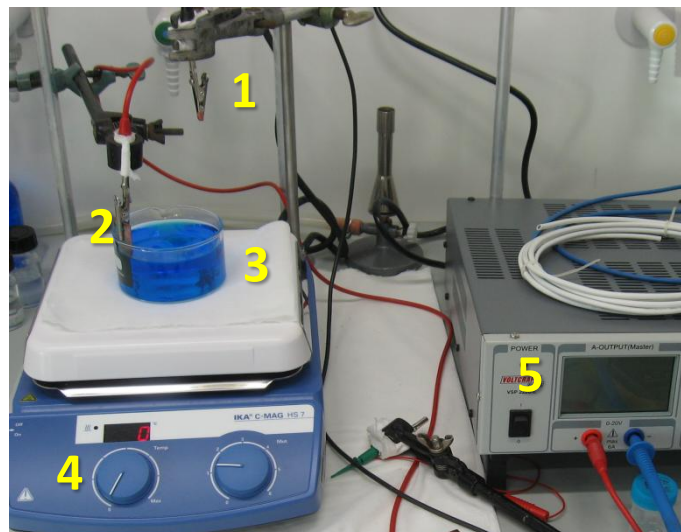


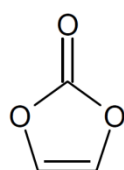
Figure 10: Image of the copper plating equipment. 1: Crocodile clip holding the electrode to be plated, cathode of the process. 2: Copper plate functioning as anode. 3: Acidic copper sulfate bath. 4: Magnetic stirrer. 5: Power supply.

2.1.3. Electrolyte preparation

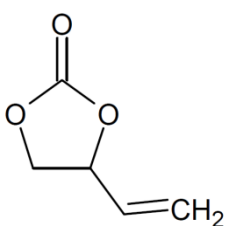
Electrolyte solutions with four different additives, vinylene carbonate (Figure 11(1), VC, Sigma Aldrich, freshly distilled); vinylethylene carbonate (Figure 11(2), VEC, Sigma Aldrich, 99 %); 4-fluorophenyl isocyanate (Figure 11(3), 4-FP, Sigma Aldrich, 99 %) and 2,3,4-trifluorophenyl isocyanate (Figure 11(4), Tri-FP, Sigma Aldrich, 97 %) in three different concentrations respectively (0.5, 1.0 and 2.0 wt.%) and a solution without additives (standard) were prepared under an argon atmosphere according to Table 4. The main components of all solutions were ethylmethyl carbonate (EMC, Merck, 99 %) and ethylene carbonate (EC, Sigma Aldrich, 99 % anhydrous) with 1 M lithium hexafluorophosphate (LiPF₆, Stella) as conductive salt. All electrolyte solutions were stored under an argon atmosphere in polypropylene bottles prior cleaned with isopropyl alcohol.

Table 4: Amount of liquids used for electrolyte solutions.

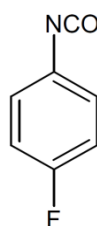
| Electrolyte solution | Ethylmethyl carbonate / g | Ethylene carbonate / g | Additive / g |
|----------------------|------------------------------|---------------------------|-----------------|
| No additive | 3.500 | 1.500 | - |
| 0,5 wt.% additive | 3.500 | 1.475 | 0.025 |
| 1,0 wt.% additive | 3.500 | 1.450 | 0.050 |
| 2,0 wt.% additive | 3.500 | 1.400 | 0.100 |



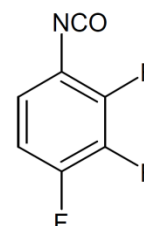
(1) Vinylene carbonate



(2) Vinylethylene carbonate



(3) 4-Fluorophenyl isocyanate



(4) 2,3,4-Trifluorophenyl isocyanate

Figure 11: Structures of used additives: From left to right: (1) Vinylene carbonate. (2) Vinylethylene carbonate. (3) 4-Fluorophenyl isocyanate. (4) 2,3,4-Trifluorophenyl isocyanate.

2.1.4. Assembling of the pouch cells

Pieces of pouch foil (5 x 3 cm, SHOWA DENKO 7 layers) were cut out and cleaned with acetone. The cathode (NCA) was fixed in the middle of the pouch foil with acrylic tape. The Si-anodes (LIBC 13) were dipped in a 1 % HF-solution (prepared from a 40 % HF-solution, Fisher Chemicals) for 30 s, thoroughly washed with water and dried. They were then placed to overlay the cathode, with a separator (two layers, 12 mm in diameter, Freudenberg 2190) in between and were secured (see Figure 12, left image).

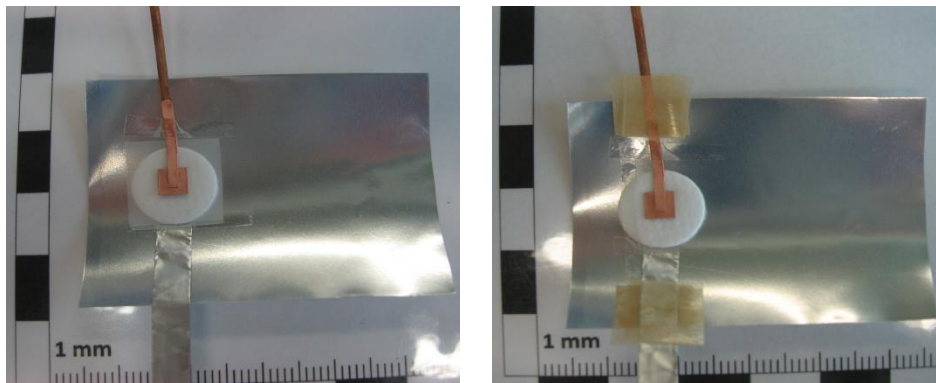


Figure 12: Images of pouch cell assembling. Left: LIBC 13 anode on top of separator and NCA cathode, with the Cu and Al current collector strips sticking out. Right: Sealing tape is put over and under the current collector strips.

A second pouch foil was placed over the first and they were welded together with welding tongs (AUDION ELEKTRO Super Poly TPS-2) on three sides (see Figure 13). To ensure airtight sealing, sealing tape (DNP Ppa-F100) was put around the copper and aluminium current collectors prior to welding (Figure 12, right image).

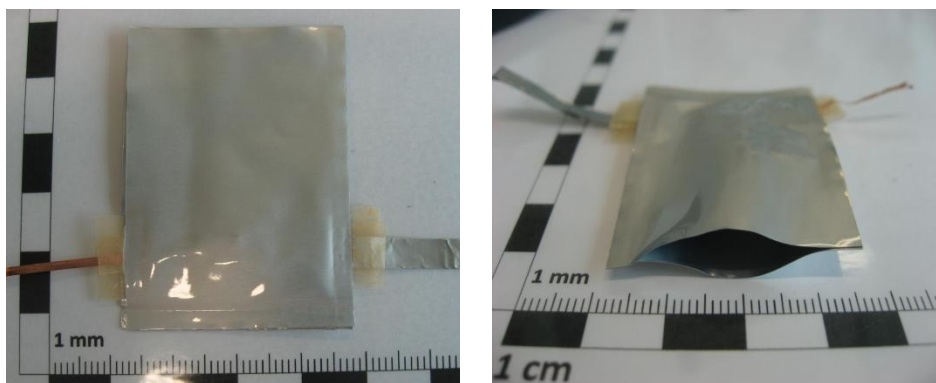


Figure 13: Images of pouch cell assembling. Left: Pouch cell after sealing on three sides, bottom, left and right. Right: Opening of the unsealed side of the pouch cell, where the electrolyte will be filled in.

The unfinished pouch cells were dried under vacuum (60 °C, BÜCHI Glass Oven B-585) for at least 24 hours and transferred into an argon filled glovebox ($H_2O < 1$ ppm, $O_2 < 1$ ppm) where they were filled with 45 μ l of electrolyte and finally closed completely using a welding technique under reduced pressure. Two cells were built according to this procedure for each different electrolyte solution (three for the standard electrolyte). Figure 14 shows the final pouch cell.

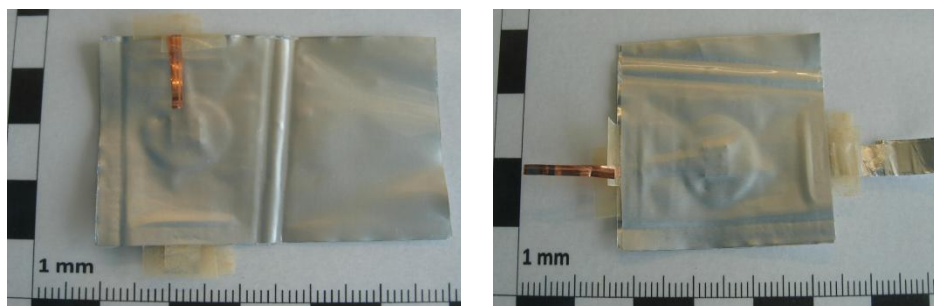


Figure 14: Images of the finished pouch cell. Left: Cell after welding under reduced pressure with clearly visible weldseam on the right side. Right: Finished pouch cell, with projecting pouch foil cut away.

2.1.5. Long term electrochemical testing

All tests were carried out on a Maccor 40 battery & cell testing machine. The cells were cycled according to the following technique (see Table 5).

Table 5: Cycling program for the long term cycling experiments: 100 cycles with 0.5 mAh capacity limitation and a formation step. Table continues on next page.

| Step | Type | Mode | Value | Cut off criterion |
|------|-----------|------------------|-------------|---------------------------------|
| 1 | Rest/OCV | - | - | $t = 12$ h |
| 2 | Charge | Constant current | 45 μ A | $t = 1$ h |
| 3 | Rest/OCV | - | - | $t = 8$ h |
| 4 | Charge | Constant current | 45 μ A | $Q = 0.5$ mAh $E \geq 4.2$ V |
| 5 | Discharge | Constant current | 45 μ A | $E \leq 2.5$ V |
| 6 | Discharge | Constant voltage | 2.5 V | $t = 6$ h |
| 7 | Charge | Constant current | 112 μ A | $Q = 0.5$ mAh $E \geq 4.2$ V |
| 8 | Discharge | Constant current | 112 μ A | $E \leq 2.5$ V |
| 9 | Discharge | Constant voltage | 2.5 V | $t = 6$ h |

| Step | Type | Mode | Value | Cut off criterion |
|------|--------------------------------|------------------|-------------|---|
| 10 | Charge | Constant current | 225 μ A | $Q = 0.5 \text{ mAh}$ $E \geq 4.2 \text{ V}$ |
| 11 | Discharge | Constant current | 225 μ A | $E \leq 2.5 \text{ V}$ |
| 12 | Discharge | Constant voltage | 2.5 V | $t = 6 \text{ h}$ |
| 13 | Repeat steps 10 to 12 97 times | | | |
| 14 | Rest/OCV | - | - | $t = 12 \text{ h}$ |

2.1.6. Post mortem investigation of pouch cells

After electrochemical testing, all cells were cut open and disassembled with great care under argon atmosphere (see Figure 15). Cathodes and separator were discarded after brief examination, while the anodes were deposited in diethyl carbonate (DEC, Sigma Aldrich, 99 %) for 24 h, dried afterwards and stored in argon filled tubes for further investigation.

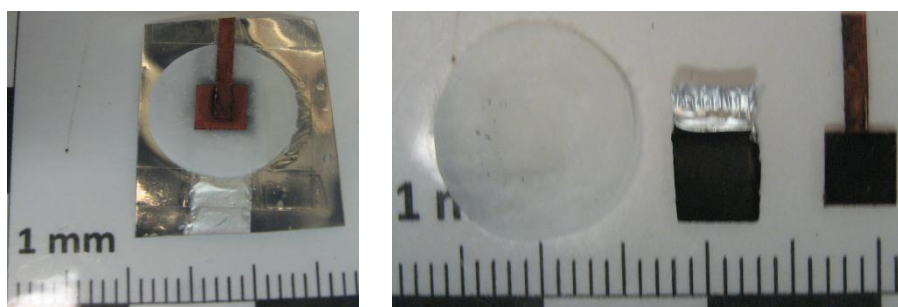


Figure 15: Images of post mortem investigation. Left: Removal of pouch foil to access the electrode stack. Right: Electrode stack disassembled into separator, NCA cathode and LIBC 13 anode.

2.2. Short term cycling experiments in Swagelok cells

2.2.1. Cathode preparation for Swagelok cells

All preparatory steps (with the following exceptions) were carried out as described in chapter 2.1.1. The thickness for the blade coating process was 150 μ m and after drying and calendaring the cathode film was 70-80 μ m thick. The cathodes that were cut out, using a round hollow punch 12 mm in diameter, are shown in Figure 16.

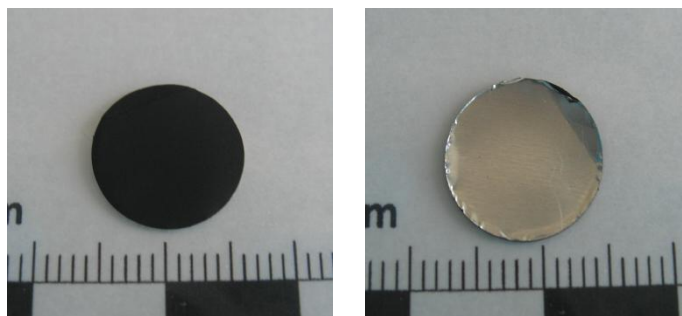


Figure 16: Images of the cathodes for the Swagelok cells. Left: Front. Right: Back.

2.2.2. Anode preparation for Swagelok cells

Silicon anodes, similar to LIBC 13 in structure and composition (see chapter 2.1.2), but with phosphor doping instead of boron doping, subsequently referred to as LIBC 23, were also obtained from IFX (see Figure 17). They were dipped in a 1 % HF-solution for 30 s, washed with water, dried under vacuum for 24 h (60 °C, BÜCHI Glass Oven B-585) and stored under argon atmosphere.

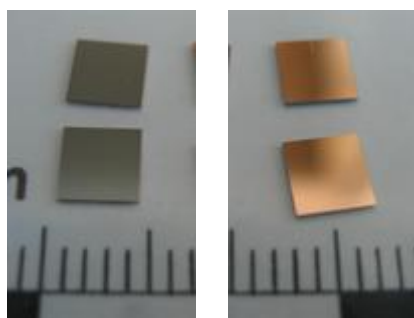


Figure 17: Image of the anodes for the Swagelok cells. Left: Front. Right: Back.

2.2.3. Electrolyte preparation

For this experiment, the same electrolyte solutions were used as for the long term cycling experiments. For a detailed description of their preparation see chapter 2.1.3.

2.2.4. Assembling the Swagelok cells

T-shaped Swagelok cells (see Figure 18) were assembled in an argon filled glovebox ($\text{H}_2\text{O} < 1 \text{ ppm}$, $\text{O}_2 < 1 \text{ ppm}$) using a three electrode setup. LIBC 23 anodes were used as working electrodes (WE), NCA cathodes as counter electrodes (CE) and pure lithium as a reference electrode (RE). To ensure optimal contact between anode and current collector, electrochemically treated copper foil (diameter 12 mm, thickness $20 \mu\text{m}$) was put in between. Two separators were used, one for the RE (Freudenberg 2190, two layers, 5 mm diameter) and one for the other electrodes (Freudenberg 2190, six layers, 12 mm diameter). Mylar foil (BoPET, Typo, $70 \mu\text{m}$ thickness) was used on the inside of the tube to ensure electrical insulation. Each cell was filled with $110 \mu\text{l}$ of electrolyte and closed airtight. Two cells were assembled for each different electrolyte solution.

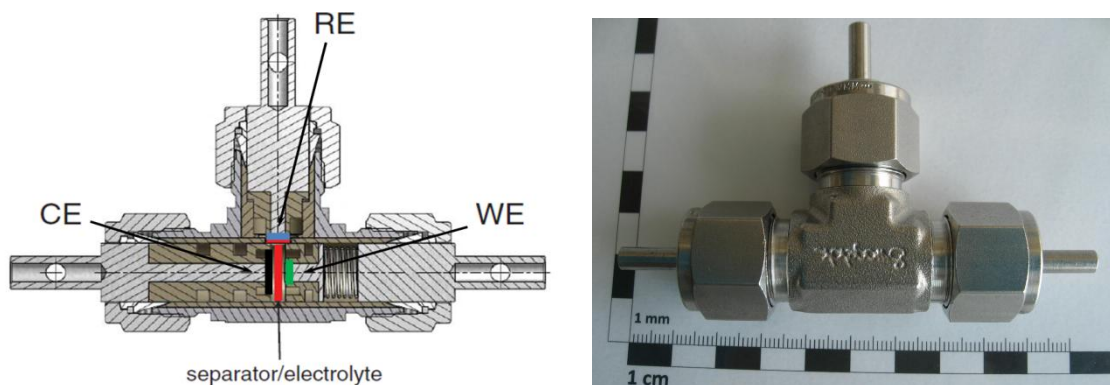


Figure 18: Three electrode setup of a T-shaped Swagelok cell. Left: Schematic view inside a cell, with highlighted NCA cathode as CE (black), Si anode as WE (green), metallic lithium as RE (blue) and separator wetted with electrolyte (red) [33]. Right: Image of complete assembled Swagelok cell.

2.2.5. Short term electrochemical testing

All tests were carried out on a Maccor 40 battery & cell testing machine. The cells were cycled according to the technique listed in Table 6. Potential was controlled through the lithium reference electrode, therefore the NCA electrode was considered as being a lithium anode, while the LIBC 23 electrode was essentially a cathode.

Table 6: Cycling program for the short term cycling experiments: 100 cycles with 0.5 mAh capacity limitation, a formation step and potential limitation for the discharge and current limitation for the charge steps.

| Step | Type | Mode | Value | Limit | Cut off criterion |
|------|-------------------------|------------------|-------------|-------------------|-------------------|
| 1 | Rest/OCV | - | - | - | $t = 12$ h |
| 2 | Discharge | Constant current | 45 μ A | $E = 0.02$ V | $Q = 0.045$ mAh |
| 3 | Rest/OCV | - | - | - | $t = 8$ h |
| 4 | Discharge | Constant current | 45 μ A | $E = 0.02$ V | $Q = 0.955$ mAh |
| 5 | Charge | Constant current | 45 μ A | - | $E \geq 1.0$ V |
| 6 | Charge | Constant voltage | 1.0 V | $I = 45$ μ A | $t = 6$ h |
| 7 | Discharge | Constant current | 225 μ A | $E = 0.02$ V | $Q = 1.0$ mAh |
| 8 | Charge | Constant current | 225 μ A | - | $E \geq 1.0$ V |
| 9 | Charge | Constant voltage | 1.0 V | $I = 225$ μ A | $t = 6$ h |
| 10 | Repeat step 7 to 9 once | | | | |
| 11 | Rest/OCV | - | - | - | $t = 12$ h |

2.2.6. Post mortem investigation of Swagelok cells

After cycling, the Swagelok cells were opened and disassembled under an argon atmosphere with great care. While NCA electrodes and separator were discarded after a brief examination, LIBC 23 electrodes were deposited in DEC for 24 h, dried and stored in argon filled tubes for further investigations. Figure 19 shows the active parts of the Swagelok cell during post mortem investigation.

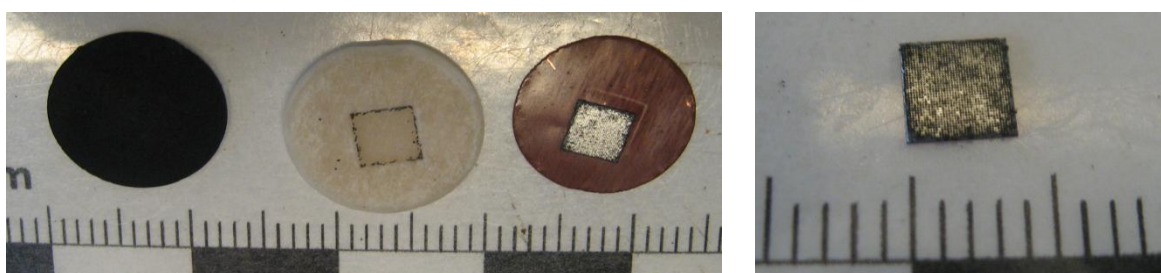


Figure 19: Images of active parts of the Swagelok cell during post mortem investigation. Left: Round NCA cathode, separator and a 4 x 4 LIBC 23 anode on a round copper foil. Right: Close up image of the Si anode.

2.3. SEM investigations

Selected electrodes from long term and short term cycling experiments for each additive were investigated using scanning electron microscopy (SEM). This work was done at the Institute for Electron Microscopy and Nanoanalysis (FELMI) of Graz University of Technology (TU Graz).

2.4. Peel test of pouch foil|sealing tape welded on different surfaces

2.4.1. Sample preparation

Seven wafers (20.34 cm in diameter) with different surface modifications were obtained from IFX. Those different modifications are listed in Table 7.

Table 7: Overview of the wafers with different surface modifications and compositions.

| No. | Substrate | Surface description |
|-----|-----------|---|
| 1 | Silicon | Bare silicon with no modification = reference |
| 2 | Glass | Mechanically thinned silicon |
| 3 | Glass | Etched silicon |
| 4 | Silicon | ECD-Cu |
| 5 | - | RU302507V01 (5) |
| 6 | Silicon | TiW/AlCu |
| 7 | Silicon | 1300 nm TEOS |

Each of those wafers were cut or broken into 3.5 x 1.5 cm pieces and the same pouch foil as used in chapter 2.1.4. was cut into slices of similar size. Everything was cleaned with acetone, dried under compressed air and stacked together, with the pouch foil on top and sealing tape (9.5 mm width, same as used in chapter 2.1.4.) as interlayer (see Figure 20).

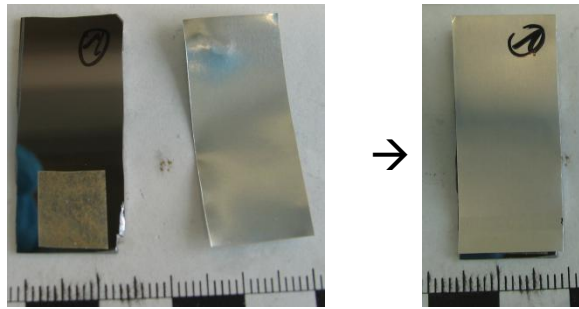


Figure 20: Images of substrate preparation for welding. Left: Substrate (with a number on it), a piece of sealing tape on the substrate and pouch foil lying on its front. Right: Pouch foil flipped over onto the sealing tape and substrate.

Using the welding tongs already used in chapter 2.1.4., wafer and pouch foil were then welded together with the highest setting and three pulse activations. For each different substrate, three to four samples were prepared in this way to look like the ones in Figure 21.

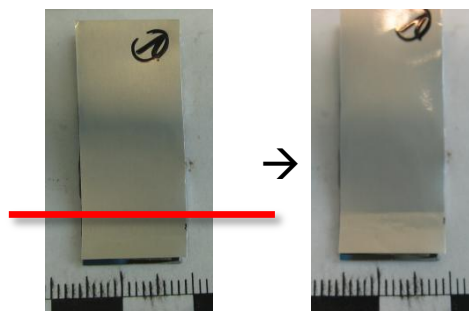


Figure 21: Welding the pouch foil onto the substrate. Left: Test sample prior to welding. The red line indicates the area of the welding. Right: Sample after welding with visible weld seam in the same area.

2.4.2. Peel test

Peel tests were carried out for each sample on a tensile testing machine (SHIMADZU AGS-X 5 kN). First, the loose end of the pouch foil was bent back at 180° (Figure 22, upper images) and the substrate and pouch foil were then fixed in the two jaws of the testing machine (distance 20 mm) and pulled apart with a constant velocity ($v = 5 \text{ mm/min}$) (Figure 23). This resulted in the pouch foil being peeled from the substrate in a 180° angle (Figure 22, lower image).

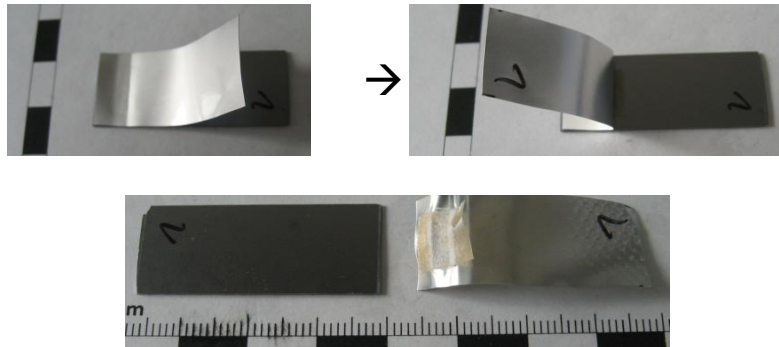


Figure 22: Images of samples. Upper images: Preparation of the samples for the peel test. The loose end of the pouch foil is bent back at 180°. Lower image: Sample after the peel test. Substrate and pouch foil are clearly separated. The sealing tape is fused with the pouch foil.

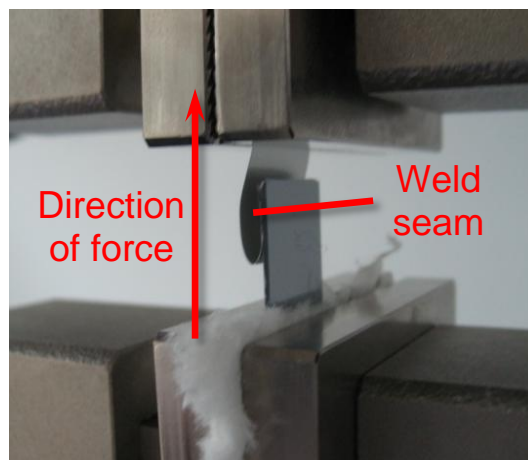


Figure 23: Image of the peel test set up. The lower jaw was fixed and the upper one was being pulled upwards with a constant velocity. The weld seam is on the averted side of the sample.

2.4.3. Analysis of the peel test

Graphical analysis was done with TRAPEZIUM LITE X software. The force was plotted against the stroke and the mean force for each graph, starting from first peak until break, was calculated. Using Microsoft Excel, average force values and standard deviation were calculated out of those mean force values. Additionally the broken residues of the samples were examined.

3. Results and discussion

3.1. Impact of electrolyte additives: Long term cycling experiments

As mentioned before, the influence of the additive on the cycle stability and irreversible capacity were measured and compared to the results from cells without additive. Furthermore, SEM images were made from the anodes after the cycling experiments. All these results are presented in the following chapters.

3.1.1. Cycling behavior

To gain a first impression of the cycling behavior and performance, discharge capacity (lower graphs, Figure 24) and coulometric efficiency (upper graphs, Figure 24, calculated from charge capacity 0.5 mAh) were combined in a single chart (Figure 24). This overview shows two cells per additive per concentration and three cells for the standard. As it can be seen, after 100 cycles there is almost no visible difference between any of the graphs, neither for discharge capacity nor for efficiency. The seemingly great deviations seen in the efficiency graphs are only ranging between 98 and 102 % at maximum and thus are more likely a result of temperature fluctuations than of electrochemical processes. A strong capacity fading is not occurring until the 100th cycle and possibly after.

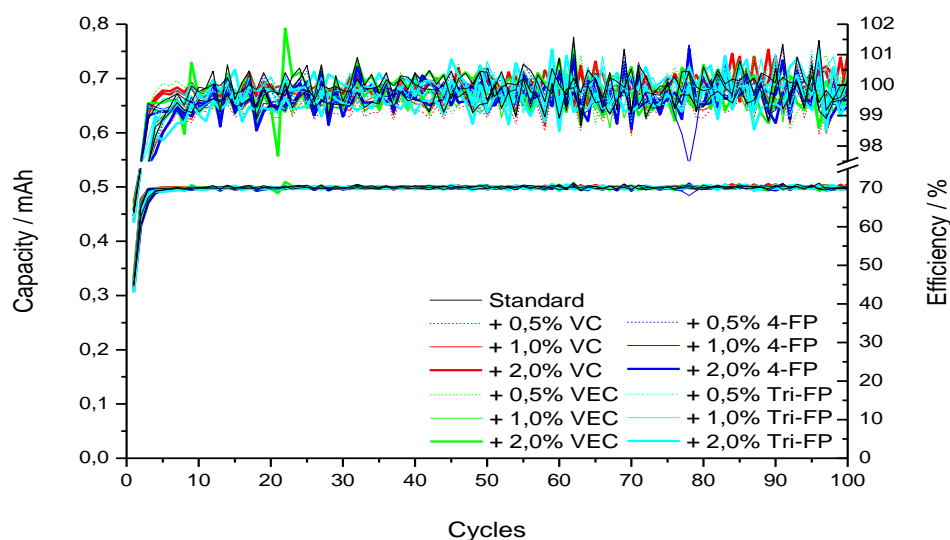


Figure 24: Overview: Capacity and efficiency vs. cycles of all cells: LIBC 13 50 μm cubic structures vs. NCA, 100 cycles, 0.5 mAh capacity limitation, EC:EMC 3:7 (w/w), 1 M LiPF_6 + different additives.

The lower efficiency and discharge capacity during the first five cycles seen in the chart are credited to the formation of the SEI, which is characteristic for lithium ion batteries. At a closer look, however, some minor differences can be noticed in the different efficiency graphs during the SEI forming phase.

For better visibility, the overview (Figure 24) was split into separate charts for each additive. Figure 25 shows the standard cells, without additives. The charts for vinylene carbonate (VC, Figure 26), vinylethylene carbonate (VEC, Figure 27), 4-fluorophenyl isocyanate (4-FP, Figure 28) and 2,3,4-trifluorophenyl isocyanate (Tri-FP, Figure 29) additives are shown in this order on the following pages. Each of these charts consists of graphs for three different additive concentrations as well as the standard cells graphs for better comparison.

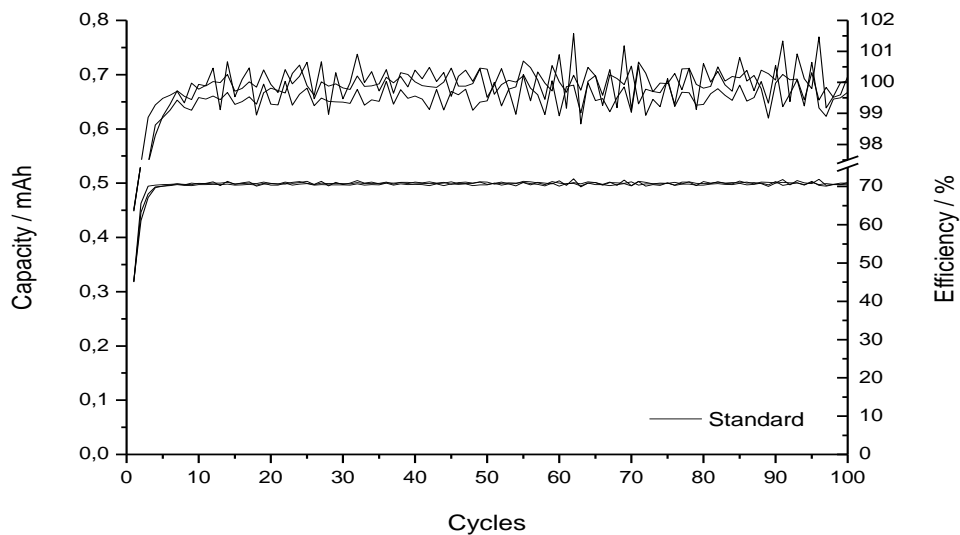


Figure 25: Cycle chart of LIBC 13 50 μm cubic structures vs. NCA, 100 cycles, 0.5 mAh capacity limitation, Standard electrolyte.

In Figure 25, the efficiency of two out of three cells is similar for the first five cycles, while the third cell shows a slightly higher efficiency (visible through the steeper gradient). After that there is no difference identifiable anymore as all data prints scatter around.

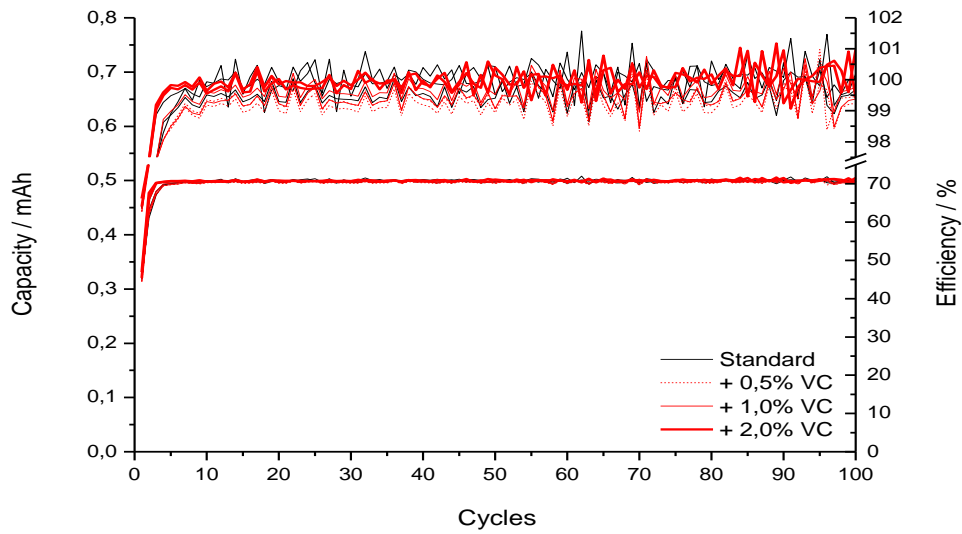


Figure 26: Cycle chart of LIBC 13 50 μm cubic structures vs. NCA, 100 cycles, 0.5 mAh capacity limitation, Standard electrolyte + VC.

In Figure 26, during the first cycles, the efficiency of the cells with the highest additive concentration (2.0 % VC, thick lines) is slightly higher than the efficiency of the “best” standard cell and higher than the efficiencies of the other cells with a lower additive concentration (1.0 % VC, thin lines and 0.5 % VC, dotted lines), which are in the range of the other standard cells. For the rest of the 100 cycles, the efficiency of the cells with 2.0 % VC additive tends to be higher than the other cell as well and the efficiency of the cells with a concentration of 0.5 % VC additive seems to be lower.

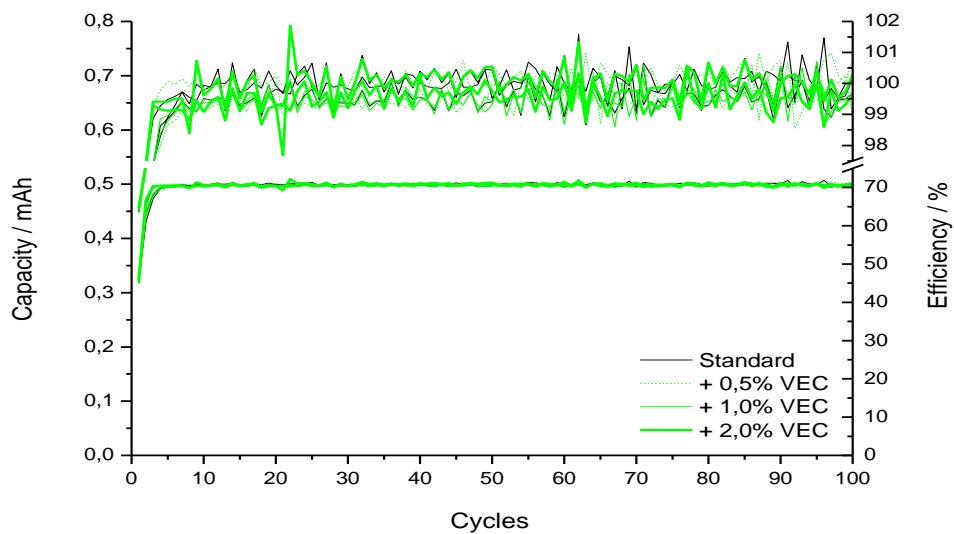


Figure 27: Cycle chart of LIBC 13 50 μm cubic structures vs. NCA, 100 cycles, 0.5 mAh capacity limitation, Standard electrolyte + VEC.

In Figure 27, it can be seen that the cells with high additive concentrations (2.0 % VEC, thick lines) and low additive concentrations (0.5 % VEC, dotted lines) have a higher efficiency at the beginning (first cycles). The cells with 1.0 % VEC (thin lines) are ranging somewhere between the efficiency of the standard cells. In the subsequent cycles, there are no clear differences between the different efficiencies. There is one strong deviation from cycle 20, although with no further impact.

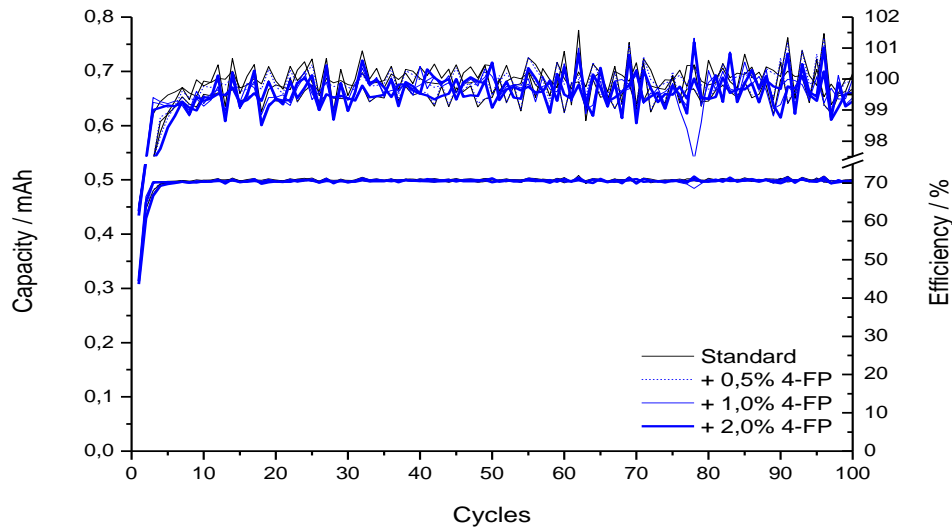


Figure 28: Cycle chart of LIBC 13 50 μm cubic structures vs. NCA, 100 cycles, 0.5 mAh capacity limitation, Standard electrolyte + 4-FP.

In Figure 28, there are no real trends identifiable. The efficiency of the cells with a higher concentration (1.0 % and 2.0 % 4-FP, thick and thin lines) starts with higher values, but drops below that of the standard cells after five cycles. Thereafter, the efficiencies of all cells are in the range of that of the standard cells.

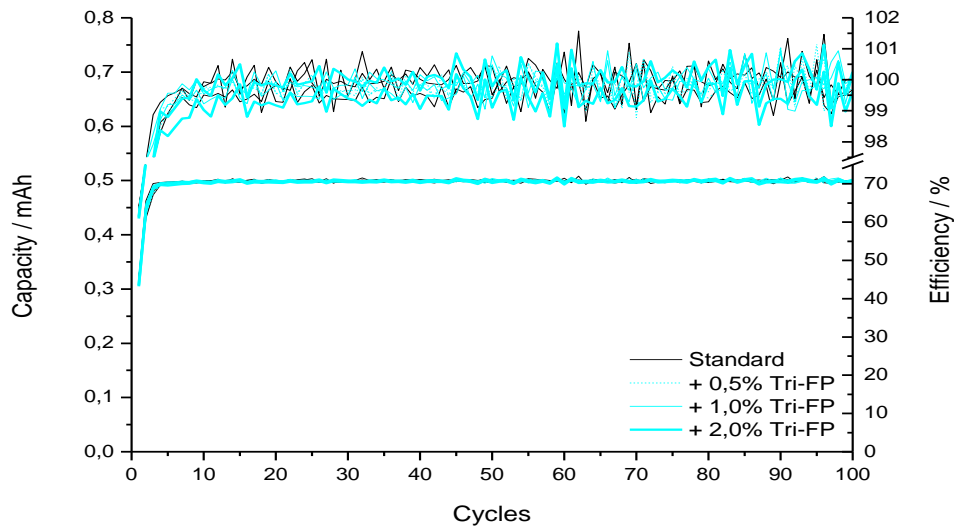


Figure 29: Cycle chart of LIBC 13 50 μm cubic structures vs. NCA, 100 cycles, 0.5 mAh capacity limitation, Standard electrolyte + Tri-FP.

The efficiencies of the additive cells in Figure 29 are not really distinguishable from one another. The efficiency of the cells of the three additive concentrations varies but mostly it is slightly below the efficiency of the standard cells (although only clearly visible for the first five cycles).

As mentioned before, under closer investigation, there are some tendencies identifiable in the efficiency and capacity charts of all the cells. An increase in cycle stability and a reduction of irreversible capacity have their origin during the most important phase of a lithium-ion battery's life, the first cycles in which SEI formation takes place. That is where the used additives should do their work. So, if each additive cell is compared to the standard cells without additives, improvements are likely in some cases (2.0 % VC, 0.5 % VEC and 2.0 % VEC). In other cases, improvement is unlikely (1.0 % VC, 1.0 % VEC, all 4-FP and all Tri-FP) or there might even be a decrease in cell performance (0.5 % VC). However, it is not possible to compare the different concentrations of one additive with each other in a significant way with the information obtained so far.

To confirm the above hypotheses, further information can be gained through the investigation of the irreversible capacity, which can be calculated from the already available capacity plots of the cells.

3.1.2. Cumulative irreversible capacity

To calculate the irreversible capacity, the discharge capacity of all cells was subtracted from the charge capacity (always 0.5 mAh) for each cycle. In this way, all the capacity “lost”, for example through SEI formation or through damage in the microstructure of the electrodes during the cycling, was obtained. Using OriginPro 8.1, these plots were then integrated to determine the cumulative irreversible capacity, which is the sum of the irreversible capacities of each cycle. To reduce the amount of data and enhance their significance for a better comparison of the results, mean values were calculated for each additive and each concentration (two cells each) as well as for the standard (three cells) and were plotted versus the cycle number in Figure 30.

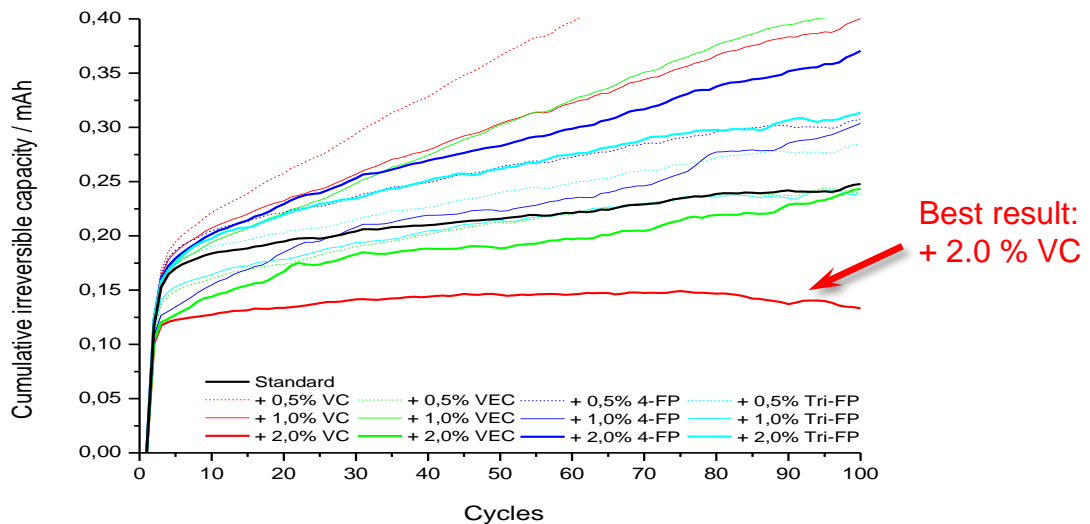


Figure 30: Cumulative irreversible capacity vs. cycles of the long term experiment. For a better overview, mean values for all samples were calculated out of the single results.

In contrast to the cycle charts (chapter 3.1.1.), there are clear differences and tendencies identifiable in Figure 30. First of all, the graphs can be divided into two different sections. The first section, up to cycle three, in which the irreversible capacity rises fast, is indicated through a very steep slope and a second section, identifiable after cycle three until the end, where the irreversible capacity rises more slowly, but still linear. In fact the graphs can almost be viewed as two linear functions with different slopes.

The fast rising of the irreversible capacity in the first section is a result of the capacity or charge lost during the first formation of the SEI or other interphases, while the second section with a lower but steady increase in irreversible capacity can be credited to the loss of active material through the damaging of the microstructure or, more likely, to the renewed formation of the SEI on freshly exposed active material because of the same damaging effects.

3.1.3. Post mortem images

To find the most representative anode for each cell system for further SEM analysis and to visually control the cells physical functionality, high resolution pictures of the silicon anodes after post mortem procedure were analyzed.

3.1.3.1. Standard electrolyte (EC:EMC 3:7 w/w, 1 M LiPF₆)

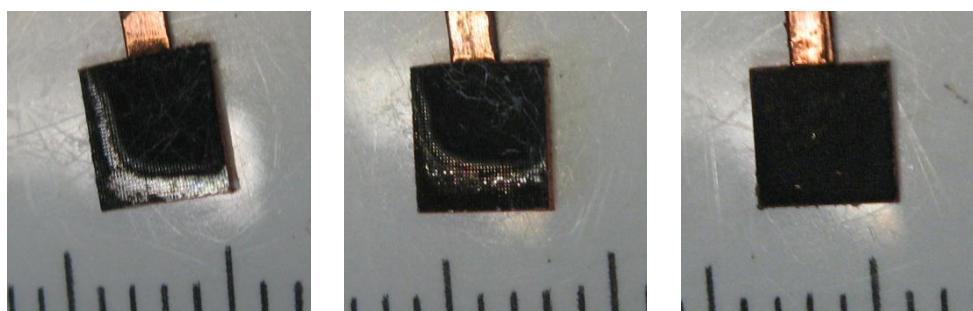


Figure 31: Standard electrolyte: Images of anodes after 100 cycles. The cells were disassembled in an argon atmosphere and the electrodes rinsed with DEC and then the pictures were taken.

Figure 31 shows the anodes of the cells with standard electrolyte after cycling and post mortem procedure. As it can be seen, almost the whole area of the electrodes was very active during the electrochemical cycling. This is noticeable through the blackened and somehow bloated material and its microstructure, which is still intact. However, on the left and middle electrode there is a small L-shaped area where the material was less active (middle electrode) or not active at all (shiny area, left electrode). There are also some separator residues visible sticking to the surface. On the right electrode, the whole material was equally active and no separator residues are visible. The anodes in the middle and on the right were selected for SEM analysis.

3.1.3.2. Standard electrolyte + 0.5 % VC

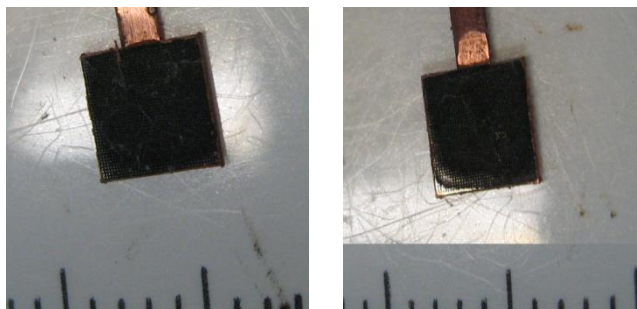


Figure 32: Standard electrolyte + 0.5 % VC: Images of anodes after 100 cycles. The cells were disassembled in an argon atmosphere and the electrodes rinsed with DEC.

Figure 32 shows the anodes of the 0.5 % VC cells. There is only a small non-active area visible on the lower left corner of the right anode. Some separator residues are visible on both. The left anode was selected for SEM analysis.

3.1.3.3. Standard electrolyte + 1.0 % VC

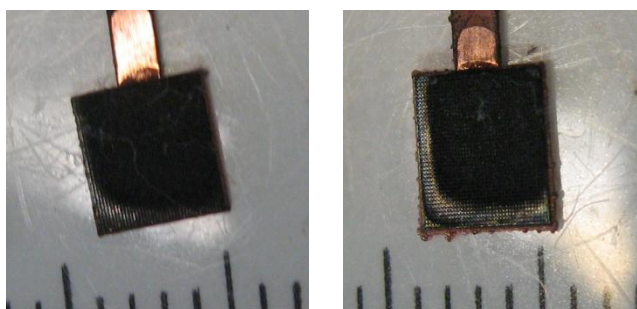


Figure 33: Standard electrolyte + 1.0 % VC: Images of anodes after 100 cycles. The cells were disassembled in an argon atmosphere and the electrodes rinsed with DEC.

In Figure 33 anodes of the 1.0 % VC cells are shown. There are some less active areas on both as well as some separator residues. The left anode was selected for SEM analysis.

3.1.3.4. Standard electrolyte + 2.0 % VC

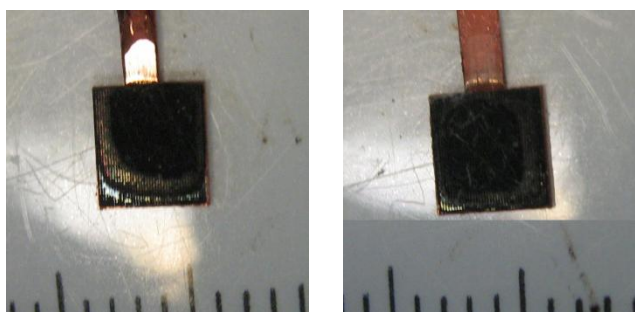


Figure 34: Standard electrolyte + 2.0 % VC: Images of anodes after 100 cycles. The cells were disassembled in an argon atmosphere and the electrodes rinsed with DEC.

Figure 34 shows the 2.0 % VC cells anodes. Although, there are some separator residues on the right electrode, it was selected for SEM analysis, because the less active areas are more homogeneous than the non-active areas on the left anode.

3.1.3.5. Standard electrolyte + 0.5 % VEC

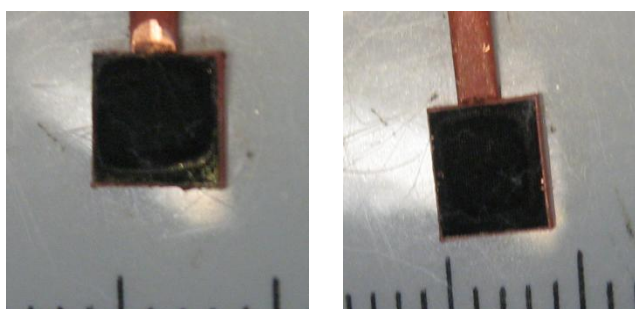


Figure 35: Standard electrolyte + 0.5 % VEC: Images of anodes after 100 cycles. The cells were disassembled in an argon atmosphere and the electrodes rinsed with DEC.

In Figure 35, anodes of the 0.5 % VEC cells are shown. There are separator residues sticking to both electrodes, but only on the left there is a small less active area visible, which is why the right one was selected for SEM analysis.

3.1.3.6. Standard electrolyte + 1.0 % VEC

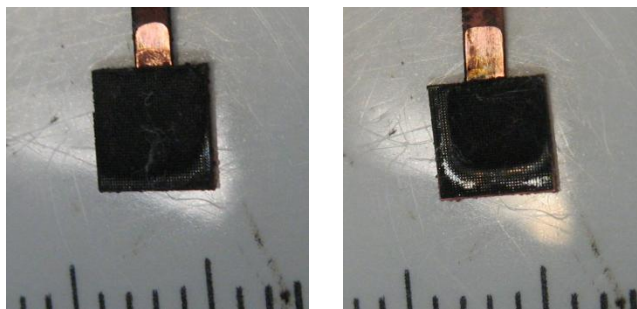


Figure 36: Standard electrolyte + 1.0 % VEC: Images of anodes after 100 cycles. The cells were disassembled in an argon atmosphere and the electrodes rinsed with DEC.

Figure 36 shows the anodes of the 1.0 % VEC cells. On the left electrode there is a small less active area, while the less and non-active areas on the right one are relatively large. On both electrodes, there are some separator residues sticking to the surface. The left anode was selected for SEM analysis.

3.1.3.7. Standard electrolyte + 2.0 % VEC

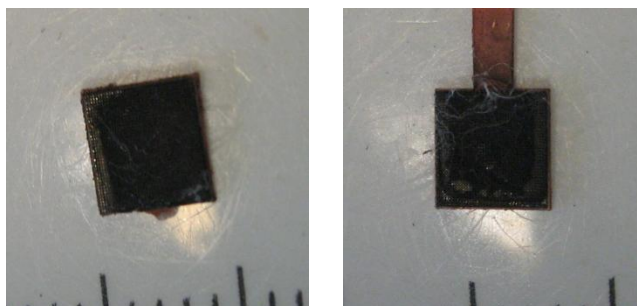


Figure 37: Standard electrolyte + 2.0 % VEC: Images of anodes after 100 cycles. The cells were disassembled in an argon atmosphere and the electrodes rinsed with DEC.

Figure 37 shows the anodes of the cells with 2.0 % VEC. There are separator residues and less active areas on both electrodes. The anode on the left was selected for SEM.

3.1.3.8. Standard electrolyte + 0.5 % 4-FP

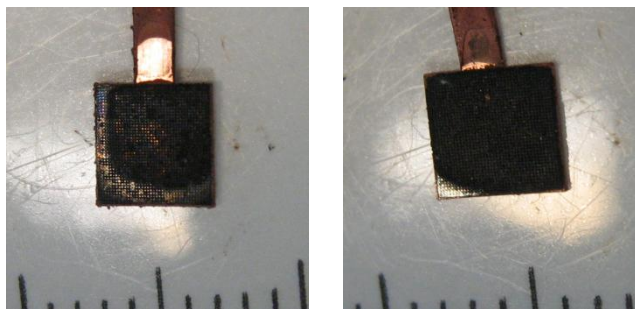


Figure 38: Standard electrolyte +0.5 % 4-FP: Images of anodes after 100 cycles. The cells were disassembled in an argon atmosphere and the electrodes rinsed with DEC.

In Figure 38 the anodes of the 0.5 % 4-FP cells are shown. There are no separator residues sticking to the surface and there is only a small non active area on the right electrode, compared to the relatively large less active areas on electrode the left one. Therefore, the anode on the right was selected for SEM analysis.

3.1.3.9. Standard electrolyte + 1.0 % 4-FP

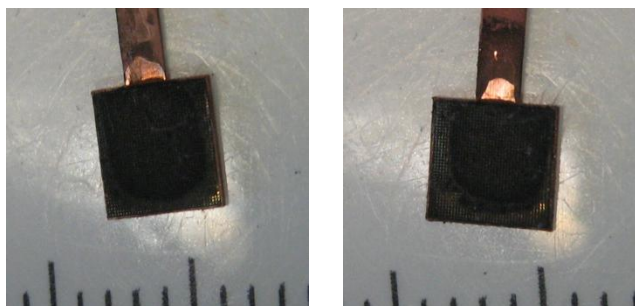


Figure 39: Standard electrolyte +1.0 % 4-FP: Images of anodes after 100 cycles. The cells were disassembled in an argon atmosphere and the electrodes rinsed with DEC.

Figure 39 shows the anodes of the 1.0 % 4-FP cells. There are no separator residues visible here either, but U-shaped less active areas on the edges of both electrodes. As those areas are smaller on the left anode, it was selected for SEM analysis.

3.1.3.10. Standard electrolyte + 2.0 % 4-FP

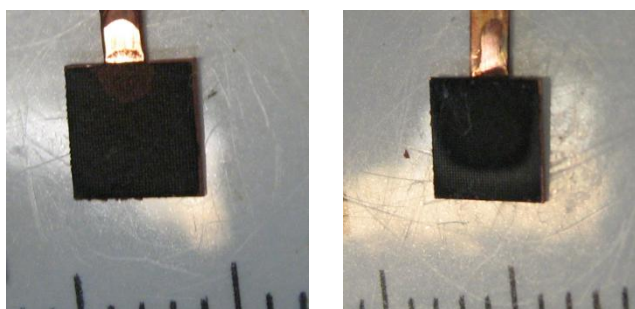


Figure 40: Standard electrolyte +2.0 % 4-FP: Images of anodes after 100 cycles. The cells were disassembled in an argon atmosphere and the electrodes rinsed with DEC.

In Figure 40, anodes of the cells with 2.0 % 4-FP are shown. The right anode has some U-shaped less active areas and separator residues sticking to the surface, while the electrode on the left does not which is why it was selected for SEM analysis.

3.1.3.11. Standard electrolyte + 0.5 Tri-FP

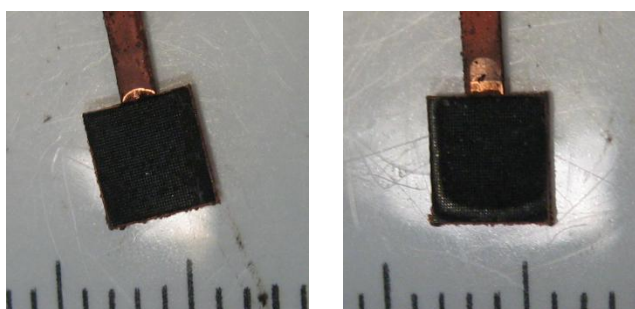


Figure 41: Standard electrolyte +0.5 % Tri-FP: Images of anodes after 100 cycles. The cells were disassembled in an argon atmosphere and the electrodes rinsed with DEC.

Figure 41 shows the anodes of the 0.5 % Tri-FP cells. There are no separator residues visible on both electrodes and only the right anode has a small less active band like area. For this reason, the anode on the left was selected for SEM analysis.

3.1.3.12. Standard electrolyte + 1.0 Tri-FP

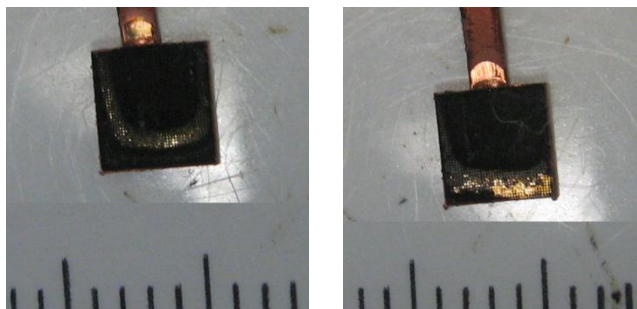


Figure 42: Standard electrolyte +1.0 % Tri-FP: Images of anodes after 100 cycles. The cells were disassembled in an argon atmosphere and the electrodes rinsed with DEC.

Figure 42 shows the anodes of the cells with 1.0 % Tri-FP. There is a U-shaped less active area on the left electrode and a broad band like non active area at the bottom of the one on the right. There are also some separator residues on the right one. The anode on the left was selected for further SEM analysis.

3.1.3.13. Standard electrolyte + 2.0 % Tri-FP

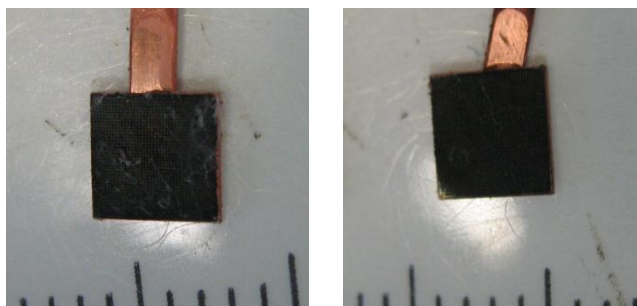


Figure 43: Standard electrolyte +2.0 % Tri-FP: Images of anodes after 100 cycles. The cells were disassembled in an argon atmosphere and the electrodes rinsed with DEC.

Figure 43 shows the anodes of the cells with 2.0 % Tri-FP. Both have a very homogeneous active surface with just a very small non active area on the bottom left corner of the right anode and some separator residues on the left one. Because separator residues are more disruptive during SEM analysis, the electrode on the right was selected.

3.1.3.14. Observations

Only two phenomena were observable during the post mortem analysis of the anodes. Firstly, sometimes there was separator residue still sticking to the surface of the electrode. One of the most likely reasons for this is the adherence of the separator fibers on the surface because of the pressure in the cell during operation. Another possible reason is that some separator fibers in close contact with the surface are built into the SEI during its formation. This, however, does not affect the functionality of the cell in any negative way. Those fibers are only an annoyance during SEM analysis, because they are masking the surface below them. This is why, if possible, anodes were chosen without separator residues on them.

Secondly, there were areas identifiable on nearly all anodes, where the material was less active than the rest or even not active at all. These areas were mainly located on the edges and had a band like or L-shaped look. Possible reasons for the appearance of these areas, where the active material obviously did not take part in the chemical reactions during the cycling of the cell, are a lower pressure on these areas, originating from minor differences in cell assembling, or lower wetting of the electrolyte in these areas and thus lower chemical activity. Either way, this phenomenon leads to differences in the active surface of the anodes during the cycling and therefore influences the comparability of the cells in a minor way. For SEM analysis, anodes with areas as small as possible were selected.

3.1.4. SEM images

To further understand the impact of additives on the investigated system and to confirm or explain some of the information obtained so far, SEM images of the previously selected anodes were analyzed. The main subject of this investigation was the influence of the different additives on the appearance of the SEI and the visible changes thereafter. Secondly, the influence of the different constructed SEIs on changing and/or damaging of the microstructure was examined. For a better picture of the whole system, images of the original anodes (unprepared, not cycled) were taken too.

3.1.4.1. Not cycled LIBC 13 and LIBC 23 anodes

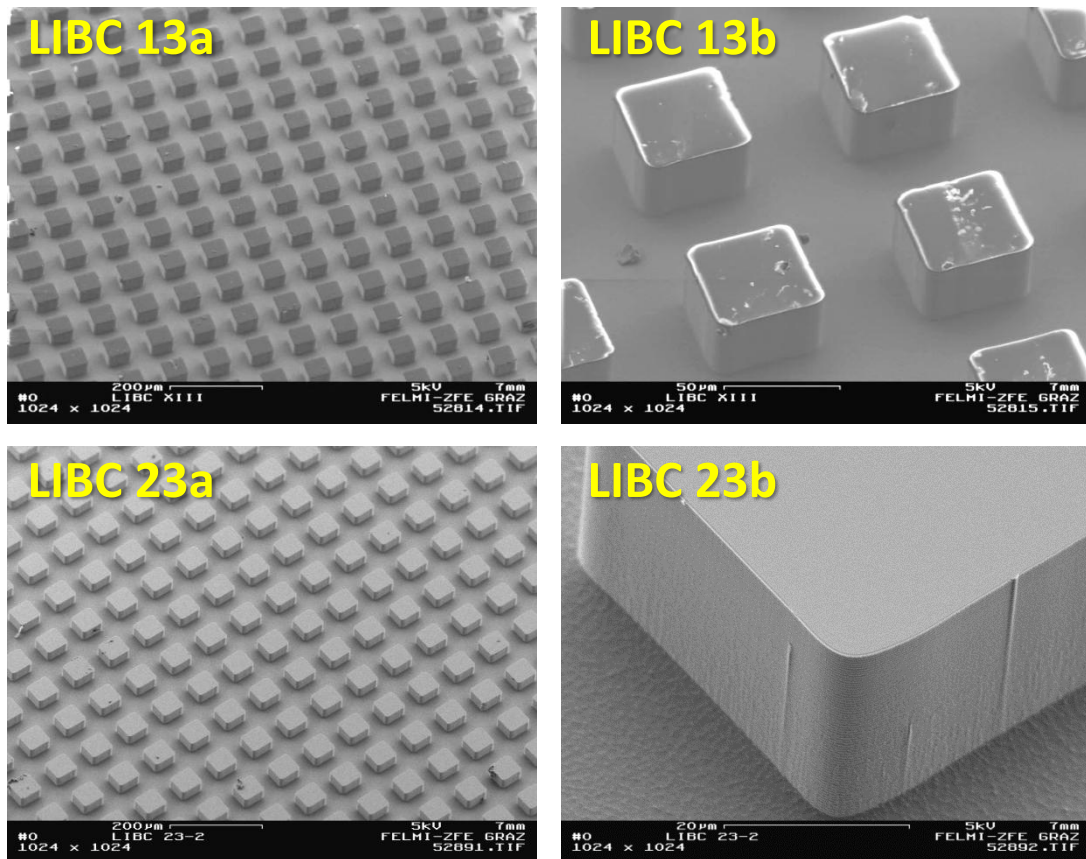


Figure 44: SEM images of the original anodes of the long term cycling experiments (LIBC 13) and of the short term cycling experiments (LIBC 23). Upper images: LIBC 13a: Magnification 100x. LIBC 13b: Magnification 500x. Lower images: LIBC 23a: Magnification 100x. LIBC 23b: Magnification 1000x.

Figure 44 shows the original silicon anodes of the types LIBC 13 and LIBC 23. On picture **LIBC 13a**, the microstructure is clearly visible. There are towers with height and edge length of 50 micrometers and gaps of equal distance in between. The corners of the top and base areas are slightly rounded. On picture **LIBC 13b**, the microstructure is shown in higher magnification; during this investigation, an unpleasant discovery was made. The towers of the LIBC 13 samples have an organic looking substance, with a thickness of at least some micrometers on their top area. The surface of this substance is clearly not as smooth as the surrounding silicon and it began to glow under the electron beam of the microscope, which indicates that this substance has insulating properties. *

*: Further inquiries on this subject led to the conclusion that this organic substance is some kind of Novolak polymer photo resist used by Infineon Technologies Austria in the lithographic process for the preparation of the microstructure of the anodes, which was not removed properly afterwards. This investigation is not part of this thesis.

To check this discovery, a LIBC 23 sample was inspected too and it showed no signs of the foreign substance (**LIBC 23 b**). This means, that only the samples of the LIBC 13 batch have this organic substance on it. Unfortunately, all experiments concerning LIBC 13 anodes were already in progress at that time and therefore the existence of this contamination has to be included in the results of the long term cycling experiments.

3.1.4.2. Standard electrolyte (EC:EMC 3:7 w/w, 1 M LiPF₆)

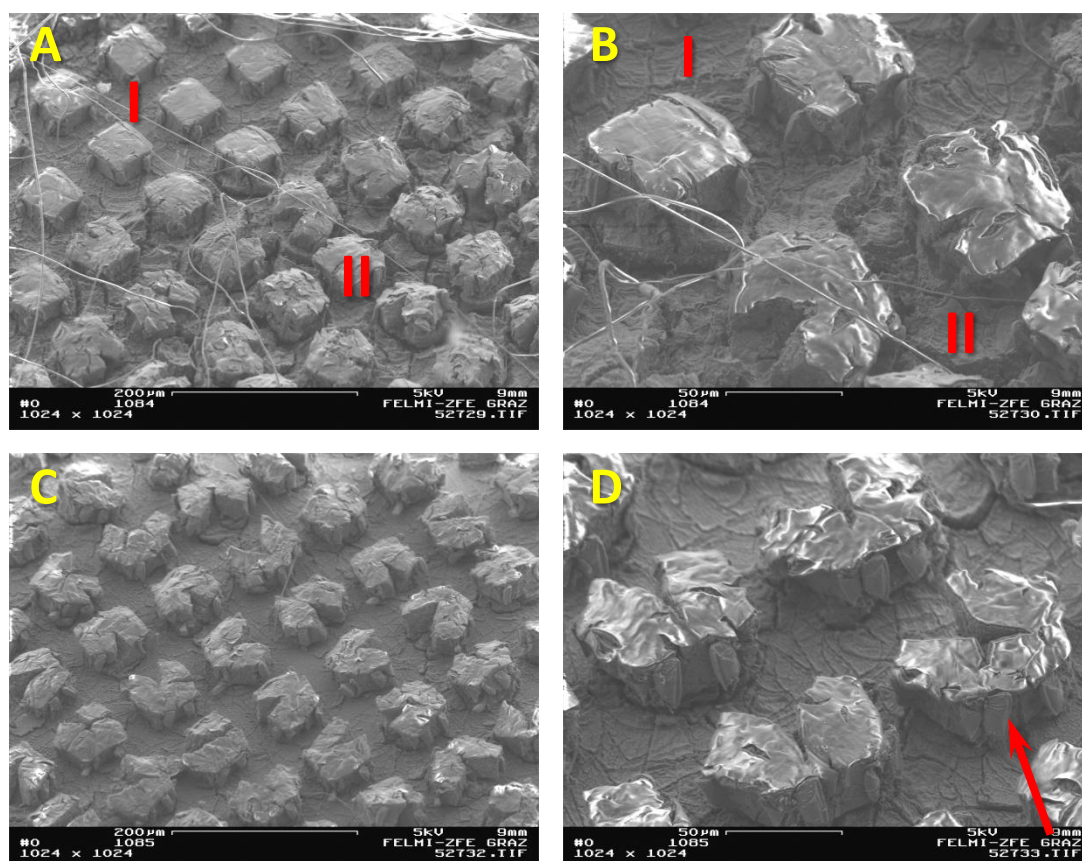


Figure 45: SEM images of the anodes of the cells with standard electrolyte. Image A: First anode, 200x. Image B: First anode, 500x. Image C: Second anode, 200x. Image D: Second anode, 500x.

Figure 45 shows two anodes of the cells with standard electrolyte. Images **A** and **C** show an overview with less magnification, while images **B** and **D** have a higher magnification for a more detailed examination. Looking at the pictures, it is obvious, that the material and its microstructure underwent some changes during the electrochemical cycling. The surfaces lost their smooth look; the cubic towers got cracks and look like they burst; the bottom surface got some minor cracks too and it seems like everything is covered with a thin film, the SEI. On a closer look, there are some separator fibers visible (Figure 45, **A** and **B**).

On image **A** and to a lesser degree on image **B**, an area where the material was less active (Figure 45, **A** and **B**, area **I**) is visible. The difference to the more active areas (Figure 45, **A** and **B**, area **II**) is that the towers with average activity are recognizable through one major crack and some minor branches (example pointed out in Figure 45, image **D**). The organic residues of the photo resist can be found again here too. The polymer film did not break apart or dissolve during cycling and can be identified on top of all towers by its shiny and glowing surface especially on images **C** and **D**.

3.1.4.3. Standard electrolyte + 0.5 % VC

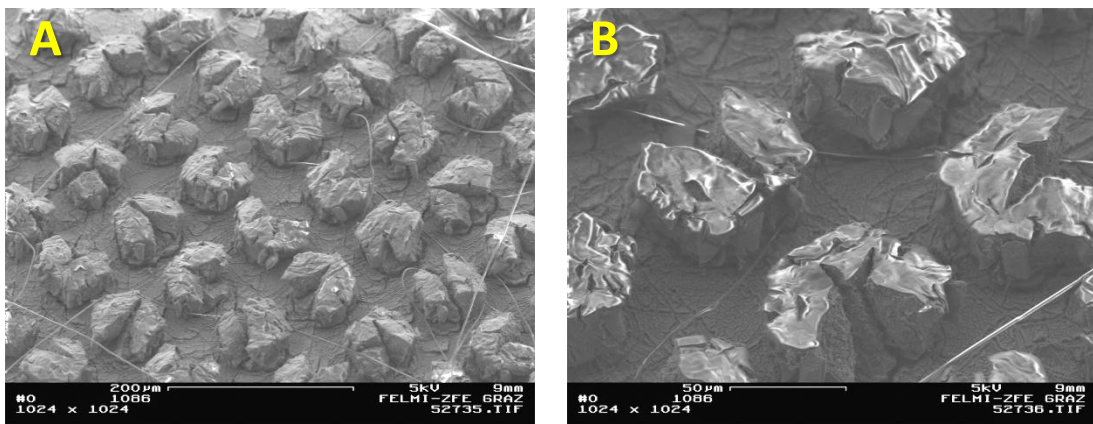


Figure 46: SEM images of the anodes of the cells with standard electrolyte + 0.5 % VC. Image A: 200x. Image B: 500x.

Figure 46 shows an anode of the cells with a concentration of 0.5 % VC. There are some separator fibers visible. All of the cubic towers of the microstructure have a major crack with some branches, but the bottom surface has almost no cracks. The photo resist film on top of the towers is clearly visible in Figure 46, image **B**.

3.1.4.4. Standard electrolyte + 1.0 % VC

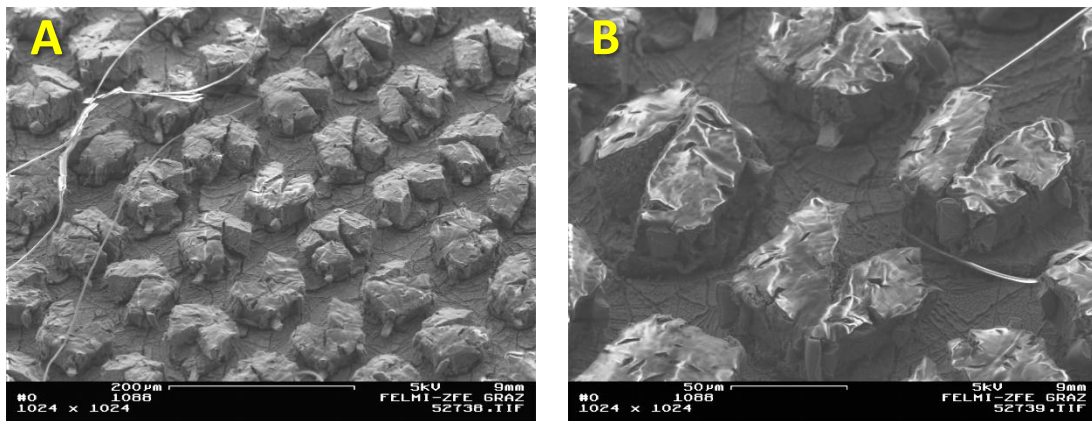


Figure 47: SEM images of the anodes of the cells with standard electrolyte + 1.0 % VC. Image A: 200x. Image B: 500x.

Figure 47 shows an anode from the cells with a concentration of 1.0 % VC. There are some separator fibers visible. The cubic towers of the microstructure all have a distinctive crack with some branches and the photo resist film on top of the towers is visible too.

3.1.4.5. Standard electrolyte + 2.0 % VC

Figure 48 shows an anode of the cells with a concentration of 2.0 % VC. This electrode had large areas that were less active (Figure 48, image A, area I) and some that were more active (Figure 48, image A, area II). It seems that less activity in one region leads to more activity in another. The differences between these regions are better visible in the higher magnification images of the less active area (Figure 48, image B) and the more active area (Figure 48, image C).

While the bottom surface is still smooth and not cracked on image **B**, it is heavily broken up in **C** and because of that some of the towers are even lifted (highlighted with red arrows). The towers in both areas have some cracks. Separator fibers and the shimmering photo resist are visible too.

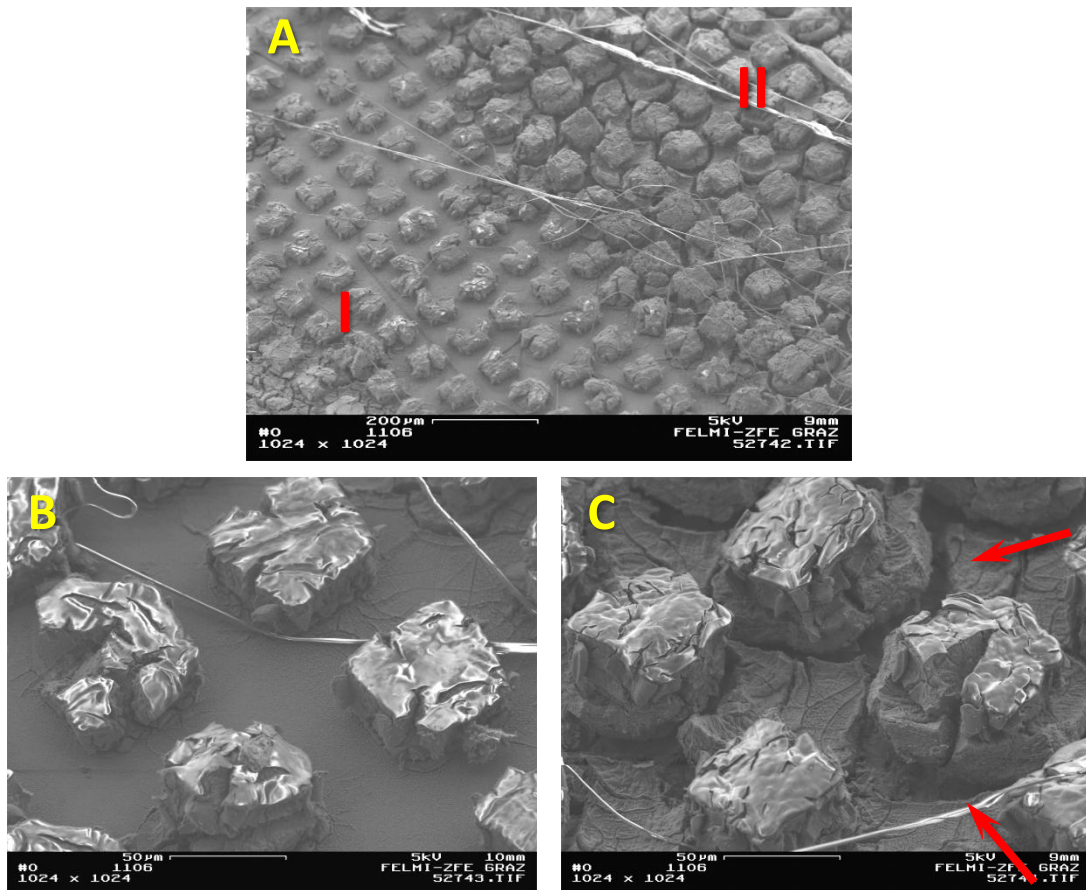


Figure 48: SEM images of the anodes of the cells with standard electrolyte + 2.0 % VC. Image A: 100x. Image B: Area I of image A, 500x. Image C: Area II of image A, 500x.

3.1.4.6. Standard electrolyte + 0.5 % VEC

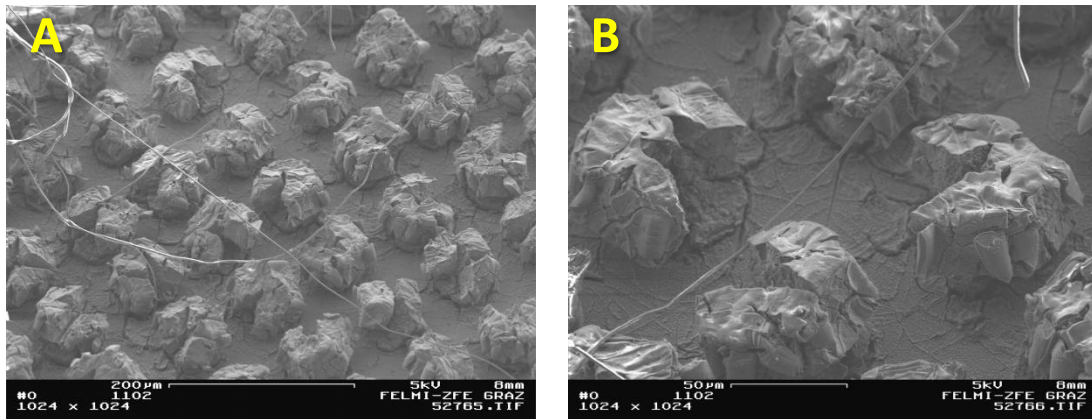


Figure 49: SEM images of the anodes of the cells with standard electrolyte + 0.5 % VEC. Image A: 200x. Image B: 500x.

Figure 49 shows the anode of the cell with a concentration of 0.5 % VEC. This anode looks very much like the one from the 0.5 % VC cells (see chapter 3.1.4.3.). Most of the towers have a branched major crack, while there are only a few minor cracks on the bottom surface. Separator fibers and the polymer photo resist film are visible again.

3.1.4.7. Standard electrolyte + 1.0 % VEC

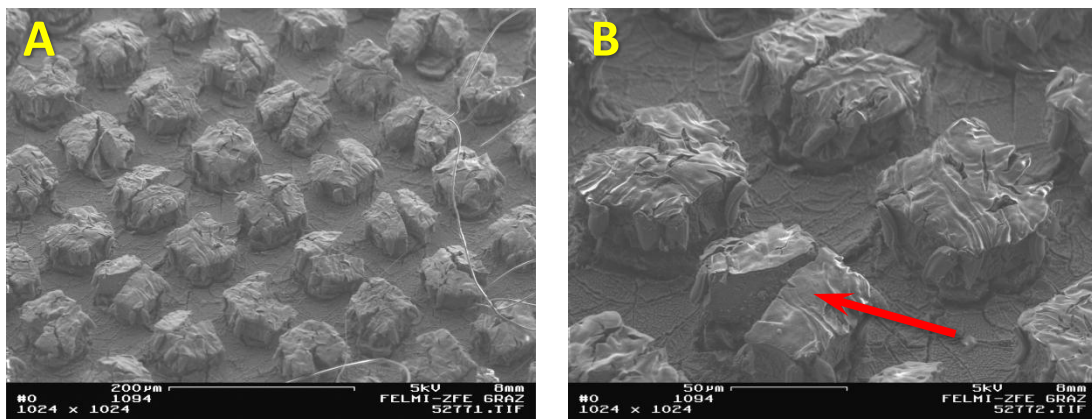


Figure 50: SEM images of the anodes of the cells with standard electrolyte + 1.0 % VEC. Image A: 200x. Image B: 500x.

Figure 50 shows the anode of the cell with a concentration of 1.0 % VEC. There again, most of the microstructure towers have a major crack, but this time it looks slightly different. The crack is not branched at the end; it looks more like the towers were split almost completely in half (Figure 50, image B, pointed out with red arrow). Separator fibers and the polymer photo resist film are visible too.

3.1.4.8. Standard electrolyte + 2.0 % VEC

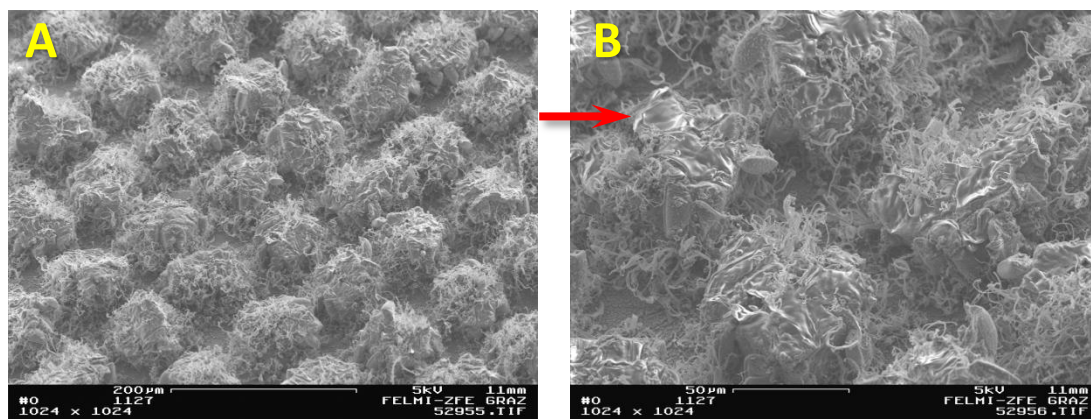


Figure 51: SEM images of the anodes of the cells with standard electrolyte + 2.0 % VEC. Image A: 200x. Image B: 500x.

Figure 51 shows an anode of the cells with a concentration of 2.0 % VEC. This electrode provides a different image compared to the ones shown before. The whole surface, towers and bottom, is covered in thread like structures protruding from the surface. Most likely, this is a rare appearance of the SEI, because of its formation under certain conditions. The towers themselves are still identifiable and it seems like they have no major cracks like the ones before. Maybe this form of the SEI prevented the towers from splitting. The photo resist film is still identifiable between the SEI (Figure 51, image B, red arrow).

3.1.4.9. Standard electrolyte + 0.5 % 4-FP

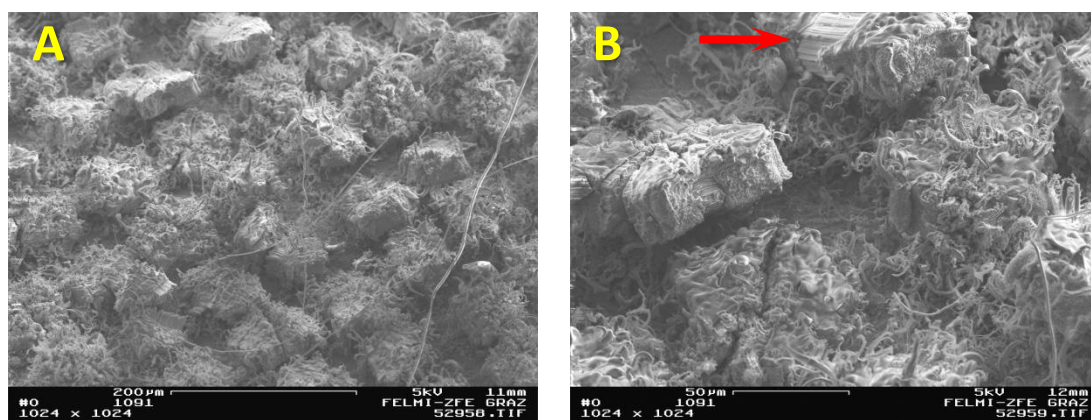


Figure 52: SEM images of the anodes of the cells with standard electrolyte + 0.5 % 4-FP. Image A: 200x. Image B: 500x.

Figure 52 shows the anode of the cell with a concentration of 0.5 % 4-FP. The SEI visible on these images looks similar to the one shown before (see chapter 3.1.4.8.). Although these thread-like structures do not cover the whole surface in a homogeneous way, it is obvious that this is the preferred appearance of the SEI for this sample. Some of the towers partially lost contact to the bottom or broke apart and were turned upside down, while between other towers, or parts of the same tower, a thread-like bond was formed from the additive (Figure 52, image **B**, red arrow). Separator fibers and some photo resist residues are visible too.

3.1.4.10. Standard electrolyte + 1.0 % 4-FP

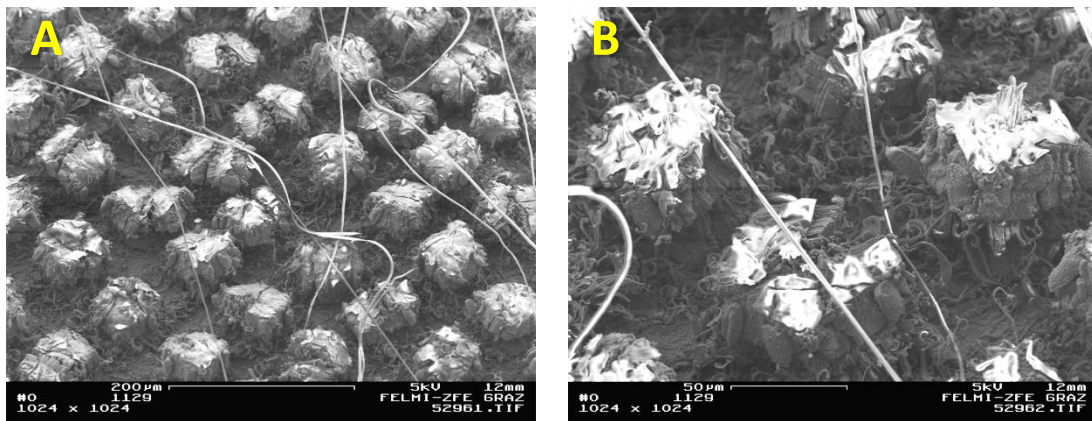


Figure 53: SEM images of the anodes of the cells with standard electrolyte + 1.0 % 4-FP. Image A: 200x. Image B: 500x.

Figure 53 shows an anode from the cells with a concentration of 1.0 % 4-FP. Unfortunately, because of the brightness of the nonconductive photo resist film on top of the tower microstructure and the resulting bad contrast these images are more difficult to analyze. Nevertheless, the SEI is identifiable again as a film with small and curly thread-like extensions (Figure 53, image **B**, on the bottom surface) and some towers with a major crack are visible, while most towers have no cracks.

3.1.4.11. Standard electrolyte + 2.0 % 4-FP

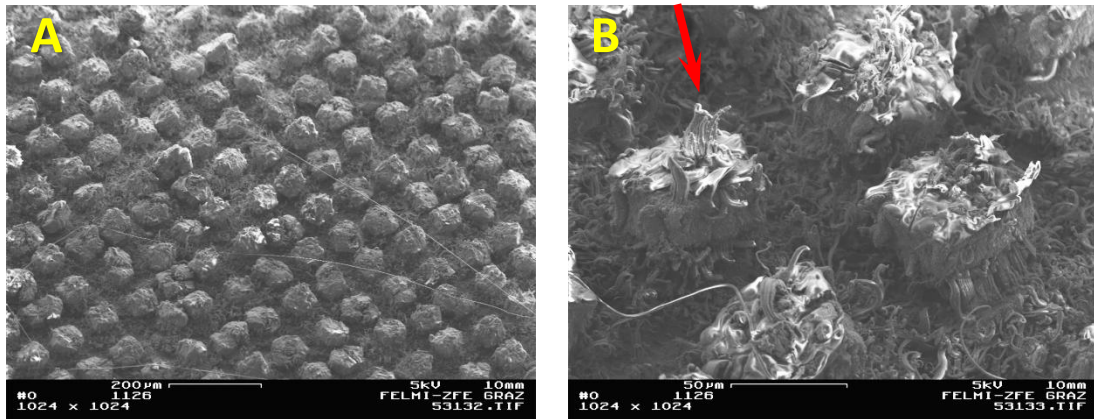


Figure 54: SEM images of the anodes of the cells with standard electrolyte + 2.0 % 4-FP. Image A: 200x. Image B: 500x.

Figure 54 shows the anode of the cell with a concentration of 2.0 % 4-FP. On this anode it looks like some of the photo resist film on top of the towers was broken up by antenna-like SEI structures (Figure 54, image B, red arrow), while the bottom surface is again covered in small and curly thread-like extensions. Unlike most of the other anodes, the towers of the microstructure have no major cracks nor were they damaged badly. A few separator fibers are visible.

3.1.4.12. Standard electrolyte + 0.5 % Tri-FP

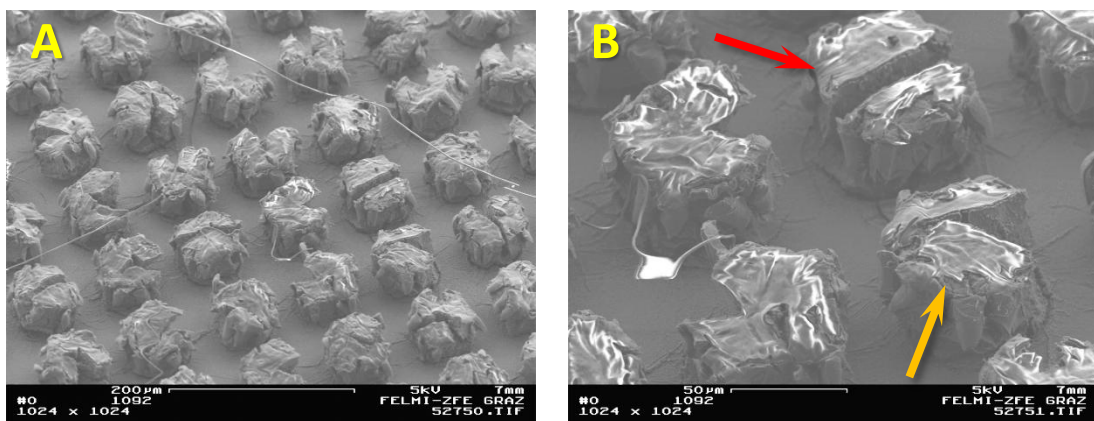


Figure 55: SEM images of the anodes of the cells with standard electrolyte + 0.5 % Tri-FP. Image A: 200x. Image B: 500x.

Figure 55 shows an anode of the cells with a concentration of 0.5 % Tri-FP. On these images, all the towers have one of two different types of cracks. One that splits the tower straight in half (Figure 55, image **B**, red arrow) and one that looks like a wedge was cut out of the tower (Figure 55, image **B**, orange arrow).

3.1.4.13. Standard electrolyte + 1.0 % Tri-FP

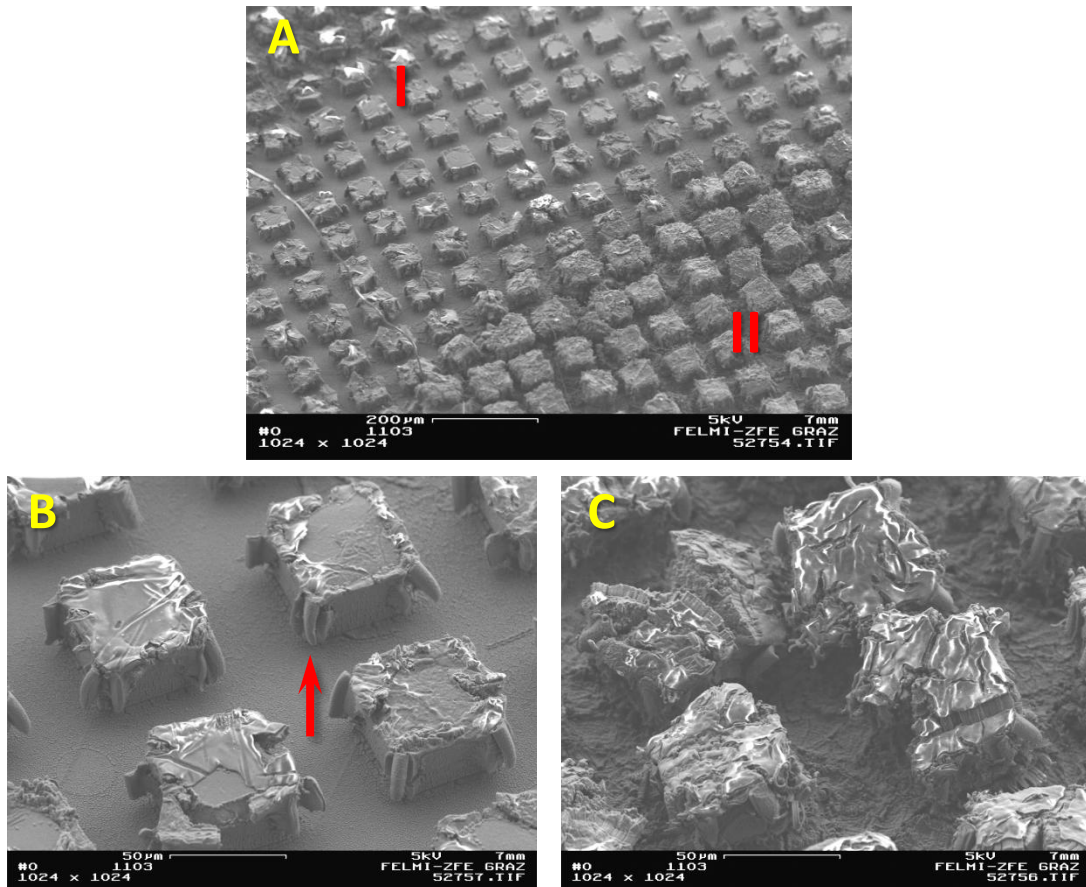


Figure 56: SEM images of the anodes of the cells with standard electrolyte + 1.0 % Tri-FP. Image A: 100x. Image B: Area I of image A, 500x. Image C: Area II of image A, 500x.

Figure 56 shows the anode of the cell with a concentration of 1.0 % Tri-FP. There is a large area on this anode, where the material was less active (Figure 56, image **A**, area **I**) and because of that the rest of the anode was slightly more active (Figure 56, image **A**, area **II**). In the less active area, the towers were not deformed except on the lateral edges, where some material splintered to form a cylinder like structure (Figure 56, image **B**, red arrow). In the more active area, some towers got large cracks, were lifted up a bit or lost their cubic structure. The bottom surface got a lot of minor cracks too. The photo resist broke off of some of the towers in the less active area, while the film is still intact on the other towers in both areas.

3.1.4.14. Standard electrolyte + 2.0 Tri-FP

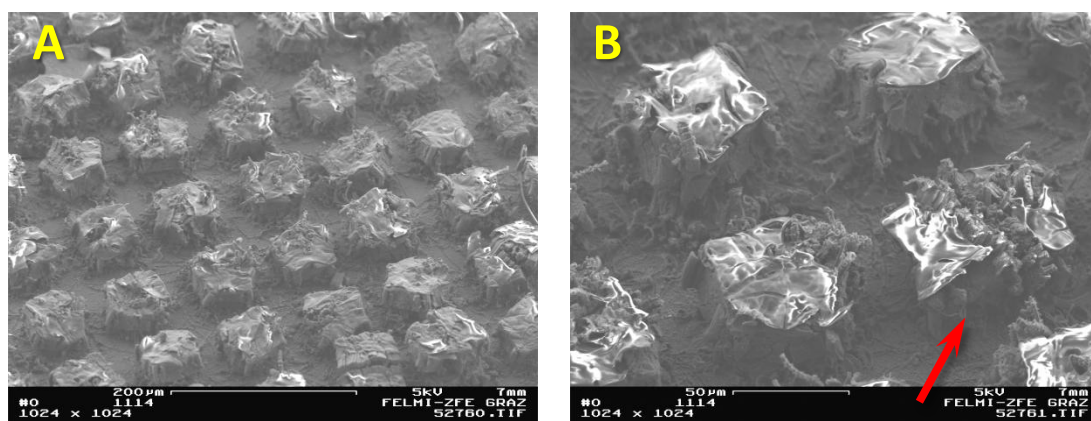


Figure 57: SEM images of the anodes of the cells with standard electrolyte + 2.0 % Tri-FP. Image A: 200x. Image B: 500x.





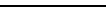



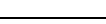
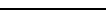



Figure 57 shows an anode of the cells with a concentration of 2.0 % Tri-FP. There are some burst towers (Figure 57, image B, red arrow), but mainly the towers were not damaged extensively. Neither the bottom nor any other surface shows signs of large cracks. The photo resist film is clearly visible on top of all the towers.

3.1.5. Analysis and comparison of the results

The observations obtained from the cycling charts in chapter 3.1.1. were not significant enough to justify statements about the quality of the improvement of the cycling behavior through the addition of additives to the electrolyte. Thus, to be able to compare the influence of the single additives to each other and to the cells with standard electrolyte, the cumulative irreversible capacity, the capacity that is irretrievably lost through the first formation of the SEI, ongoing damaging of it and possible side reactions, was calculated over the course of the whole experiment (see chapter 3.1.1., Figure 30).

Looking at the graphs in Figure 30 in detail, it can be seen that there are roughly two major groups for the first section (until cycle three). Cells with a concentration of 2.0 % VC, 2.0 % VEC and 1.0 % 4-FP and a lower end value of about 0.12 and the other cells with higher end values of about 0.16 to 0.18, with exceptions from the cells with 0.5 % VEC and 1.0 % Tri-FP, which are somewhere in between (with 0.14 as end value). From that point on, in section two, all cells develop with different slopes until they reach end values (after 100 cycles) of about 0.15 to more than 0.40. Table 8 shows all values in ascending order for comparison.

Table 8: Irreversible capacity values for the two sections that were defined for the graphs in Figure 30 (chapter 0.). The samples are listed from overall best results to worst ones.

| No. | Electrolyte | End value section one | End value section two | Graph |
|-----|----------------|-----------------------|-----------------------|---|
| 1 | + 2.0 % VC | 0,117 | 0,133 |  |
| 2 | + 2.0 % VEC | 0,120 | 0,244 |  |
| 3 | + 1.0 % 4-FP | 0,127 | 0,304 |  |
| 4 | + 0.5 % VEC | 0,137 | 0,240 |  |
| 5 | + 1.0 % Tri-FP | 0,141 | 0,239 |  |
| 6 | Standard | 0,153 | 0,248 |  |
| 7 | + 1.0 % VEC | 0,154 | 0,415 |  |
| 8 | + 0.5 % Tri-FP | 0,157 | 0,285 |  |
| 9 | + 2.0 % Tri-FP | 0,158 | 0,314 |  |
| 10 | + 2.0 % 4-FP | 0,160 | 0,370 |  |
| 11 | + 1.0 % VC | 0,163 | 0,400 |  |
| 12 | + 0.5 % 4-FP | 0,165 | 0,307 |  |
| 13 | + 0.5 % VC | 0,168 | 0,523 |  |

Based on this data, the following conclusions can be drawn from the comparison of the cells.

There are cells from each additive, where the irreversible capacity was reduced more or less significantly, compared to the standard cells. On the other hand, there were also cells of each additive where the irreversible capacity increased. The difference between those cells was the additive concentration, which is obviously a great factor regarding the impact of the additive, since it determines the boundary between the desired (decrease of the irreversible capacity) and undesired (increase of the irreversible capacity) effect the additive has on the system.

The Tri-FP additive shows the best results with a concentration of 1.0 %. The irreversible capacity of these cells is slightly lower than that of the standard cells. The 0.5 % and 2.0 % cells of Tri-FP, on the other hand, have slightly higher irreversible capacities, with values of about the same level.

The cells with a concentration of 1.0 % 4-FP have a lower irreversible capacity than the cells with standard electrolyte too, however only for region one. Then the irreversibly capacity rises faster than that of the reference. The 0.5 % and 2.0 % cells are among the worst results in this experiment, with a strong increase in irreversible capacity, for the cells with a concentration of 2.0 % 4-FP more than for the cells with a concentration of 0.5 % 4-FP.

The VEC additive shows some contradictory results. Both, the cells with a concentration of 0.5 % and 2.0 %, have a lower irreversible capacity, while the cells with a concentration of 1.0 % have a much higher increase of the irreversible capacity than the standard cells.

The best result was achieved with the VC additive. The cells with a concentration of 2.0 % were the only ones with a distinctive decrease of the irreversible capacity compared to the reference cells. The worst result, on the other hand, was achieved with VC too. The cells with a concentration of 0.5 % have the greatest increase in irreversible capacity, closely followed by the cells with a concentration of 1.0 %. However, compared to the VEC additive cells, the results are not contradictory, as the irreversible capacity decreases with increasing additive concentration.

Obviously, there is a perfect concentration for each additive to affect the system as desired and decrease the irreversible capacity. For the VC and VEC additives this concentration is higher, about 2.0 %, while for the other additives, 4-FP and Tri-FP, the 1.0 % concentration seems to be the most promising. The VC and VEC additives, as well as the 4-FP and Tri-FP additives, are more similar in their way of affecting the system to each other as to the others, which is a coherent fact too. This means that the best way to improve the overall effectiveness of the system is to use VC and VEC like additives (especially VC) in high concentrations around or above 2.0 %.

Obviously, there are some differences in the formation of the SEI because of the use of different additives and thus the behavior of the anode or its microstructure during cycling. However, from the pictures shown so far it is not understandable why or how the ideal concentration for each additive affects the cell in a more positive way than the other concentrations. The following chapter tries to give some explanations concerning that question by comparing different SEM images.

3.1.5.1. Standard electrolyte and VC

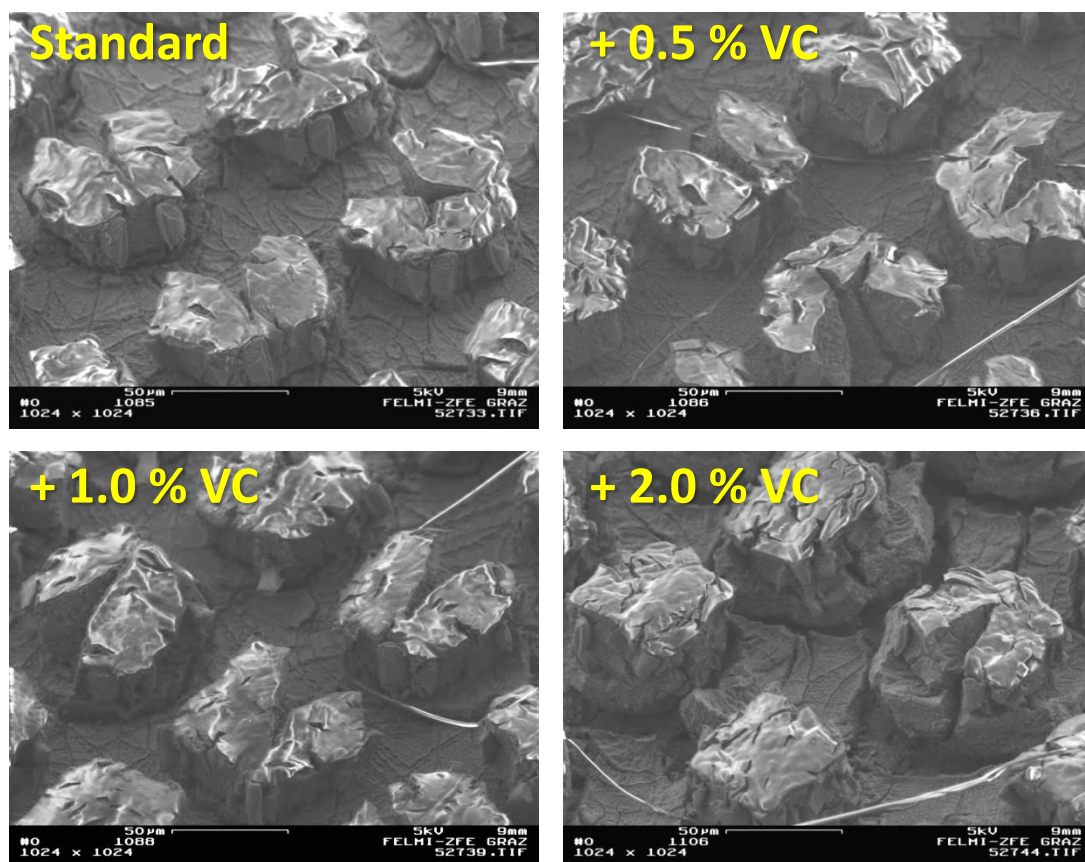


Figure 58: SEM images of the anodes of the cells with standard electrolyte and added VC in different concentrations.

Compared to the cells with standard electrolyte, the anodes of the cells with a 0.5 % and a 1.0 % VC concentration look very similar (Figure 58). On all three anodes, the towers have a major crack that is branched at the end in some cases. The only difference is that the bottom surface of the 0.5 % VC anode has slightly fewer minor cracks than that of the anode with 1.0 % VC concentration, which itself has slightly fewer cracks than the bottom surface of the reference. The 2.0 % VC concentration electrode, on the other hand, has much larger cracks on the bottom surface than on the towers and some cracks are so deep that they lift the towers on them. Since there are no differences visible in the SEI appearance or thickness (although the film may simply be too thin to be able to clearly identify differences), it is not clear, why the cells with a concentration of 2.0 % VC additive have a much less irreversible capacity than the other VC cells and the standard cells (see Table 8).

Eventually, because of a more stable and elastic SEI formed by the additive that somehow stabilized the structure, the higher additive concentration led to fewer major cracks on the towers during the first cycles. The cracks on the bottom were most likely formed on an advanced point of cycling, when the tension in the material became too high. It seems that in this way, much less irreversible capacity was generated than during the initial cracking of the towers seen on the other VC and standard anodes.

3.1.5.2. Standard electrolyte and VEC

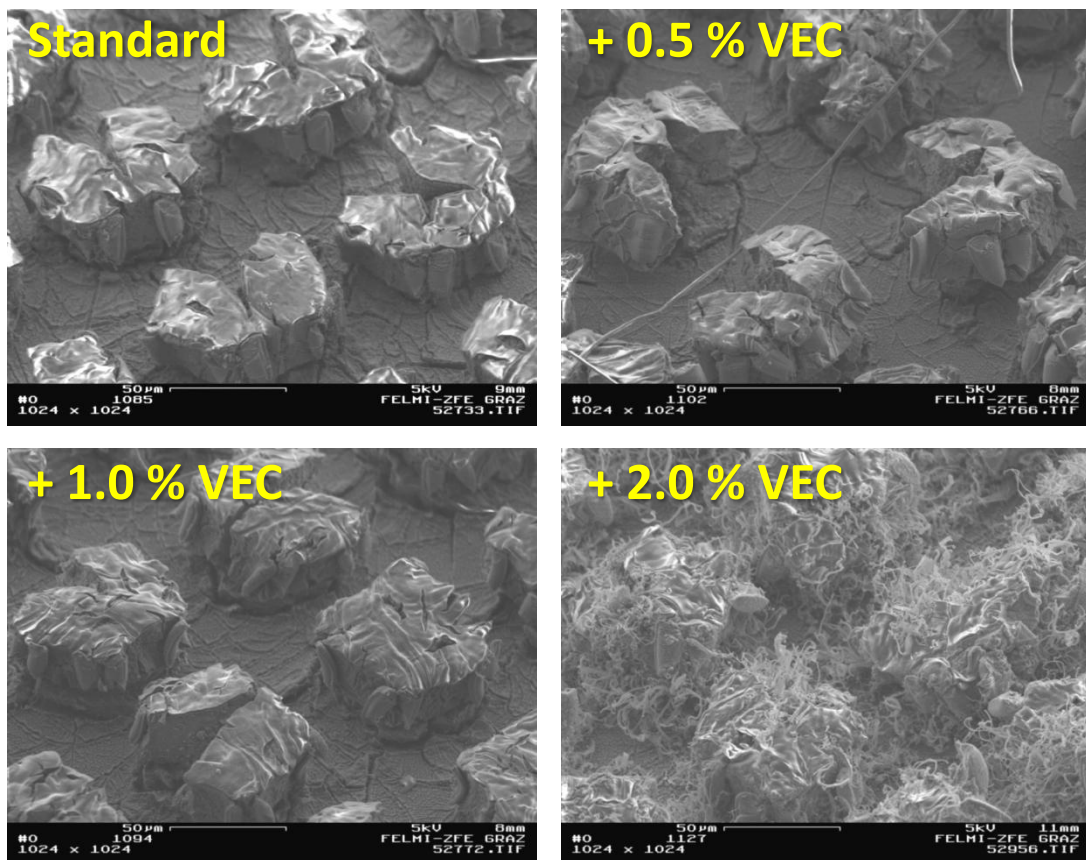


Figure 59: SEM images of the anodes of the cells with standard electrolyte and added VEC in different concentrations.

The representative anode of the cells with a concentration of 0.5 % VEC additive looks very much like the one from the reference cells. Both have large branched cracks on their towers and many very small cracks on the bottom surface. The anode of the cell with a concentration of 1.0 % VEC has smaller cracks on its towers and the 2.0 % VEC anode looks completely different, because the SEI has a different appearance here. It looks like a more stable or stabilizing SEI was formed with a higher additive concentration (see Figure 59).

The only contradiction is that, while the cells with a concentration of 0.5 % VEC had a similar irreversible capacity to that of the standard cells and the 2.0 % VEC concentration cells had less, the cells with 1.0 % VEC had a much higher irreversible capacity (see Table 8). According to the look of the microstructure and the SEI and assuming that fewer cracks lead to less irreversible capacity, the irreversible capacity of the 1.0 % VEC cells should range between that of the 0.5 % and 2.0 % cells. It is not clear, why it does not. Another unclear aspect is the different appearance of the SEI on the anodes from the 2.0 % VEC concentration cells. Maybe this is a characteristic of having too much additive in the electrolyte solution after the first forming of the SEI.

3.1.5.3. Standard electrolyte and 4-FP

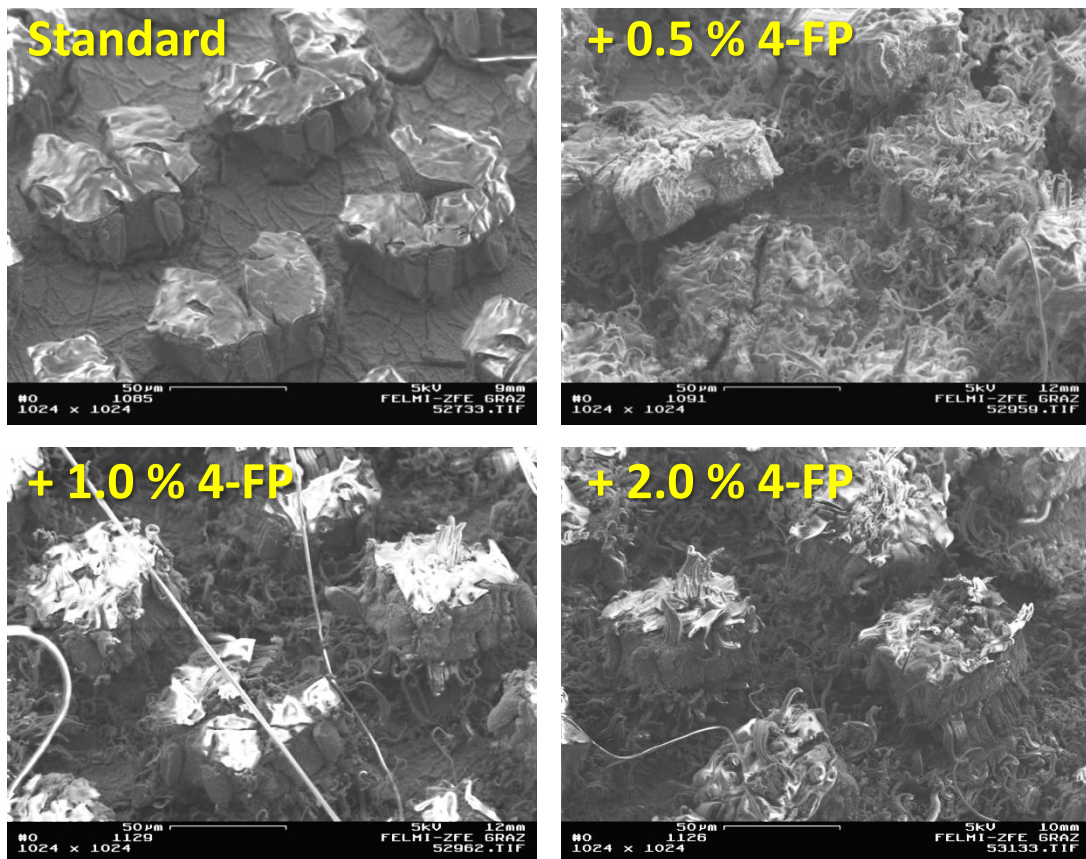


Figure 60: SEM images of the anodes of the cells with standard electrolyte and added 4-FP in different concentrations.

All three of the 4-FP additive anodes differ greatly from the cells with standard electrolyte in the appearance of the SEI. It looks like the formation of these curly thread-like extensions from the SEI film are occurring predominantly with this additive, as they appear on all cells on all concentrations. These extensions look a bit more bulky on the 1.0 % and 2.0 % anodes than on the 0.5 % anode, where they are smaller and thinner.

Additionally it looks like the extensions in the cells with higher concentrations (1.0 % and 2.0 %) break apart some of the photo resist film on top of the towers and grow from underneath. The towers show fewer cracks and disorder on these concentrations too. On the anode of the 0.5 % concentration, some of the towers broke in half or were turned upside down or lifted because of the cracks (see Figure 60).

In the initial phase of the cycling the irreversible capacity of the cells with 1.0 % 4-FP additive are lower than that of the standard cells and the irreversible capacity of the cells with 0.5 % and 2.0 % concentration is higher. As the cycling goes on, however, the irreversible capacity of all cells with 4-FP additive steadily increases until in the end even the cells with 1.0 % concentration have a much higher irreversible capacity than the standard cells (see Table 8). Taking the information from the images into account, the following conclusions can be drawn: For the initial SEI formation the best additive concentration would be 1.0 % 4-FP as there are fewer cracks visible than on the 0.5 % 4-FP anode and the irreversible capacity is less than that of the cells with 2.0 % 4-FP, although they look very similar. But then (maybe because of the excess of additive) those thread-like structures are formed and thus the irreversible capacity greatly increases. This increase seems to depend on the concentration of the additive, as it is lower for the lower concentrations and higher for the higher ones.

3.1.5.4. Standard electrolyte and Tri-FP

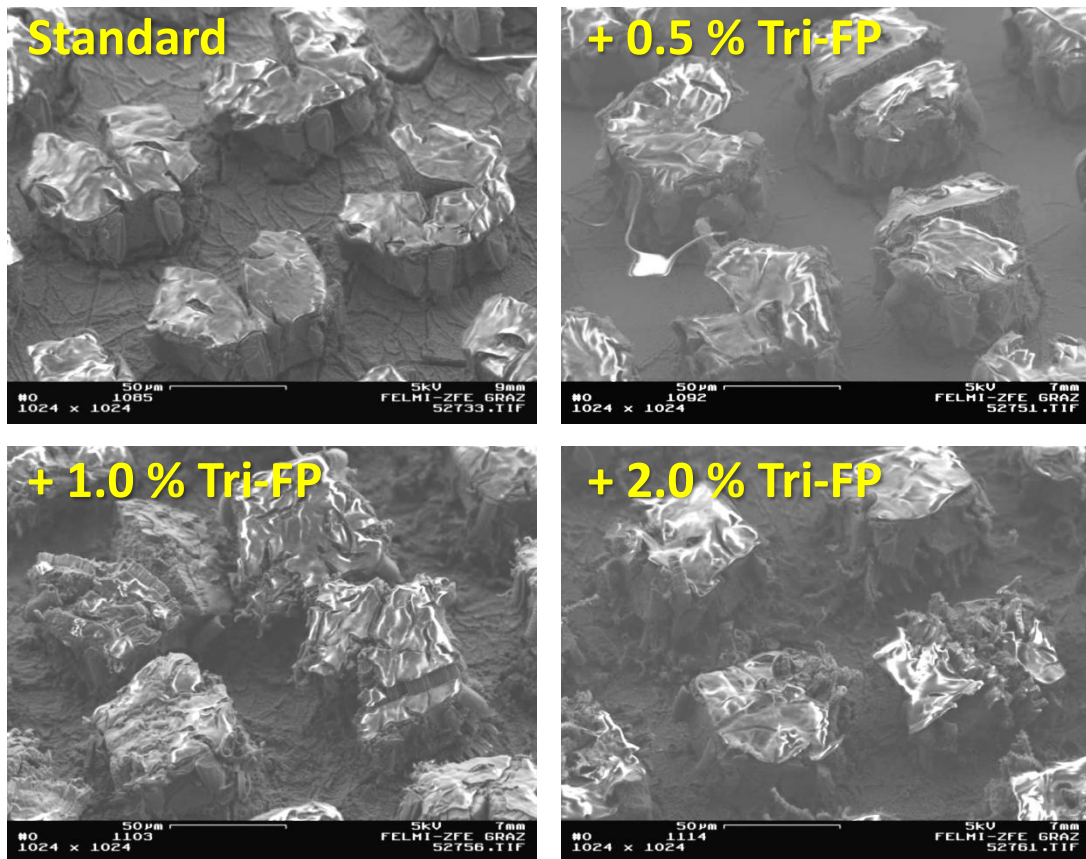


Figure 61: SEM images of the anodes of the cells with standard electrolyte and added Tri-FP in different concentrations.

On the additive anodes in Figure 61, the increasing influence of the additive on the formation of the SEI with increasing concentration can be seen clearly. On the 0.5 % Tri-FP anode, the SEI film looks very thin and smooth and the towers have random cracks. The SEI of the cells with 1.0 % Tri-FP concentration looks rougher and bulkier on the bottom surface and fewer towers have a major crack. With 2.0 % Tri-FP additive, some organic-looking structures were added on the top and bottom edges of the towers and none of the towers look like they were split in half.

Unfortunately, the irreversible capacity does not decrease with increasing additive concentration (see Table 8). While the cells with 1.0 % Tri-FP concentration have a slightly lower irreversible capacity than the reference cells, the others (0.5 % and 2.0 %) do not. For the 0.5 % Tri-FP cells, the formed SEI may be too thin and the additive may be used up after the first cycles, which increases irreversible capacity. For the 2.0 % Tri-FP cells, the excess additive may lead to an increase in the irreversible capacity as it is still reactive, forming unnecessary structures. Thus, a concentration of 1.0 % Tri-FP additive led to the best results, because there is enough additive to form a stable SEI and not too much to still cause reactions afterwards.

3.1.6. Conclusion

Obviously, using additives can improve the cell performance through the reduction of the irreversible capacity and it was shown that all of the used additives (VC, VEC, 4-FP and Tri-FP) were more or less able to achieve this. However, it is interesting that apparently there is an ideal window of concentration for each additive within which its effects are most positive. On the other hand, outside this window (which means if too much or too little additive is used) the cell performance can get significantly worse as the irreversible capacity may strongly increase compared to cells where no additive was added.

As the effectiveness of the used additives lies in affecting the SEI formation, its composition and its properties, visual analysis of the anodes, the microstructure on them and the SEI film led to some theories about why the irreversible capacity was decreased or increased depending on the additive and its concentration.

First of all, depending on the current density and the charge or discharge capacity, the single crystal micro structured silicon anode underwent heavy transformation during cycling. With each new cycle, the volume changes caused by the delithiation and lithiation lead to new cracks on the surface of the material or in the SEI and if strong tensions were built up, even to bursting of the microstructure. This is the main effect causing irreversible capacity, as either active material is lost, because it breaks off the bulk and loses electrical contact, or new SEI has to be formed on the now freshly exposed silicon. The additives decreasing irreversible capacity were able to reduce these effects, because the SEI they formed was either stabilizing the active material in a way that fewer cracks occurred (2.0 % VEC, 1.0 % 4-FP and 1.0 % Tri-FP) or the SEI that had to be formed on newly exposed material was formed very fast and effectively (2.0 % VC and 0.5 % VEC). Furthermore, the initial forming of the SEI from these additives was more effective than that of the standard electrolyte.

On the other hand, in some cases (4-FP, 2.0 % VEC and to a lesser extent 1.0 % and 2.0 % Tri-FP) the additive led to a more or less drastic increase of the irreversible capacity after the initial cycles. The reason for this is most likely the formation of additional thread-like structures on the SEI film resulting from the excess of additive in the electrolyte solution and its reactivity or instability. This effect was very strong with the 4-FP additive and increased with its concentration, while the cells with 2.0 % VEC and 1.0 % Tri-FP additives still had a slightly lower irreversible capacity, than that of the standard cells in the end.

The other additives that led to an increase of the irreversible capacity (0.5 % VC, 1.0 % VC, 1.0 % VEC and 0.5 % Tri-FP) did so for other reasons. Most likely, the additive concentration for the initial SEI formation was too low and therefore an unstable or imbalanced (concerning its composition) SEI was formed. In the subsequent cycles, the SEI had to be repaired or reworked constantly, which caused an increase of the irreversible capacity.

Summing up, the additives 2.0 % VC, 0.5 % and 2.0 % VEC and 1.0 % Tri-FP are possible choices for a successful improvement of the investigated system. This improvement comes from the reduction of the irreversible capacity and thus prolongs cell life. However, as the results from the VEC additive are not really consistent (only the anodes of the 2.0 % cells showed those thread-like structures; the irreversible capacity of the 0.5 % and 2.0 % cells was low, while that of the 1.0 % was much higher), those results should be regarded with cautiousness.

Moreover, two more aspects should be taken into consideration: Firstly, the individual assembling of the cells and the preparation of the anodes through copper plating may have led to some small differences in the pouch cells that could not be predicted and thus have to be considered negligible, but may have slightly influenced the result of the cycling experiments. Secondly, it is completely unclear whether or not the photo resist film on top of the microstructure that was accidentally left there influenced the performance of the additive or the whole cell in any positive or negative way, as no cells without this photo resist polymer were analyzed in these experiments.

To verify the results so far and to see if the photo resist influenced the cells in any way, another shorter cycling experiment was done in Swagelok cells, the results of which will be presented in the next chapter.

3.2. Impact of electrolyte additives: Short term cycling experiments

3.2.1. Target and hypothesis

When the discovery was made that the anode samples for the long term cycling experiments (LIBC 13, 100 cycles) were contaminated with photo resist film that was not properly removed after the lithographic process, a new set of anode samples was obtained (LIBC 23). After ensuring that the top surfaces of the microstructure of these new samples were clean (SEM images of these new samples were already shown in chapter 3.1.4.1, Figure 44), they were used for new experiments. However, because of the lack of time, it was not possible to repeat the entire long term experiment and therefore shorter experiments (3 cycles instead of 100) were carried out in Swagelok cells, which are faster to prepare. All other procedures were carried out similarly to the long term experiment.

The purpose of these new experiments was to determine if the contamination of the electrodes influenced the cells performance in any way and if the results regarding the influence of the additives on the initial SEI formation (which was done in the first cycles) from the previous experiments can be confirmed.

3.2.2. Cumulative irreversible capacity

Similar to chapter 0. mean values for the cumulative irreversible capacity were calculated out of the cycle charts for the cells with standard electrolyte and the ones with additives. The cycle charts themselves are not shown anymore, because of their little information value.

In Figure 62, the irreversible capacity over the three cycles is shown. Even though they are small, there are some differences identifiable. Obviously, most of the additives led to a reduced irreversible capacity compared to the standard electrolyte and only three actually led to an increase in the cumulative irreversible capacity. The irreversible capacity that is shown can most likely only be credited to the initial formation of the SEI. Other effects that may lead to an increase of irreversible capacity only play a minor role at such early stages of the life of an electrode.

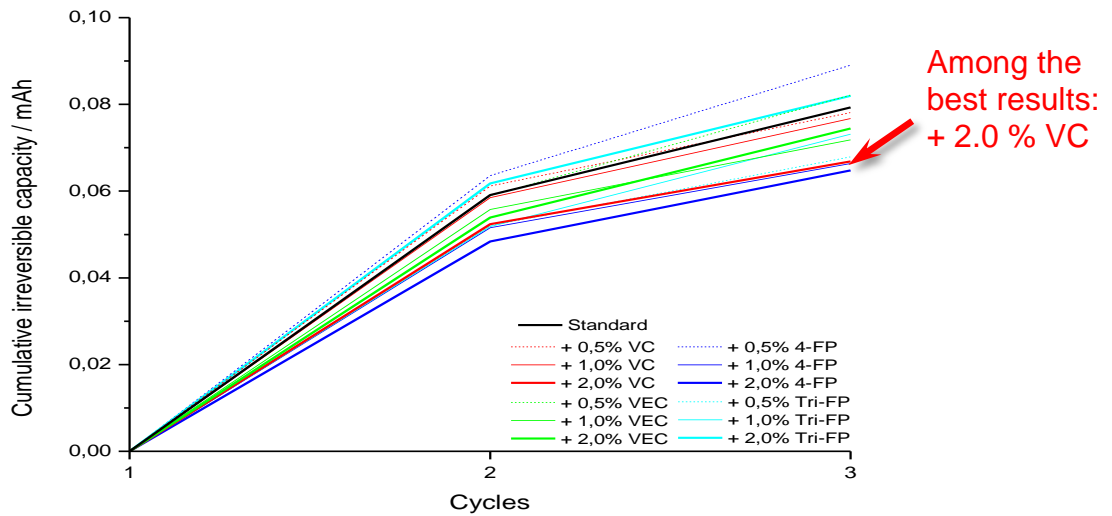


Figure 62: Cumulative irreversible capacity vs. cycles of the short term experiment. For a better overview, mean values for all samples were calculated from the single results.

3.2.3. SEM images

As no pictures were taken of the anodes during or after the post mortem procedure, an overview SEM picture was taken of each additive and for the standard instead of an image with medium magnification. This was done to gain a better insight into the behavior of the anodes. The second set of images has the same magnification level as the ones from the long term experiment.

3.2.3.1. Standard electrolyte (EC:EMC 3:7 w/w, 1 M LiPF₆)

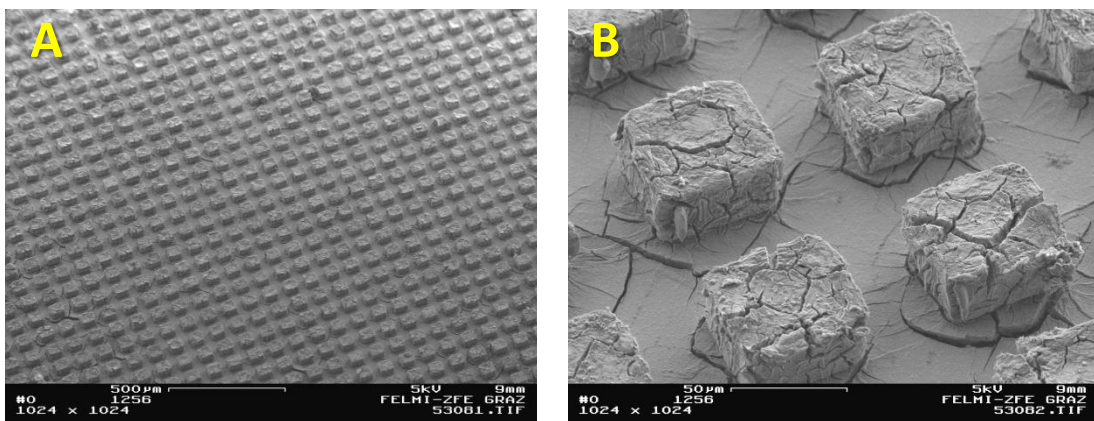


Figure 63: SEM images of the anodes of the cells with standard electrolyte after three cycles. Image A: 50x. Image B: 500x.

A representative anode of the cells with standard electrolyte is shown in Figure 63. In the overview image (Figure 63, image **A**) it can be seen that the surface of the anode was used very homogeneously. On the image with a higher magnification level (Figure 63, image **B**) the microstructure can be seen and small cracks are evenly distributed on the towers and the bottom surface.

3.2.3.2. Standard electrolyte + 0.5 % VC

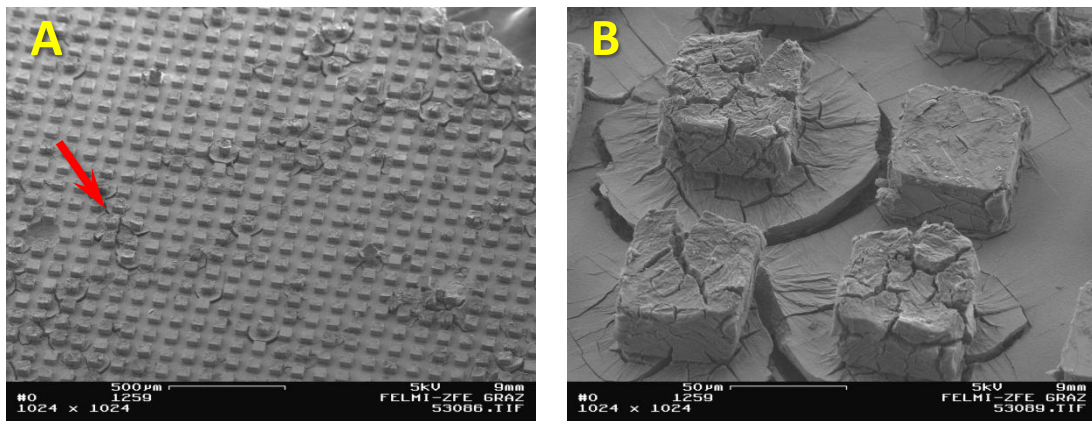


Figure 64: SEM images of the anodes of the cells with standard electrolyte + 0.5 % VC after three cycles. Image A: 50x. Image B: 500x.

On the overview image of the anode from the cell with 0.5 % VC (Figure 64, image **A**), it looks as if only small areas, or even only some single towers were active (see red arrow, image **A**), while others were not. On the other image (Figure 64, image **B**), this difference can be seen more clearly. The tower on the upper left side has cracks on all sides and is surrounded by a deep ring-like crack on the bottom surface. The tower on the upper right side on the other hand was mainly left untouched and has only some very small cracks.

3.2.3.3. Standard electrolyte + 1.0 % VC

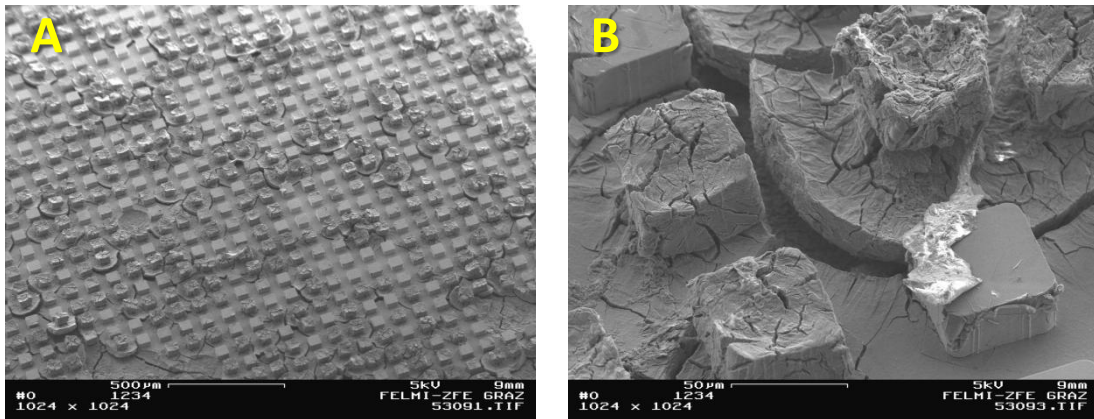


Figure 65: SEM images of the anodes of the cells with standard electrolyte + 1.0 % VC after three cycles. Image A: 50x. Image B: 500x.

These images (Figure 65) of the anode from the cells with 1.0 % VC show the same effect as on the previous images (chapter 3.2.3.2.). On the image with higher magnification (Figure 65, image B), it can be seen again that the upper right tower suffered from heavy deformation and a ring-like crack was formed around it, while the lower right tower looks almost like the ones from the not cycled samples (see chapter 3.1.4.1.). Additionally, there is a substance of unknown origin visible on that tower.

3.2.3.4. Standard electrolyte + 2.0 % VC

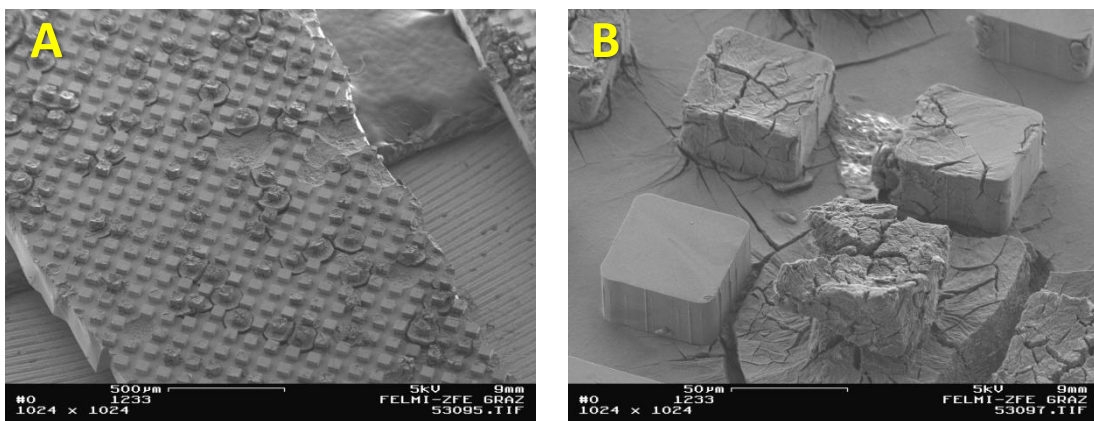


Figure 66: SEM images of the anodes of the cells with standard electrolyte + 2.0 % VC after three cycles. Image A: 50x. Image B: 500x.

In Figure 66, SEM images from the 2.0 % VC sample are shown. On the overview image (Figure 66, image **A**), some craters are visible where some tower groups obviously broke off. The reason for this may be the uneven activity of the towers, as can be seen in the other image (Figure 66, image **B**). The lower right tower is again very deformed and has a deep ring-like crack around, while the lower left tower was completely inactive. Those deep cracks on the bottom surface are most likely the reason for those areas where the material exfoliated.

3.2.3.5. Standard electrolyte + 0.5 % VEC

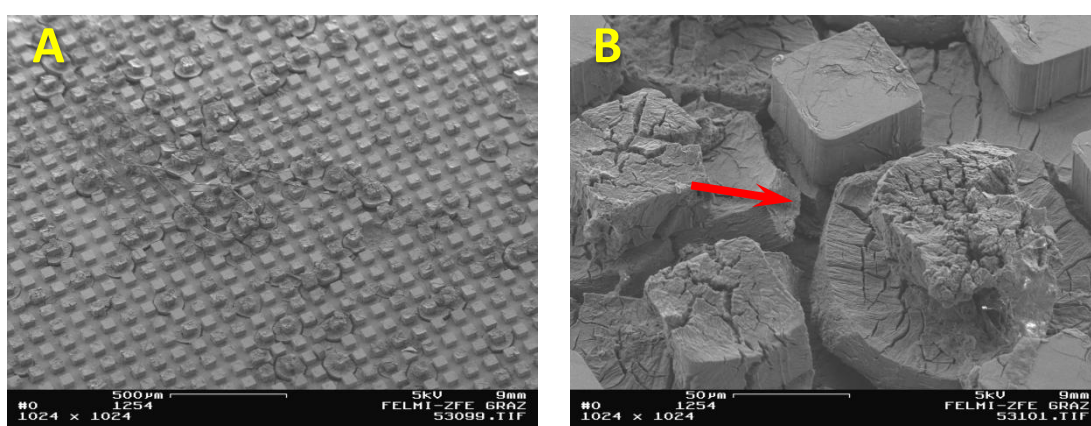


Figure 67: SEM images of the anodes of the cells with standard electrolyte + 0.5 % VEC after three cycles. Image A: 50x. Image B: 500x.

In Figure 67, the anode of the 0.5 % VEC sample is shown. On the overview image (Figure 67, image **A**), it can be seen that there are domains where the material was very active and other areas where it was not. On the second image (Figure 67, image **B**) towers that were very active are directly identifiable besides an inactive one. The cracks surrounding the active towers are deep enough to undermine the other tower (red arrow, image **B**).

3.2.3.6. Standard electrolyte + 1.0 % VEC

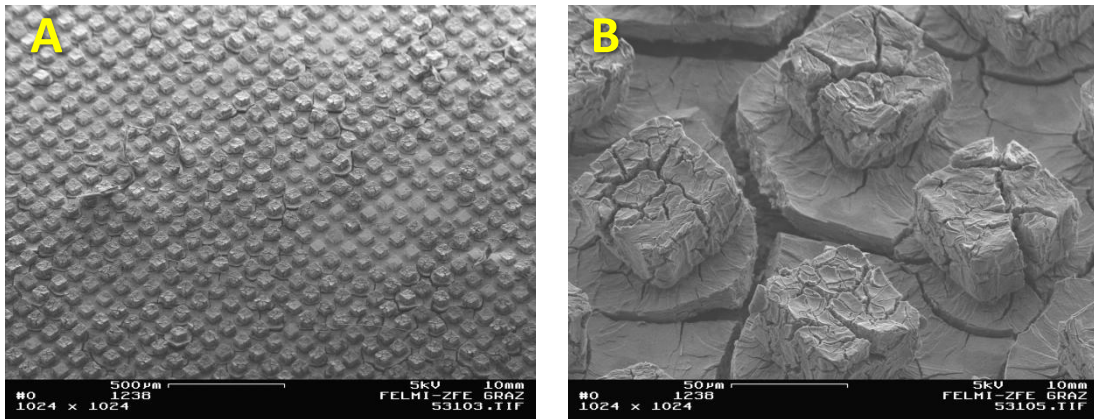


Figure 68: SEM images of the anodes of the cells with standard electrolyte + 1.0 % VEC after three cycles. Image A: 50x. Image B: 500x.

Figure 68 shows images of a 1.0 % VEC anode. The activity was distributed more evenly, as can be seen in image **A** (Figure 68), but there are still areas that were less active. In image **B**, the visible towers all have cracks of the same size and the bottom surface has a deep crack as well.

3.2.3.7. Standard electrolyte + 2.0 % VEC

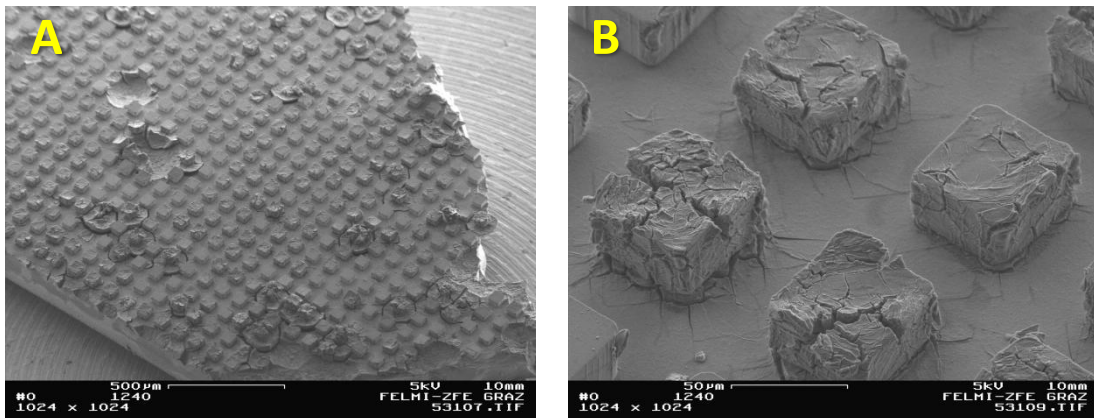


Figure 69: SEM images of the anodes of the cells with standard electrolyte + 2.0 % VEC after three cycles. Image A: 50x. Image B: 500x.

The representative anode for the cells with 2.0 % VEC is shown in Figure 69. Some craters are visible on the first image (Figure 69, image **A**), where the microstructure was detached because of the formation of these round deep cracks on the surface (seen on the previous images, for example in chapter 3.2.3.5.). On image **B**, an area that showed moderate activity can be seen.

3.2.3.8. Standard electrolyte + 0.5 % 4-FP

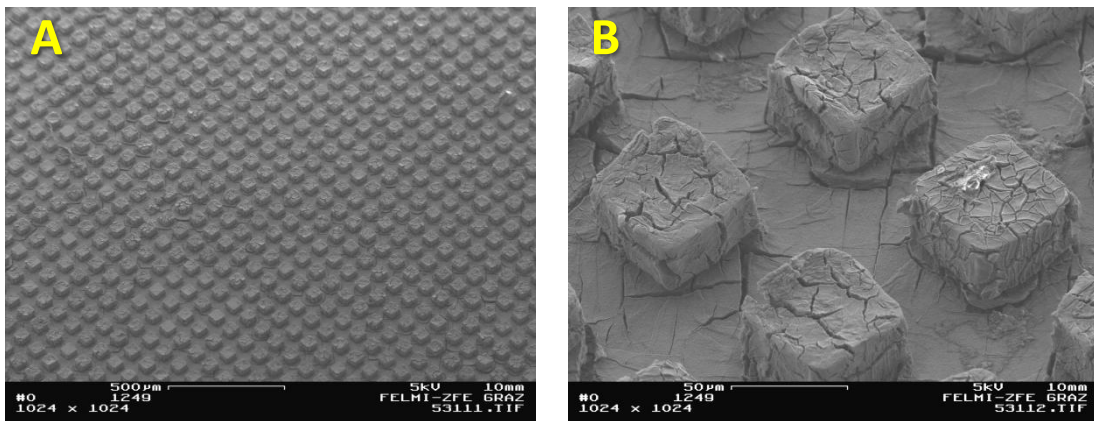


Figure 70: SEM images of the anodes of the cells with standard electrolyte + 0.5 % 4-FP after three cycles. Image A: 50x. Image B: 500x.

The images of the cell with 0.5 % 4-FP in Figure 70 have a very homogeneous looking surface. The towers and the bottom surface (Figure 70, image B) have similar small cracks.

3.2.3.9. Standard electrolyte + 1.0 % 4-FP

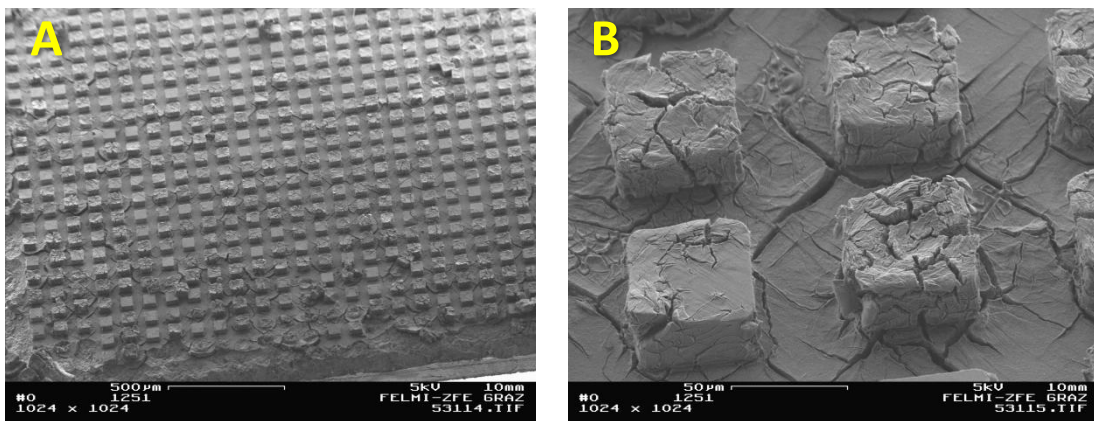


Figure 71: SEM images of the anodes of the cells with standard electrolyte + 1.0 % 4-FP after three cycles. Image A: 50x. Image B: 500x.

Figure 71 shows the SEM images of the 1.0 % 4-FP anode. Some minor differences in the activity are identifiable on image A. Image B shows those differences in a greater magnification. For example, the lower two towers are looking slightly different concerning the number and size of the cracks on their surface.

3.2.3.10. Standard electrolyte + 2.0 % 4-FP

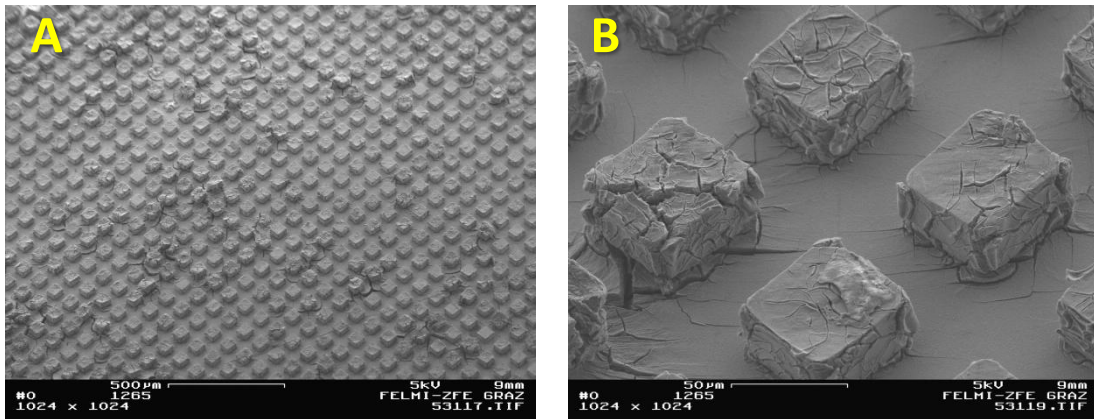


Figure 72: SEM images of the anodes of the cells with standard electrolyte + 2.0 % 4-FP after three cycles. Image A: 50x. Image B: 500x.

Figure 72 shows images of the 2.0 % 4-FP anode. The same observations as in the previous chapter (3.2.3.9.) can be made.

3.2.3.11. Standard electrolyte + 0.5 % Tri-FP

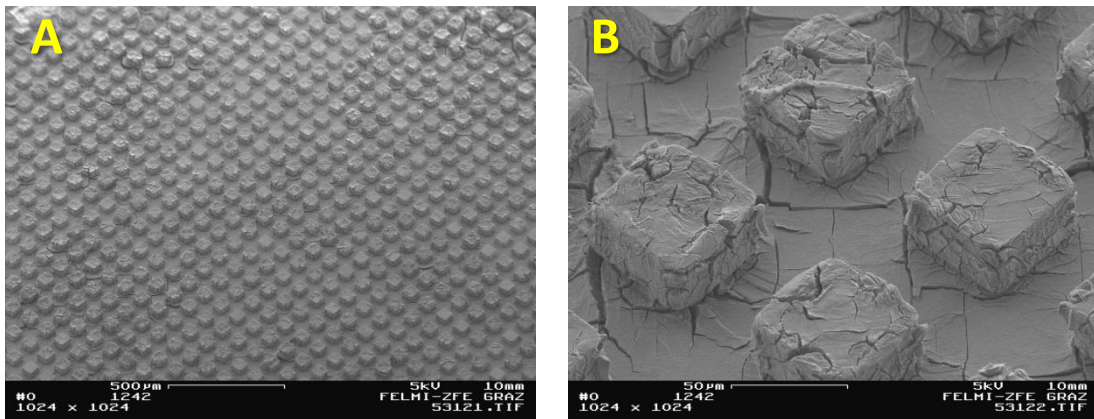


Figure 73: SEM images of the anodes of the cells with standard electrolyte + 0.5 % Tri-FP after three cycles. Image A: 50x. Image B: 500x.

The anode of the cells with 0.5 % Tri-FP has a very homogeneous looking surface, as can be seen in the overview image in Figure 73 (image **A**). On a higher magnification (Figure 73, image **B**), small cracks are visible on the towers and the bottom surface of the sample.

3.2.3.12. Standard electrolyte + 1.0 % Tri-FP

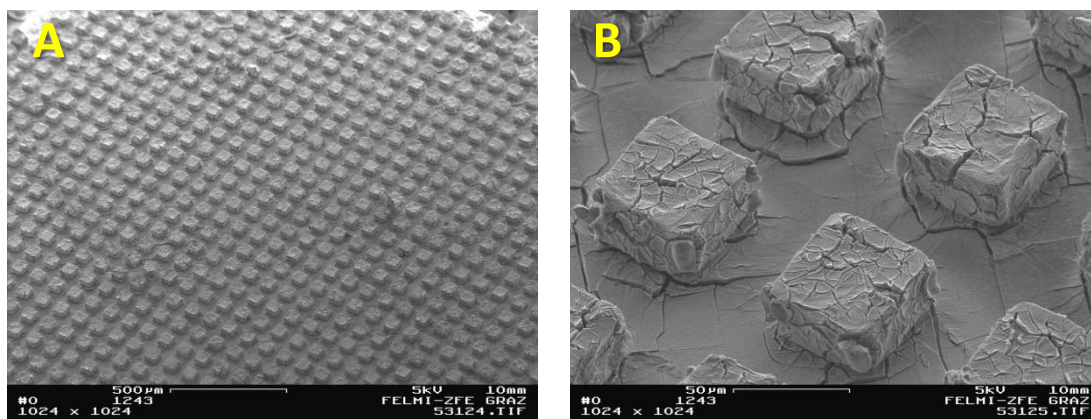


Figure 74: SEM images of the anodes of the cells with standard electrolyte + 1.0 % Tri-FP after three cycles. Image A: 50x. Image B: 500x.

Figure 74 shows the anode of the cell with 1.0 % Tri-FP. Similar to the one with 0.5 % Tri-FP (see chapter 3.2.3.11.), this electrode has a very homogeneous looking surface and the towers and the bottom surface have similar cracks.

3.2.3.13. Standard electrolyte + 2.0 % Tri-FP

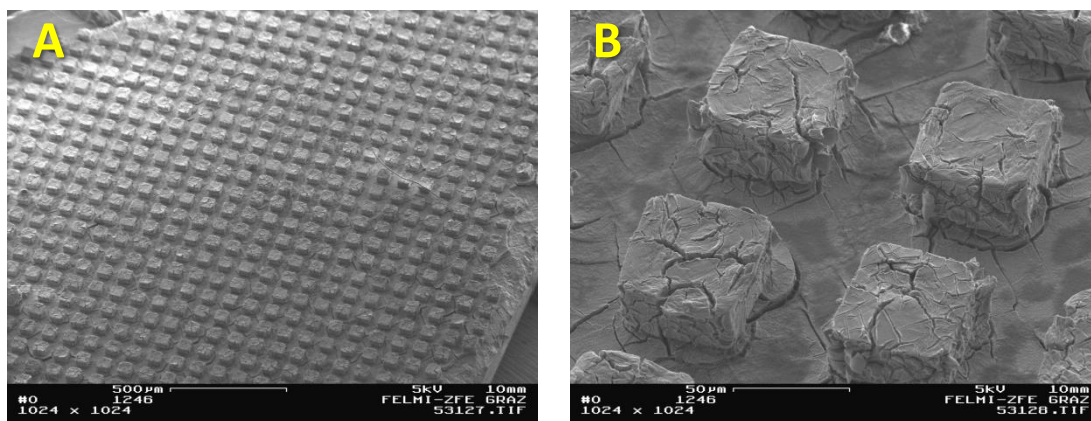


Figure 75: SEM images of the anodes of the cells with standard electrolyte + 2.0 % Tri-FP after three cycles. Image A: 50x. Image B: 500x.





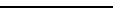
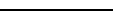


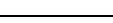

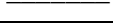


In Figure 75, the 2.0 % Tri-FP anode is shown. Again, this electrode looks very similar to the one from the 0.5 % Tri-FP sample in chapter 3.2.3.11. The only difference is the somehow patterned bottom surface that can be seen in image **B**.

3.2.4. Analysis

Taking a closer look at the results of the short term experiment (the SEM images of the anodes and the irreversible capacity), it is difficult to make a connection between the appearance of the anodes after cycling and the cumulative irreversible capacity. Firstly, the difference of the absolute values of the irreversible capacity is very low at the end of the experiment (cycle three), as can be seen in chapter 3.2.2. (Figure 62) and in Table 9. Secondly, no difference could be identified on the SEM images between electrodes of the same additive but with different concentrations. Thus, no assumption can be made as to why the different additives increased or decreased the irreversible capacity.

However, the results for the irreversible capacity can at least be compared with the ones from the long term cycling experiment. This is shown in Table 9.

Table 9: Cumulative irreversible capacity of the short term experiment, sorted from best to worst result (taken from Figure 62). For comparison reasons, the values of the long term experiment at the same point in time (cycle three) are given as well as the rank of each additive respectively.

| No. | Electrolyte | End value short term | Graph | Cycle three long term | No. long term |
|-----|----------------|----------------------|---|-----------------------|---------------|
| 1 | + 2.0 % 4-FP | 0.065 |  | 0.160 | 10 |
| 2 | + 1.0 % 4-FP | 0.066 |  | 0.127 | 3 |
| 3 | + 2.0 % VC | 0.067 |  | 0.117 | 1 |
| 4 | + 0.5 % Tri-FP | 0.068 |  | 0.157 | 8 |
| 5 | + 1.0 % VEC | 0.072 |  | 0.154 | 7 |
| 6 | + 1.0 % Tri-FP | 0.073 |  | 0.141 | 5 |
| 7 | + 2.0 % VEC | 0.074 |  | 0.120 | 2 |
| 8 | + 1.0 % VC | 0.077 |  | 0.163 | 11 |
| 9 | + 0.5 % VC | 0.078 |  | 0.168 | 13 |
| 10 | Standard | 0.079 |  | 0.153 | 6 |
| 11 | + 0.5 % VEC | 0.082 |  | 0.137 | 4 |
| 12 | + 2.0 % Tri-FP | 0.082 |  | 0.158 | 9 |
| 13 | + 0.5 % 4-FP | 0.089 |  | 0.165 | 12 |

When comparing the results of the long and short term irreversible capacity, the first thing that can be noticed is that the values of the long term cycling are at least twice as high as the one from the short term experiment. The reason for this may be the photo resist contamination on the electrodes of the long term experiments that influenced the SEI formation in a negative way and thus led to an increase of irreversible capacity loss.

On the other hand this could simply be because of the different test setup (Swagelok cell vs. pouch cell) or for other unknown reasons.

The single results for each additive and concentration also differ greatly. While only five additives (or concentrations) actually decreased the irreversible capacity compared to the standard electrolyte in the long term experiment, all but three decrease it in the short term cycling. For example, 2.0 % 4-FP, which was among the worst ones in the long term cycling, shows the best result in the short term experiment and 0.5 % VEC, which was a good one for the long term cycling, is among the worst for the short term experiments. Only 1.0 % 4-FP and 2.0 % VC show similarly good results as before. There is no clear explanation for this inconsistency.

3.2.4.1. VC/VEC vs. 4-FP/Tri-FP

Regardless of the results, another interesting observation can be made. Comparing the SEM images of the four additives it can be seen that when using VC and VEC, only small areas of the surface were active during cycling, while 4-FP and Tri-FP led to a more evenly distributed activity (see Figure 76).

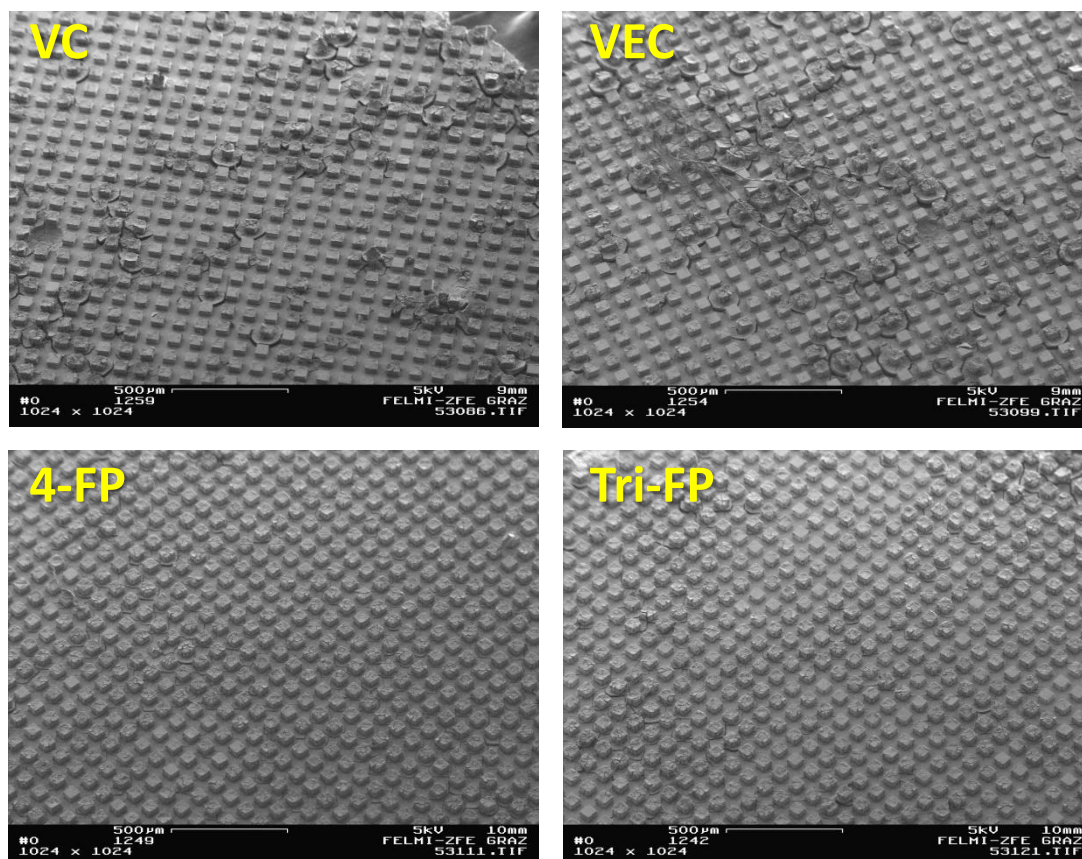


Figure 76: SEM images of the 0.5 % cells of all additives. Magnification: 50x.

Since VC and VEC are similar in their functionality, as are 4-FP and Tri-FP, the additive may be the reason for this occurrence. If this is the case and 4-FP and Tri-FP are favoring a more homogeneous usage of the available surface than VC and VEC, the use of 4-FP and Tri-FP should be preferred. In Figure 77, the negative effect of the irregularly distributed activity on the electrode surface can be observed.

The unevenly distributed activity that may be favored by the use of VC and VEC leads to an above-average lithium insertion into single areas or towers. During the course of the cycling, the activity towards lithium increases even further, as the insertion into areas that are already accessible is easier. On the other hand, inactive areas remain inactive. However, the mechanical stress that is negligible if distributed over the whole surface leads to enough deformation for those small active areas to be exfoliated from the surface (see Figure 77, red arrows). This, in turn, means a loss of active material and decreases the performance and stability of the cell.

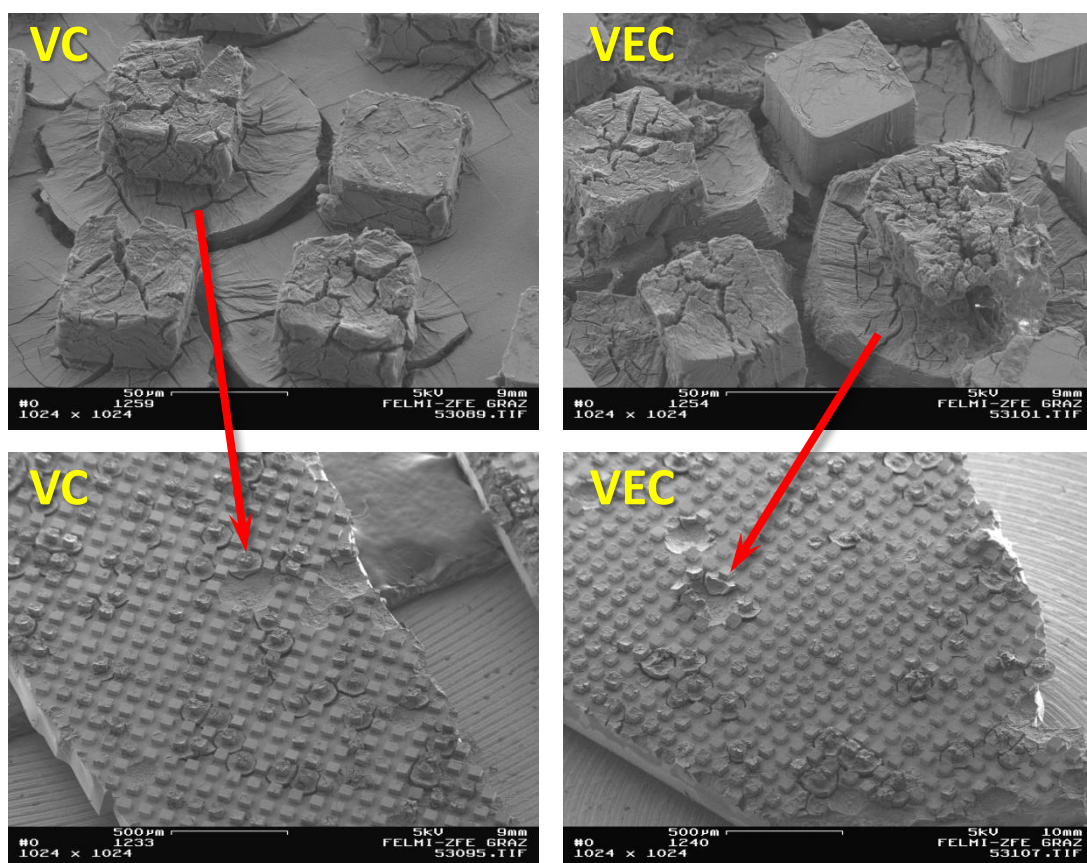


Figure 77: SEM images of the anodes of the cells with VC and VEC. Magnification upper images: 500x. Magnification lower images: 50x. The red arrows indicate that the single towers that are surrounded by a deep ring-like crack (upper images) will break off and leave these craters behind (lower images).

3.2.5. Conclusion

The short term cycling experiments yielded some interesting results on their own. Compared to the standard electrolyte, the used additives (with the exceptions of 0.5 % VEC, 2.0 % Tri-FP and 0.5 % 4-FP) were able to decrease the irreversible capacity generated during SEI formation. Additionally, a possible connection between the used types of additives (VC/VEC vs. 4-FP/Tri-FP) and the homogeneity of the activity of the electrode surface could be identified.

However, when comparing the results of the short term experiments with those of the long term experiment, some inconsistencies can be observed. The values of the same point of time during the experiments (after cycle three) of the cumulative irreversible capacity were compared. Additives that led to an increase of the irreversible capacity in the long term experiments decreased the irreversible capacity in the short term cycling (like 2.0 % 4-FP and 0.5 % Tri-FP). On the other hand, 0.5 % VEC, which was among the best of the long term cycling increased the irreversible capacity during the short term experiment. Only 1.0 % 4-FP and 2.0 % VC showed similarly good results in the short term as in the long term experiment. Effectively, all other additives did not confirm the results of the long term experiment.

Another important aspect is the overall much lower irreversible cumulative capacity of the short term cycling. The cumulative irreversible capacity of the long term experiment is approximately twice as high at the same point of the experiment. It cannot be said for sure whether the missing photo resist contamination on the anodes of the short term experiments is the reason for this drastic decrease of the cumulative irreversible capacity.

In general, the second, shorter cycling experiment did not yield very significant results as they are contradictory to the first, long term experiment and are not very meaningful on their own. Because of this, further investigations on this topic are highly recommended.

3.3. Adhesion of pouch foil/sealing tape welded on different surfaces

In the following chapter, the results of the peel test are presented and an analysis is made. As mentioned before, the aim was to find a way to compare the adhesive bond of the different surface modifications to that of the unmodified silicon and to find the best suited modification for this application.

3.3.1. Analysis

3.3.1.1. Reference (unmodified silicon wafer)

Figure 78 shows force-stroke graphs for the reference samples. This figure shows the typical graph for a peel experiment. At first, as long as the sample is slouching little force is necessary to stretch it. Then the sample is stretched to the point where adhesive forces start to counteract the applied force of the testing machine (first peak). At the slightly sloping plateau afterwards, the adhesive begins to stretch or peel away until it breaks or is peeled off (second peak and steep decline at the end, breaking point). The mean force for every sample was calculated at this plateau phase (area of calculation).

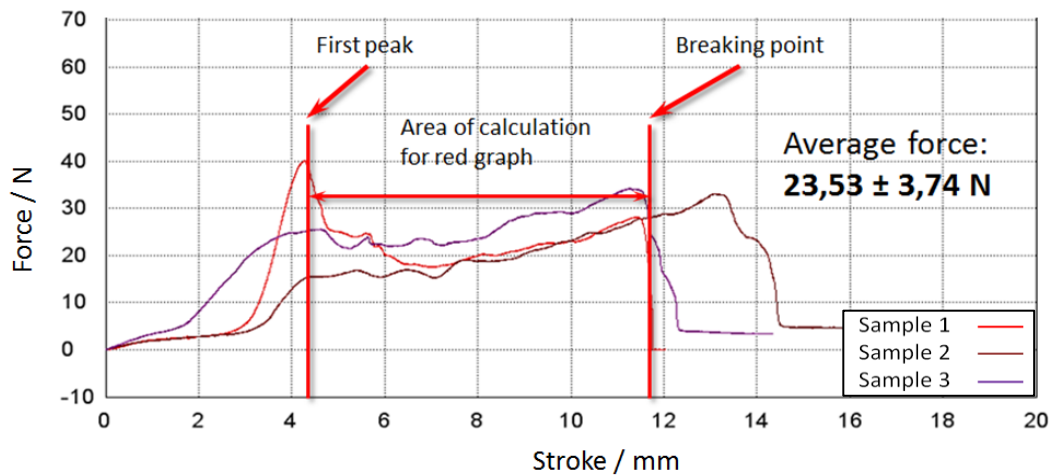


Figure 78: Results peel test: Force-stroke-diagram of the reference (three samples). The first peak and the breaking point for sample one (red) are highlighted. Between them, the mean force for the peel process was calculated (area of calculation). The average force shows the combined value for all samples.

The behavior of all three samples was similar. The only difference was that the first peak of sample 1 was very sharp compared to the flat peaks of sample 2 and 3. A possible reason for this can be identified when looking at the pictures in Figure 79.

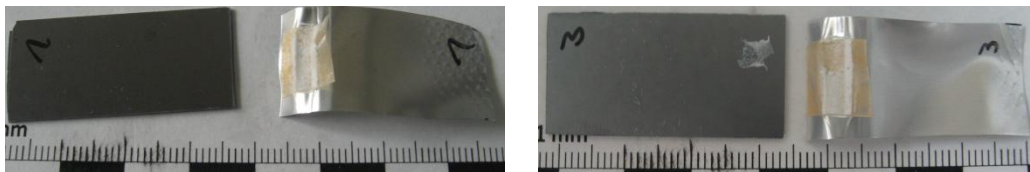


Figure 79: Images of reference samples after the peel test. Left: Sample 1: No sealing tape residues are left on the surface. The foil was neatly peeled away. Right: Sample 3: The foil was peeled away except for a very small residue still sticking to the substrate.

While the foil in sample 1 (Figure 79, left image) was neatly peeled off, there was a small residue of the sealing tape left on the surface of the substrate in sample 2 (Figure 79, right image) and 3. This may have caused the broadening of the first peak for those two samples.

3.3.1.2. Mechanically thinned silicon on glass

Figure 80 shows the diagram for the samples with mechanically thinned silicon on a glass substrate. The behavior of all three samples was similar and the first peaks and breaking points are sharp and easily identifiable.

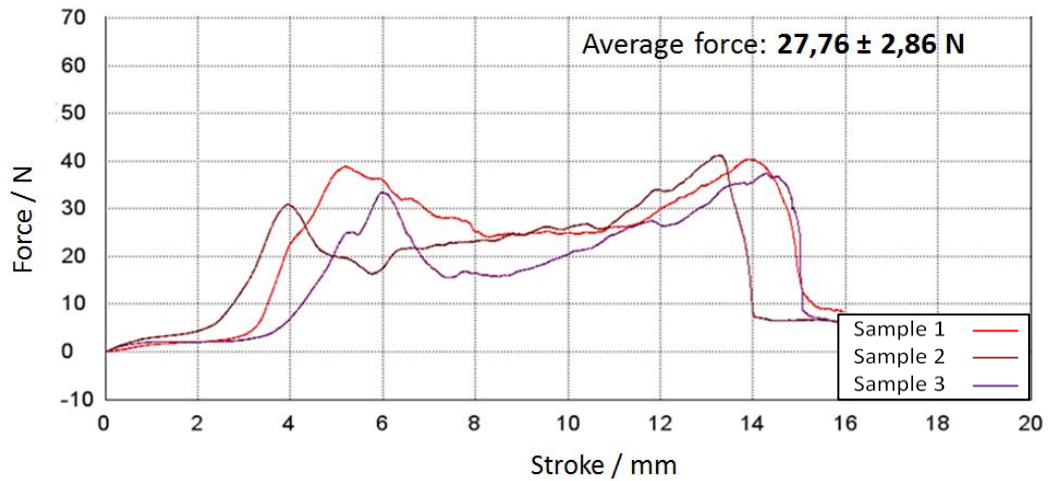


Figure 80: Results peel test: Force-stroke-diagram of mechanically thinned silicon on glass (three samples) and calculated average force for this surface modification.

The images of the samples after the test in Figure 81 show that the foil was not simply peeled off. It rather looks like the sealing tape was torn apart at the upper edge of the weld seam on sample 1 (Figure 81, left image) and 2. On sample 3 (Figure 81, right image) the silicon surface of the welding area with the foil was even pulled off the glass substrate. However, this could be due to some cracks or other damages on the very brittle surface originating from the initial cutting and breaking of the samples.

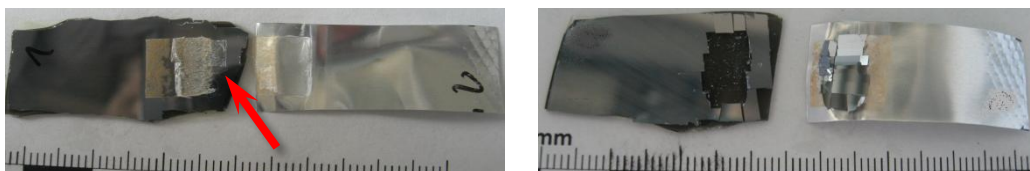


Figure 81: Images of mechanically thinned silicon on glass samples after the peel test. Left: Sample 1: The sealing tape was not peeled off, but pulled apart at the upper edge of the welding area (where the red arrow is pointing). Right: Sample 3: The silicon in the whole area where the foil was welded onto the sample was pulled off.

3.3.1.3. Etched silicon on glass

The samples with etched silicon on a glass substrate showed some non-uniform results as can be seen in Figure 82. While adhesive forces for sample 1 are very low, sample 3 has the only sharp first peak and adhesive forces of sample 4 are high. Sample 2 is somewhere in between.

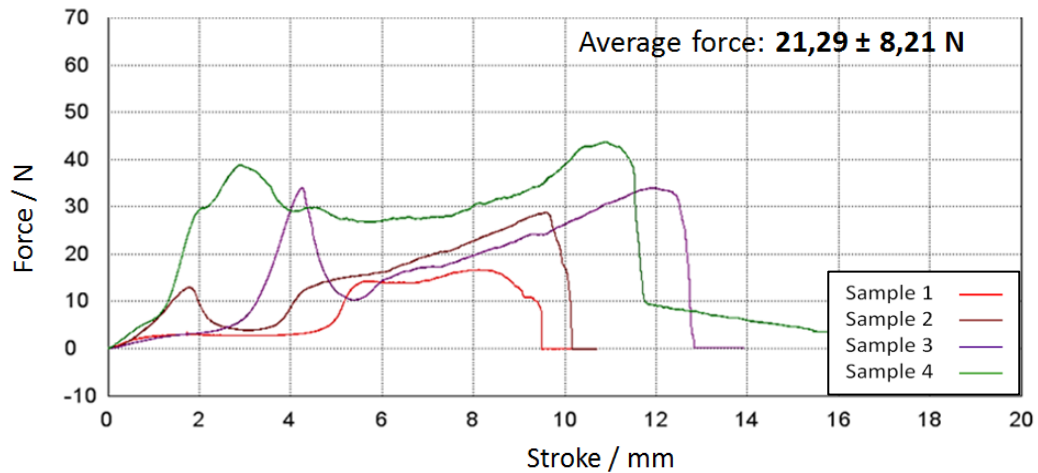


Figure 82: Results peel test: Force-stroke-diagram of etched thinned silicon on glass (four samples) and calculated average force for this surface modification.

The reason for the poor reproducibility of this experiment is unknown. A possible reason could be that the rough surface of this modification heat transfer during welding and thus adhesion of the foil was incomplete or not reproducible. The images of the samples after the peel test do not offer any reason for the inconsistency either. In sample 1 (Figure 83, left image) 2 and 3, the foil was peeled off and left no residues behind. On sample 4 (Figure 83, right image) some sealing tape residues remained on the surface.

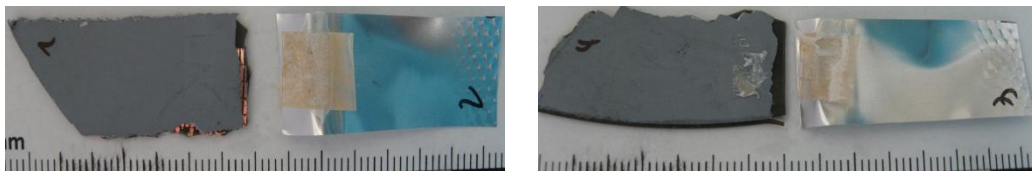


Figure 83: Images of etched silicon on glass samples after the peel test. Left: Sample 1: The foil was peeled away without leaving residues. Right: Sample 4: Some pieces of the sealing tape broke and are still sticking to the surface.

3.3.1.4. ECD-Cu on silicon

All the ECD-Cu samples reacted in the same way, except for sample 4 (Figure 84). Instead of a single peak at the beginning of the experiment, as with the other samples, two small peaks are visible for this sample.

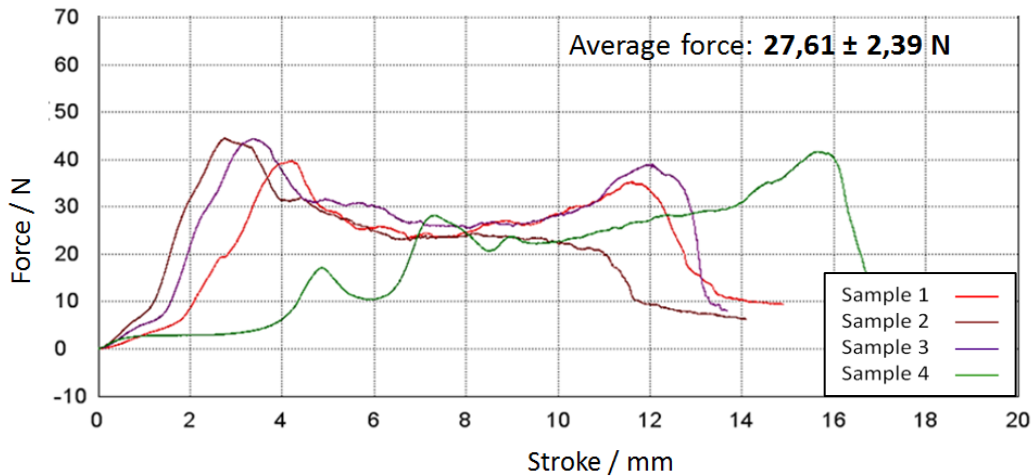


Figure 84: Results peel test: Force-stroke-diagram of ECD-Cu on silicon (four samples) and calculated average force for this surface modification.

On the images of the samples after the test (Figure 85) no differences could be identified. On all samples, the sealing tape was pulled apart at the upper edge of the weld seam and parts of the sealing tape were still left on the sample and the pouch foil.

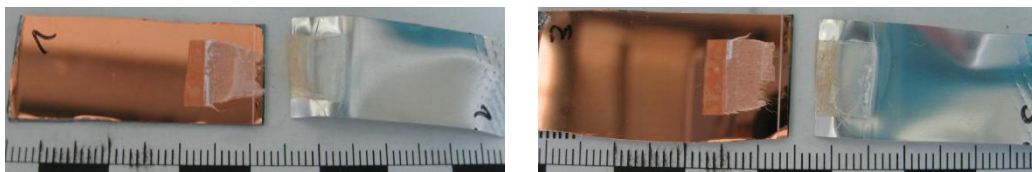


Figure 85: Images of ECD-Cu on silicon samples after the peel test. Left: Sample 1. Right: Sample 3. On both samples, the sealing tape was pulled apart rather than peeled off.

3.3.1.5. RU302507V01 (5)

This modification was the only one that was not applied onto a glass or silicon substrate. This means that these samples were not as thick as the others and the wafer could be broken without the help of any tools. The lesser thickness may have had a positive influence on the welding as this sample showed good results. Another interesting fact are the great fluctuations of the applied force during the plateau-phase that did not occur with any other samples (Figure 86).



Figure 86: Results peel test: Force-stroke-diagram of RU302507V01 (5) (four samples) and calculated average force for this surface modification.

As the results of these samples are very similar so are the images of the samples after the test. The sealing tape of all samples was pulled apart and no differences were observable (Figure 87).

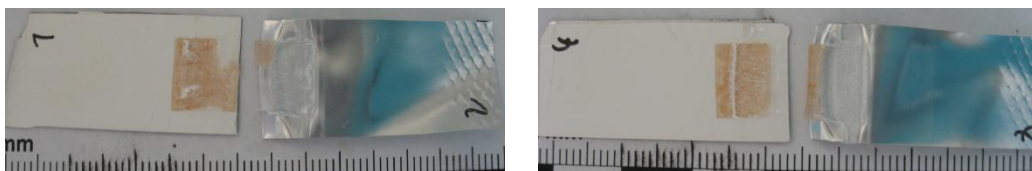


Figure 87: Images of RU302507V01 (5) samples after the peel test. Left: Sample 1. Right: Sample 4. On both samples, the sealing tape was pulled apart rather than peeled off.

3.3.1.6. TiW/AlCu on silicon

In Figure 88, the results of this modification are shown. Sample 1 and 2 and sample 3 and 4 showed similar results respectively. The graphs of the first two samples have a single peak at the beginning, while sample three and four show two smaller peaks, similar to the one from the ECD-Cu modification.

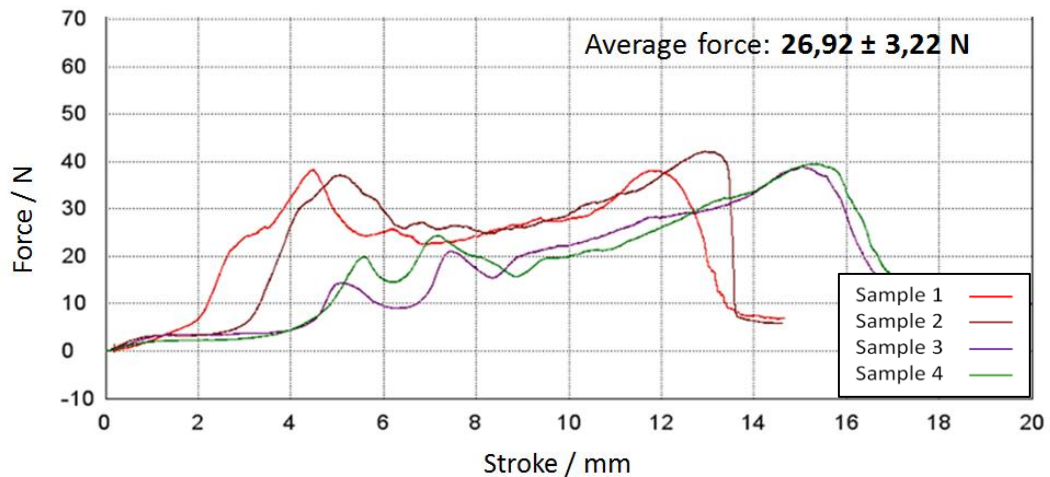


Figure 88: Results peel test: Force-stroke-diagram of TiW/AlCu on silicon (four samples) and calculated average force for this surface modification.

This time a difference can be observed after the test, between the samples that had only this single peak and those that had two smaller ones. The sealing tape of sample 1 and 2 (Figure 89, left image) was pulled apart at the edge of the weld seam. On sample 3 and 4 (Figure 89, right image) the foil was partly peeled away and partly pulled part and only a smaller residue is left sticking to the surface.

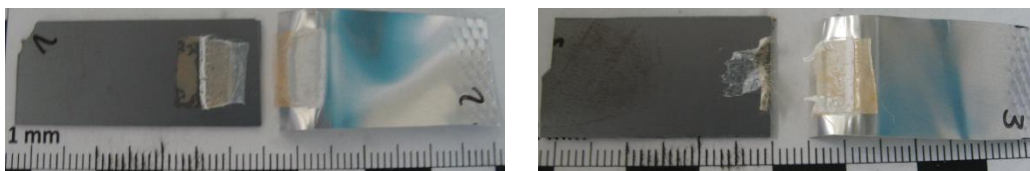


Figure 89: Images of TiW/AlCu on silicon samples after the peel test. Left: Sample 1: The foil was pulled apart rather than peeled off. Right: Sample 3: The sealing tape was partly pulled apart and partly peeled off.

3.3.1.7. 1300 nm TEOS on silicon

The samples of this last modification all showed similar behavior. The graphs shown in Figure 90 have almost the same shape, which is an indicator for a very good reproducibility.

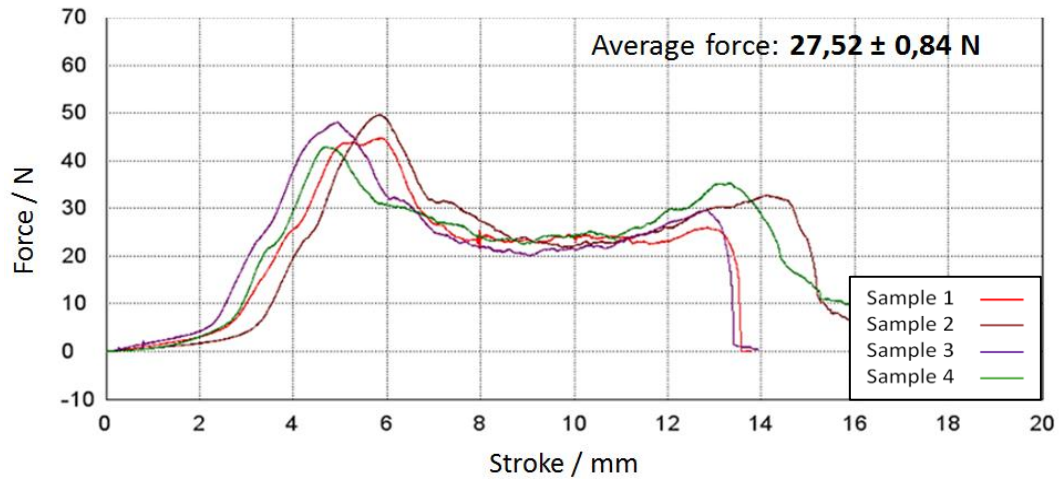


Figure 90: Results peel test: Force-stroke-diagram of 1300 nm TEOS on silicon (four samples) and calculated average force for this surface modification.

On the samples after the test, there were no differences found either. The sealing tape of all four samples was pulled apart in the middle of the welding area, as is illustrated in Figure 91.

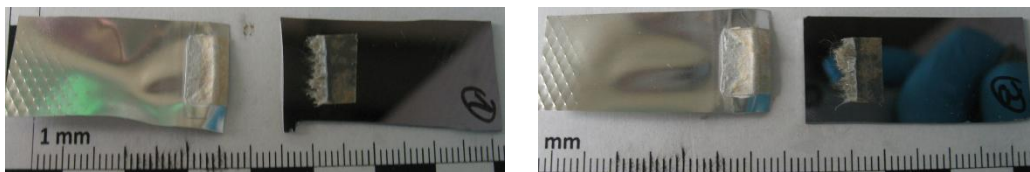


Figure 91: Images of 1300 nm TEOS on silicon samples after the peel test. Left: sample 1. Right: Sample 3. On both samples the sealing tape was pulled apart in the middle.

3.3.2. Conclusion

The results of this simple experiment and the observations made during its execution can be used to determine some factors with which the quality of the adhesive bond between pouch foil and surfaces of different modifications can be compared, with the sealing tape taking the part of the actual adhesive. First of all, the average force for every surface modification that was calculated out of the mean forces from the peel test for every sample can be used to compare the overall adhesive strength the sealing tape pouch foil compound has towards the given surface modification. The actual peel or breaking behavior of the samples at the end of the test can be used for orientation as well. Last but not least, the reproducibility of the test as well as the form of the force-stroke graphs obtained can give information regarding the adhesive bond.

With this factors in mind, the tested surface modifications can be ranked from best suited, (meaning the bond between surface, sealing tape and pouch foil was good) to worst suited (meaning that it showed an unsatisfactory behavior of the bond). In Table 10, this ranking is listed.

Table 10: Overview of the results for different surface modifications from best suited (No. 1) to worst suited (No. 7). Reproducibility ranking: Very high - high - medium - poor - very poor.

| No. | Modification | Average force / N | Sealing tape was | | Reproducibility |
|-----|------------------------------|----------------------|------------------|---------------|-----------------|
| | | | pulled apart | peeled off | |
| 1 | Mechanically thinned silicon | 27,76 ± 2,86 | ++ | | high |
| 2 | 1300 nm TEOS | 27,52 ± 0,84 | ++ | | Very high |
| 3 | ECD-Cu | 27,61 ± 2,39 | ++ | | medium |
| 4 | RU302507V01 (05) | 27,36 ± 1,87 | ++ | | high |
| 5 | TiW/AlCu | 26,92 ± 3,22 | ++ | + | poor |
| 6 | No modification - reference | 23,53 ± 3,74 | + | ++ | poor |
| 7 | Etched silicon | 21,29 ± 8,21 | + | ++ | Very poor |

Looking at the combined results, at least four of the tested surface modifications showed better results than the reference (bare silicon). Those four modifications are mechanically thinned silicon, 1300 nm TEOS, ECD-Cu and RU302507V01 (05). They had a high average force of the adhesive bond, which resulted in the sealing tape being pulled apart in the middle or at the edge of the welding area rather than simply being peeled off. Reproducibility of these samples ranges from very high to good.

Between the four samples, mechanically thinned silicon and 1300 nm TEOS showed even slightly better results than the others. Mechanically thinned silicon had the highest average force towards the sealing tape pouch foil compound and 1300 nm TEOS showed the best reproducibility, although it had a lower average force than ECD-Cu. The RU302507V01 (05) modification has to be viewed with caution as it was the only modification that was not on a glass or silicon substrate and therefore was much thinner. Thus, a direct comparison with the others may not be accurate.

The remaining modifications are TiW/AlCu that had indeed better results than the reference but showed a lower average force and reproducibility than the previously named modifications. Etched silicon showed even worse characteristics than the bare silicon.

The reasons for these results may be found in the roughness or micro-roughness of the used materials. While bare silicon (reference) has a very smooth surface, the other samples, especially mechanically thinned silicon and the metallic modifications, have a surface that looks smooth to the eye, but may have a distinctive micro-roughness. On the other hand, the surface of the etched silicon was even very rough on a macroscopic scale, which may have been too much. Other factors that may have influenced the experiment are heat capacity and heat transfer rates of the materials, as the welding has a different efficiency when these factors are different.

To sum up, the peel test was a simple and convenient way for a fast determination of the best suited surface modification that can be used to improve the adhesive bond of a sealing tape pouch foil compound towards a silicon or glass wafer. A silicon wafer without any modifications was used as a reference and at least four other samples showed superior results. These results can only be viewed in relation to the reference as the carried out peel test was not a standard test, but an improvised one.

4. Summary

The construction of a lithium-ion micro battery based on a single crystal, micro-structured silicon anode is a novel approach to make use of the very high specific capacity of silicon. In this thesis, two aspects that are important for the final realization of such a battery system were investigated.

The first aspect examined was the effect of selected electrolyte additives on the electrochemical performance of the silicon anode was tested. The aim was to improve the cycle stability of the anode through a reduction of the irreversible capacity and an increase of the mechanical stability of the microstructure, thereby influencing the formation of the SEI. For this purpose, four different additives (VC, VEC, 4-FP and Tri-FP) were used in three different concentrations respectively. Long term cycling experiments (100 cycles) in pouch cells were carried out and cycle stability, coulometric efficiency and cumulative irreversible capacity were analyzed. Afterwards, an additional visual analysis of the cycled silicon anodes was carried out using SEM. It was shown that certain additives indeed have a positive effect on the cycling behavior at certain concentrations, as they were able to decrease the cumulative irreversible capacity and mechanical stress of the material through the formation of a more stable SEI.

Unfortunately, at this point, a contamination of all the previously used silicon anodes was discovered and it was decided to repeat the whole experiment with new anodes that were not contaminated. Due to the lack of time, a much shorter version of the experiment was carried out (only three cycles) and instead of pouch cells, Swagelok cells were used as a test system. In this short term cycling experiment, it was again shown that the cumulative irreversible capacity could be reduced and the morphological behavior of the anode could be influenced by the use of additives. However, the exact results from the long term cycling experiment could not be reproduced. On the contrary, additives that showed good behavior in the long term experiment, showed bad results in the short term experiment and vice versa. Only two out of twelve samples (VC in 2.0 % concentration and 4-FP in 1.0 % concentration) had similarly good results in both experiments. The reason for this inconsistency is unclear, but a possible reason could be the contamination of the first anodes or the use of two different test cells. In either case, a further and deeper investigation on this topic is strongly advised.

The second focus was on the investigation of the adhesive bond between different modified surfaces and aluminium laminated film (pouch foil) with sealing tape as interlayer. Pouch foil is a possible enclosure material for the cavity on a silicon wafer that may function as housing for the micro-battery. For a very tight sealing, the pouch foil was welded onto the silicon surface, with the sealing tape being the actual bonding agent. Via an improvised peel test and a subsequent analysis, factors could be determined with which the quality and the strength of the adhesive bond between the surface and the pouch foil could be described. These factors enabled the comparison of the different modifications and it was shown that, compared to unmodified silicon, the strength of the adhesive bond strongly increases with certain surface modifications (mechanically thinned silicon, 1800 nm TEOS and ECD-Cu).

5. References

- [1] Obrovac, M. N.; Christensen, L., Structural Changes in Silicon Anodes during Lithium Insertion/Extraction. *Electrochemical and Solid-State Letters* **2004**, *7*, (5), A93-A96.
- [2] Li, H.; Huang, X.; Chen, L.; Wu, Z.; Liang, Y., A High Capacity Nano - Si Composite Anode Material for Lithium Rechargeable Batteries. *Electrochemical and Solid-State Letters* **1999**, *2*, (11), 547-549.
- [3] Maranchi, J. P.; Hepp, A. F.; Kumta, P. N., High Capacity, Reversible Silicon Thin-Film Anodes for Lithium-Ion Batteries. *Electrochemical and Solid-State Letters* **2003**, *6*, (9), A198-A201.
- [4] Boukamp, B. A.; Lesh, G. C.; Huggins, R. A., All-Solid Lithium Electrodes with Mixed-Conductor Matrix. *Journal of The Electrochemical Society* **1981**, *128*, (4), 725-729.
- [5] Dimov, N.; Xia, Y.; Yoshio, M., Practical silicon-based composite anodes for lithium-ion batteries: Fundamental and technological features. *Journal of Power Sources* **2007**, *171*, (2), 886-893.
- [6] Liu, W.-R.; Guo, Z.-Z.; Young, W.-S.; Shieh, D.-T.; Wu, H.-C.; Yang, M.-H.; Wu, N.-L., Effect of electrode structure on performance of Si anode in Li-ion batteries: Si particle size and conductive additive. *Journal of Power Sources* **2005**, *140*, (1), 139-144.
- [7] Ohara, S.; Suzuki, J.; Sekine, K.; Takamura, T., A thin film silicon anode for Li-ion batteries having a very large specific capacity and long cycle life. *Journal of Power Sources* **2004**, *136*, (2), 303-306.
- [8] Jung, H.; Park, M.; Yoon, Y.-G.; Kim, G.-B.; Joo, S.-K., Amorphous silicon anode for lithium-ion rechargeable batteries. *Journal of Power Sources* **2003**, *115*, (2), 346-351.
- [9] Xu, K., Nonaqueous Liquid Electrolytes for Lithium-Based Rechargeable Batteries. *Chemical Reviews* **2004**, *104*, (10), 4303-4418.
- [10] Zhang, S. S., A review on electrolyte additives for lithium-ion batteries. *Journal of Power Sources* **2006**, *162*, (2), 1379-1394.
- [11] Simon, B.; Boeueve, J.-P. Rechargeable lithium electrochemical cell. U.S. Patent 5626981, 1997.
- [12] Aurbach, D.; Gamolsky, K.; Markovsky, B.; Gofer, Y.; Schmidt, M.; Heider, U., On the use of vinylene carbonate (VC) as an additive to electrolyte solutions for Li-ion batteries. *Electrochimica Acta* **2002**, *47*, (9), 1423-1439.
- [13] Chen, L.; Wang, K.; Xie, X.; Xie, J., Effect of vinylene carbonate (VC) as electrolyte additive on electrochemical performance of Si film anode for lithium ion batteries. *Journal of Power Sources* **2007**, *174*, (2), 538-543.

- [14] Chen, G.; Zhuang, G. V.; Richardson, T. J.; Liu, G.; Ross, P. N., Anodic Polymerization of Vinyl Ethylene Carbonate in Li-Ion Battery Electrolyte. *Electrochemical and Solid-State Letters* **2005**, 8, (7), A344-A347.
- [15] Zhang, S. S., Aromatic isocyanate as a new type of electrolyte additive for the improved performance of Li-ion batteries. *Journal of Power Sources* **2006**, 163, (1), 567-572.
- [16] Korepp, C.; Kern, W.; Lanzer, E. A.; Raimann, P. R.; Besenhard, J. O.; Yang, M. H.; Möller, K. C.; Shieh, D. T.; Winter, M., Isocyanate compounds as electrolyte additives for lithium-ion batteries. *Journal of Power Sources* **2007**, 174, (2), 387-393.
- [17] Showa Denko Packaging Co., Ltd. <http://sdk-pack.co.jp/en/product/#electronics> (04.12.2013).
- [18] Peel Adhesion Test Standards. <http://www.mecmesin.com/knowledge-center-peel-test-adhesion-testing> (14.11.2013).
- [19] How to Perform ASTM D903 Peel or Stripping Strength of Adhesive Bonds. <http://www.massdevice.com/blogs/debbi-cohen/how-perform-astm-d903-peel-or-stripping-strength-adhesive-bonds> (14.11.2013).
- [20] How to Perform an Adhesive Strength T-Peel Test - ASTM D1876. <http://info.admet.com/specifications/bid/43840/How-to-Perform-an-Adhesive-Strength-T-Peel-Test-ASTM-D1876> (15.11.2013).
- [21] Wahl, D., Eine kleine Geschichte der Elektrochemie Teil 1. *Galvanotechnik* **2005**, 7, 1600-1610.
- [22] Dunsch, L., *Geschichte der Elektrochemie*. VEB Deutscher Verlag für Grundstoffindustrie Leipzig: **1985**.
- [23] Winter, M.; Besenhard, J. O., Wiederaufladbare Batterien. *Chemie in unserer Zeit* **1999**, 33, (5), 252-266.
- [24] Linden, D.; Reddy, T. B., *Handbook of batteries*. 2nd ed.; McGraw-Hill, Inc.: **1995**.
- [25] Daniel, C.; Besenhard, J. O., *Handbook of Battery Materials*. 2nd ed.; Wiley-VCH Verlag GmbH & Co. KGaA: **2011**; Vol. 1.
- [26] Winter, M.; Besenhard, J. O., Wiederaufladbare Batterien. *Chemie in unserer Zeit* **1999**, 33, (6), 320-332.
- [27] Schematic structure of an alkaline-manganese dioxide cell. <http://electrochem.cwru.edu/encycl/art-c01-carbon.htm> (12.11.2013).
- [28] Peled, E., The Electrochemical Behavior of Alkali and Alkaline Earth Metals in Nonaqueous Battery Systems—The Solid Electrolyte Interphase Model. *Journal of The Electrochemical Society* **1979**, 126, (12), 2047-2051.
- [29] Wakihara, M.; Yamamoto, O., *Lithium Ion Batteries - Fundamentals and Performance*. Kodansha Ltd. WILEY-VCH Verlag GmbH: **1998**.

- [30] Winter, M.; Besenhard, J. O.; Spahr, M. E.; Novák, P., Insertion Electrode Materials for Rechargeable Lithium Batteries. *Advanced Materials* **1998**, 10, (10), 725-763.
- [31] Schematic of a lithium-ion battery. http://www.tft.kit.edu/564_619.php (02.05.2013).
- [32] Daniel, C.; Besenhard, J. O., *Handbook of Battery Materials*. 2nd ed.; Wiley-VCH Verlag GmbH & Co. KGaA: **2011**; Vol. 2.
- [33] Ender, M.; Weber, A.; Ellen, I.-T., Analysis of Three-Electrode Setups for AC-Impedance Measurements on Lithium-Ion Cells by FEM simulations. *Journal of The Electrochemical Society* **2011**, 159, (2), A128-A136.